Electronic Supplementary Material (ESI) for Chemical Communications.

Supporting Information

Mono-mercapto-functionalized pillar[5]arene: a host-guest complexation accelerated reversible redox dimerization

Jianbing Jin[a], Jiarong Miao[a], Chuyang Cheng[*a]

a. *College of Chemistry, Sichuan University, Chengdu, 610064, China.*

The corresponding author: cycheng@scu.edu.cn

Table of Contents

1. General Materials and Methods 3
2. Syntheses and Characterizations of Mono-SH-pillar[5]arene J1 and Di(mono-SH-pillar[5]arene)mer J2 4
   Synthetic Procedures 5
   1D NMR Spectra 13
   2D NMR Spectra 21
   HR-MS (ESI-TOF) Spectra 41
3. Reversible Redox Conversion between J1 and J2 47
   The oxidative self-dimerization of J1 in the presence of O_2 and K_2CO_3 48
   The reduction of J2 in the presence of DTT and K_2CO_3 49
   Determination of oxidative self-dimerization rate constant of J1 by linear fitting 55
   The changes of oxidative self-dimerization conversion ratio of J1 by nonlinear curve-fitting 56
4. Host-guest Complexation 59
   NMR spectra of HDPB (1-hexadecylpyridinium bromide) in the absence and presence of J1 59
   NMR spectra of HDPB (1-hexadecylpyridinium bromide) in the absence and presence of J2 63
   NMR spectra of titration 66
   Molar ratio plot for the complexation by ^{1}H NMR titration 70
   Determination of association constants by ^{1}H NMR titration 71
5. The Reversible Redox Conversion of the Host-guest Complexes between G0⊂J1 and $(G0)_2$⊂J2. 74
6. Control Experiments for Further Elucidating the Mechanism of Accelerated Redox Conversion Process. 77
7. References 87

1. General Materials and Methods

All reagents were purchased from commercial suppliers: Innochem, Aladdin, Adamas, Greagent and used without further purification. All solvents used in synthesis were purchased from commercial suppliers: KESHI. Anhydrous solvents were purchased from commercial suppliers: Energy Chemical and used without further purification from a drying agent under a nitrogen atmosphere.

^{1}H NMR, ^{13}C NMR, ^{1}H-^{1}H COSY, ^{1}H-^{1}H NOESY, ^{1}H-^{13}C HSQC, ^{1}H-^{13}C HMBC spectra were recorded on 400 MHz Agilent ProPulse (^{1}H 400 MHz, ^{13}C 100 MHz) instruments. Chemical shifts (δ) are reported in parts per million (ppm). Coupling constants are reported in Hertz (Hz), and signal multiplicity is denoted as singlet (s), doublet (d), doublet of doublets (dd), triplet (t), dt (doublet of triplets), td (triplet of doublets), dtd (doublet of triplets of doublets), q (quartet), h (heptet), multiplet (m) and broad (br). All spectra were acquired at 20 °C (293 K) and were referenced to the residual solvent peaks. The common solvent impurities in ^{1}H and ^{13}C NMR in small amounts were water, dichloromethane.

The high-resolution mass spectra (HR-MS) data was acquired on a Bruker MaXis HD ESI-TOF mass spectrometer for high mass accuracy, coupled to a Thermo Scientific Dionex Ultra-High Performance Liquid Chromatography (UPLC) unit.

UPLC-MS data was collected by Ultimate 3000 Ultra-High

Performance Liquid Chromatography-ISQEM Mass Spectrometer. Acetonitrile (CH_3CN) for UPLC-MS was purchased from Adamas. Mass spectra (positive mode) were acquired in ultra-scan mode. Analytical separations were achieved by injecting 5 μL (for 1 mM DCL, scaled accordingly for dynamic combinatorial libraries (DCLs) at different concentrations) of DCL solution on to a Symmetry C18 reverse phase column (ThermoFisher Scientific, Accucore RP-MS 100 × 2.1 mm, 2.6 μm particle size) at 35 °C and a flow rate of 0.30 mL/min.

2. Syntheses and Characterizations of Mono-SH-pillar[5]arene J1 and Di(mono-SH-pillar[5]arene)mer J2

Synthetic route of J1

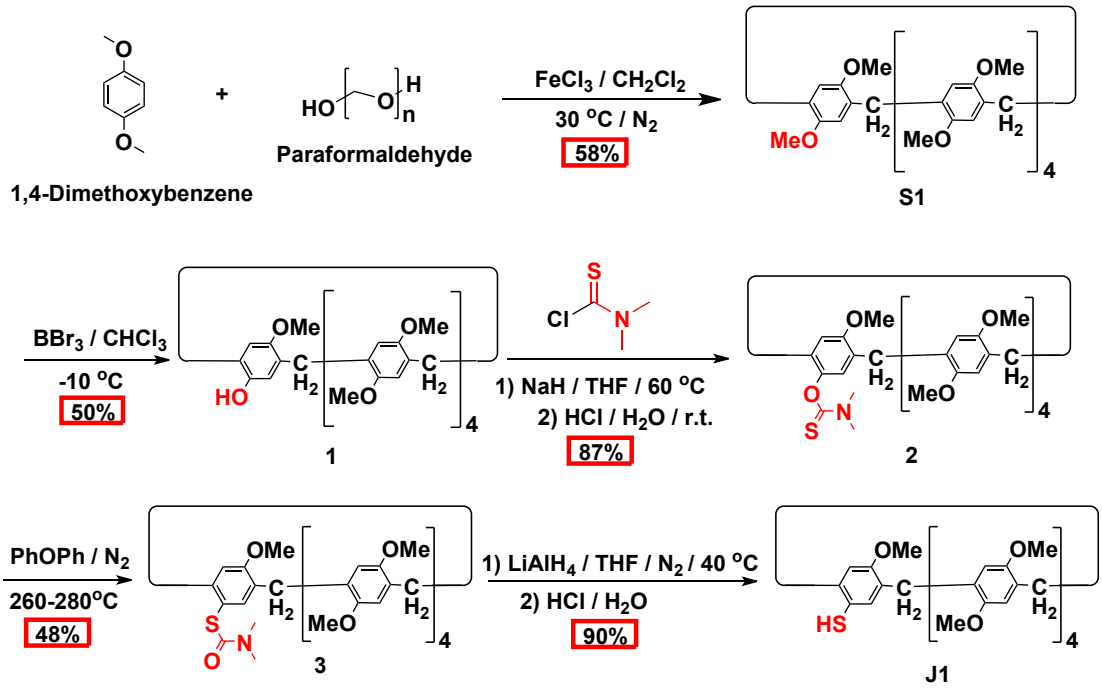

Scheme S1 The synthesis of **Mono-SH-pillar[5]arene J1**

Synthetic route of J2

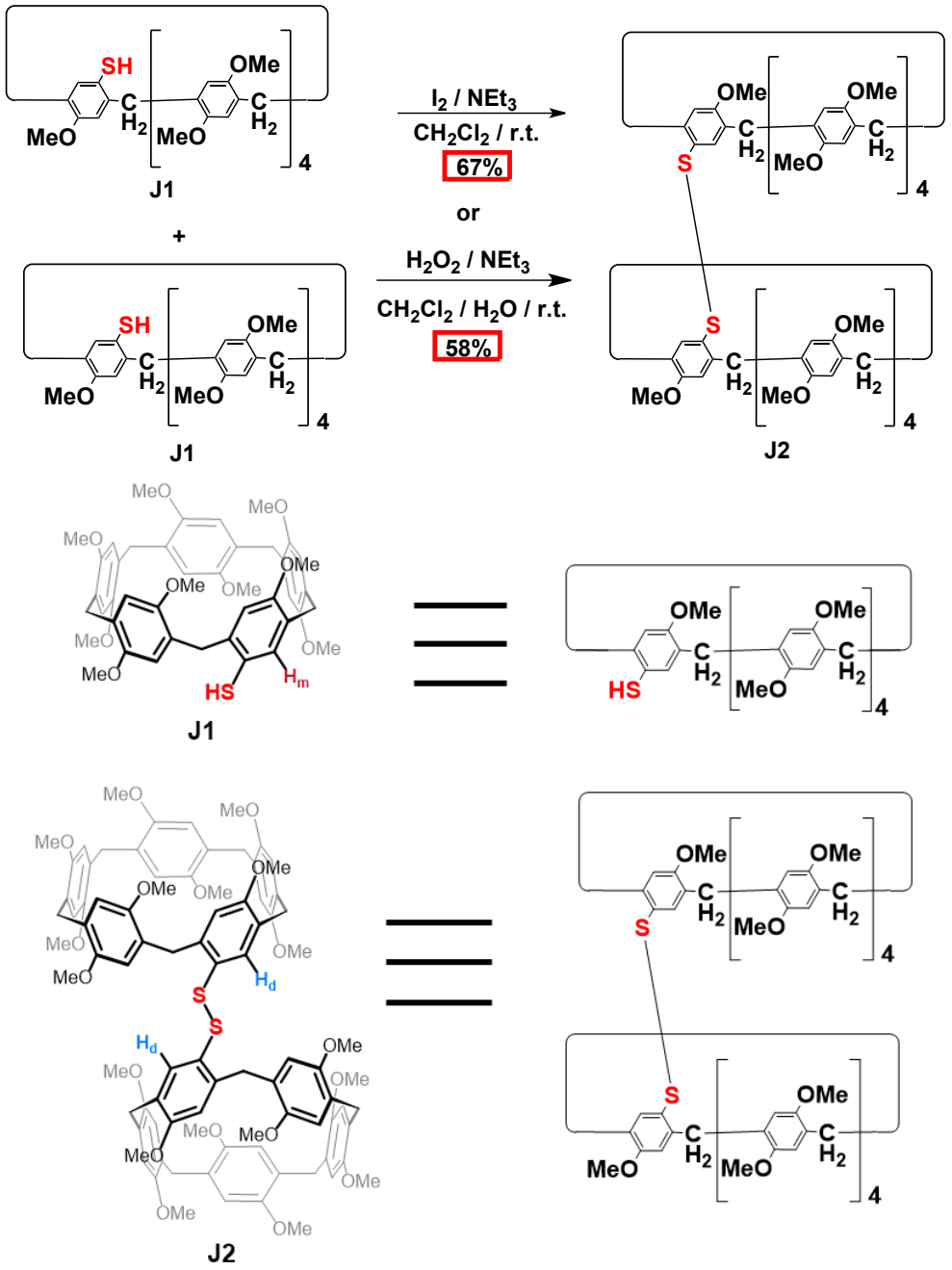

Scheme S2 The synthesis of dimer of **Mono-SH-pillar[5]arene**

Synthetic Procedures

Compound **S1** and compound **1** were synthesized according to literature procedures with necessary modification.[1, 2]

Compound S1: Dimethoxypillar[5]arene. [1] To the mixture of 1,4-dimethoxybenzene (5.80 g, 42.0 mmol), paraformaldehyde (3.60 g, 120.0 mmol, 2.86 eq) and anhydrous iron (III) chloride (1.00 g, 6.17 mmol, 0.15 eq) was added dichloromethane (A. R., analytical reagent) (CH_2Cl_2) (320 mL) in the water bath (30 ℃) under nitrogen atmosphere. After stirring at 30 ℃ for 1 h, the reaction was quenched with distilled water (125 mL). Then, the mixture was filtrated under reduced pressure and the filtrate was extracted with CH_2Cl_2 (150 mL × 2). The combined organic extracts were dried with anhydrous Na_2SO_4. After removal of the solvents under reduced pressure, the residue was further purified by column chromatography over silica gel (petroleum ether: ethyl acetate = 3:1) to afford **S1** as whitish yellow solid powder in 58% yield (3.65 g). ^{1}H NMR (400 MHz, 293 K, $CDCl_3$): δ (ppm) 6.79 (s, 10H, phenyl), 3.78 (s, 10H, -CH_2-), 3.67 (s, 30H, -OCH_3). ^{13}C NMR (100 MHz, 293 K, $CDCl_3$): δ (ppm) 150.85 (phenyl), 128.32 (phenyl), 114.10 (phenyl), 55.87 (-OCH_3), 29.71 (-CH_2-). HR-MS (ESI-TOF): *m*/*z* Calcd for $[M + NH_4]^+$ $C_{45}H_{54}NO_{10}$: 768.3748; found: 768.3725, error: -3.0 ppm.

Compound 1: Mono-OH-pillar[5]arene. [2] To a solution of **S1** (2.00 g, 2.66 mmol) in chloroform (A. R., analytical reagent, 140 mL) was added boron tribromide (2.67 g, 10.7 mmol, 1.00 mL, 4.00 eq) in the ethanol bath (-10 ℃). After stirring at -10 ℃ for 80 min, the reaction was quenched with

distilled water (100 mL). Then, the mixture was extracted with CH_2Cl_2 (100 mL × 2). The combined organic extracts were dried with anhydrous Na_2SO_4. After removal of the solvents under reduced pressure, the residue was further purified by column chromatography over silica gel (eluent: first with (petroleum ether: ethyl acetate = 9:1); next with (petroleum ether: ethyl acetate = 4:1); last with (petroleum ether: ethyl acetate = 3:1)) to afford **1** as pink solid powder in 50% yield (0.98 g). ^{1}H NMR (400 MHz, 293 K, $CDCl_3$): δ (ppm) phenyl: 6.89 (s, 1H, -OH), 6.76-6.58 (m, 10H); -CH_2-: 3.84-3.76 (m, 10H); -OCH_3: 3.75-3.50 (m, 27H). ^{13}C NMR (100 MHz, 293 K, $CDCl_3$): δ (ppm) phenyl: 151.95, 151.17, 151.07, 151.03, 151.01, 150.99, 150.90, 148.69, 147.65, 130.09, 129.41, 128.78, 128.47, 128.41, 128.36, 128.22, 127.80, 126.92, 125.13, 119.01, 114.65, 114.57, 114.37, 114.15, 113.95, 113.06, 113.00; -OCH_3: 56.47, 56.25, 56.17, 56.09, 56.00, 55.97, 55.95, 55.94; -CH_2-: 31.06, 30.17, 30.04, 29.71, 28.95. HR-MS (ESI-TOF): *m*/*z* Calcd for $[M + NH_4]^+$ $C_{44}H_{52}NO_{10}$: 754.3591; found: 754.3563, error: -3.7 ppm.

Compound 2: Mono-[(*N*,*N*′-dimethyl)thiocarbamoyl]-pillar[5]arene.[3,4] To a solution of **1** (0.98 g, 1.33 mmol) and *N*,*N*′-dimethylthiocarbamoyl chloride (DMTCC, 0.85 g, 6.65 mmol, 5.00 eq) in anhydrous THF (50 mL) was added sodium hydride (NaH, 60% wt suspension in mineral oil, 0.53 g, 13.3 mmol, 10.0 eq) at 0 °C. The

mixture was stirred at 60 °C in the oil bath for 29 h. After cooling to room temperature, the reaction was quenched by adding 20 mL solution of 2.0 M HCl in the ice-water bath. CH_2Cl_2 (150 mL) and distilled H_2O (100 mL) was added to the mixture. The mixture was extracted with CH_2Cl_2 (100 mL × 2). The obtained yellow solution was dried with anhydrous Na_2SO_4. After removal of the solvents under reduced pressure, the residue was purified first by recrystallization with methanol and dichloromethane. Then, the obtained solid was further purified by column chromatography over silica gel (eluent: first with (petroleum ether: ethyl acetate = 4:1); then with (petroleum ether: ethyl acetate = 3:1); last with (petroleum ether: ethyl acetate = 2:1)) to afford **2** as white solid powder in 87% yield (0.96 g). ^{1}H NMR (400 MHz, 293 K, $CDCl_3$): δ (ppm) phenyl: 6.80-6.74 (m, 8H), 6.70 (s, 1H), 6.56 (s, 1H); -CH_2-: 3.79-3.76 (m, 8H), 3.68 (s, 2H); -OCH_3: 3.66-3.58 (m, 27H); -$N(CH_3)_2$: 3.48 (s, 3H), 3.29 (s, 3H). ^{13}C NMR (100 MHz, 293 K, $CDCl_3$): δ (ppm) phenyl: 188.43, 154.91, 151.12, 151.10, 151.07, 150.91, 150.88, 150.87, 150.85, 150.84, 144.92, 132.58, 128.83, 128.74, 128.67, 128.60, 128.51, 128.46, 128.08, 128.04, 127.74, 124.96, 114.67, 114.40, 114.28, 114.22, 114.03, 113.92, 112.61; -OCH_3: 56.20, 56.06, 56.03, 56.00, 55.98, 55.94, 55.89, 55.24; -$N(CH_3)_2$: 43.46, 38.52; -CH_2-: 30.20, 30.17, 29.95, 29.91, 29.80. HR-MS (ESI-TOF): *m*/*z* Calcd for $[M + H]^+$ $C_{47}H_{54}NO_{10}S$: 824.3468; found: 824.3455, error: -1.6 ppm.

Compound 3: Mono-[(*N,N′*-dimethylcarbamoyl)thio]-pillar[5]arene.[4,5] The mixture of **2** (2.51 g, 3.05 mmol) and diphenyl ether (32.1 g, 188.6 mmol) was heated at 260-280 °C in the heating-mantle for 140 min under N_2 to undergo the Newman-Kwart rearrangement reaction. Then, the mixture was cooled to the room temperature and further purified by column chromatography over silica gel (eluent: first with petroleum ether; then with (petroleum ether: ethyl acetate =4:1); next with (petroleum ether: ethyl acetate = 2:1); last with (petroleum ether: ethyl acetate = 7:5)) to afford **3** as white solid powder in 48% yield (1.22 g). ^{1}H NMR (400 MHz, 293 K, $CDCl_3$): δ (ppm) phenyl: 7.32 (s, 1H), 6.86 (s, 1H), 6.80-6.70 (m, 8H); -CH_2-: 3.98 (s, 2H), 3.80-3.72 (m, 8H); -OCH_3: 3.67-3.59 (m, 27H); -$N(CH_3)_2$: 3.20-2.92 (br, 6H). ^{13}C NMR (100 MHz, 293 K, $CDCl_3$): δ (ppm) phenyl: 167.90, 158.68, 151.26, 151.07, 151.02, 150.90, 150.88, 150.85, 150.74, 150.67, 145.94, 139.69, 128.59, 128.54, 128.44, 128.41, 128.38, 128.32, 128.17, 127.90, 117.08, 114.56, 114.40, 114.27, 114.22, 114.19, 114.11, 113.94, 112.97; -OCH_3: 56.13, 56.00, 55.95, 55.92, 54.91; -$N(CH_3)_2$: 37.06; -CH_2-: 33.60, 30.22, 30.07, 29.85, 29.74. HR-MS (ESI-TOF): *m*/*z* Calcd for $[M + H]^+$ $C_{47}H_{54}NO_{10}S$: 824.3468; found: 824.3468, error: 0.0 ppm.

Compound J1: Mono-SH-pillar[5]arene. [5] To the mixture of **3** (1.22 g, 1.48 mmol) and lithium aluminum hydride ($LiAlH_4$) (0.84 g, 22.2 mmol,

15 eq) was added anhydrous THF (75 mL) in the ice-water bath under N_2 atmosphere. After that, the mixture was stirred at 40 °C in the oil bath for 4.0 h under N_2 and quenched by slowly adding 50 mL of HCl (2.0 M, deoxygenated) solution at 0 °C under nitrogen protection. The obtained solution was extracted with CH_2Cl_2 (100 mL × 2) and dried with anhydrous Na_2SO_4. After removal of the solvents under reduced pressure, the residue was further purified by column chromatography over silica gel (eluent: first with (petroleum ether: ethyl acetate = 6:1); then with (petroleum ether: ethyl acetate = 4:1)) to afford **J1** as white solid powder in 90% yield (1.00 g). ^{1}H NMR (400 MHz, 293 K, $CDCl_3$): δ (ppm) phenyl: 7.20 (s, 1H), 6.84-6.76 (m, 7H), 6.75 (s, 1H), 6.73 (s, 1H); -CH_2-: 3.95 (s, 2H), 3.80-3.77 (br, 6H), 3.72 (s, 2H); -OCH_3: 3.67-3.62 (m, 27H); -SH: 3.18 (s, 1H). ^{13}C NMR (100 MHz, 293 K, $CDCl_3$): δ (ppm) phenyl: 156.36, 151.07, 151.03, 150.96, 150.90, 150.86, 150.85, 150.82, 150.67, 140.82, 135.31, 128.80, 128.71, 128.51, 128.49, 128.45, 128.35, 128.17, 127.86, 127.62, 117.97, 114.35, 114.24, 114.21, 114.19, 114.14, 113.90, 113.37; -OCH_3: 56.04, 55.97, 55.96, 55.93, 55.80, 55.15; -CH_2-:34.22, 29.95, 29.80, 29.75, 29.53. HR-MS (ESI-TOF): *m*/*z* Calcd for $[M + NH_4]^+$ $C_{44}H_{52}NO_9S$: 770.3363; found: 770.3359, error: -0.52 ppm.

Compound J2: Di(mono-SH-pillar[5]arene)mer. [6] To a solution of **J1** (0.55 g, 0.73 mmol) in CH_2Cl_2 (A. R., analytical reagent) (130 mL)

containing triethylamine (1.48 g, 14.6 mmol, 2.00 mL, 20 eq), I_2 (0.56 g, 2.20 mmol, 3.00 eq) was added at room temperature (20 °C). After that, the solution was stirred at room temperature for 100 min and quenched by adding 30 mL of sodium thiosulfate solution (2.0 M) at room temperature. CH_2Cl_2 (20 mL) and distilled H_2O (100 mL) was added to the mixture. The obtained brown solution was extracted with CH_2Cl_2 (100 mL × 2) and dried with anhydrous Na_2SO_4. After removal of the solvents under reduced pressure, the residue was further purified by column chromatography over silica gel (eluent: first with (petroleum ether: ethyl acetate = 6:1); then with (petroleum ether: ethyl acetate = 4:1); last with (petroleum ether: ethyl acetate = 2:1)) to afford **J2** as whitish yellow solid powder in 67% yield (0.37 g). ^{1}H NMR (400 MHz, 293 K, $CDCl_3$): δ (ppm) phenyl: 7.40 (s, 2H), 6.85-6.72 (m, 18H); -CH_2-: 3.89 (s, 4H), 3.77 (s, 12H), 3.72 (s, 4H); -OCH_3: 3.68-3.63 (br, 48H), 3.57 (s, 6H). ^{13}C NMR (100 MHz, 293 K, $CDCl_3$): δ (ppm) phenyl: 158.11, 151.20, 151.03, 150.89, 150.82, 150.67, 150.51, 144.01, 137.76, 128.50, 128.38, 128.25, 128.19, 127.69, 126.11, 114.27, 114.12, 114.05, 113.80, 112.57; -OCH_3: 55.99, 55.95, 55.92, 55.89, 55.86, 55.79, 54.98, -CH_2-: 33.16, 29.89, 29.64. HR-MS (ESI-TOF): *m*/*z* Calcd for $[M + NH_4]^+$ $C_{88}H_{98}NO_{18}S_2$: 1520.6225; found: 1520.6176, error: -3.2 ppm.

Compound J2: Di(mono-SH-pillar[5]arene)mer. [6] To a solution of **J1**

(0.12 g, 0.16 mmol) in CH_2Cl_2 (A. R., analytical reagent) (30 mL) containing triethylamine (0.73 g, 7.20 mmol, 1.00 mL, 45 eq) and distilled H_2O (15 mL), hydrogen peroxide (H_2O_2) (30 wt%, 1.10 g, 9.70 mmol, 1.00 mL, 61.0 eq) was added at room temperature (20 °C). After that, the mixture was stirred at room temperature for 42.5 h and quenched by adding 10 mL of sodium thiosulfate solution (2.0 M) at room temperature. CH_2Cl_2 (30 mL) and distilled H_2O (30 mL) was added to the mixture. The obtained solution was extracted with CH_2Cl_2 (50 mL × 2) and dried with anhydrous Na_2SO_4. After removal of the solvents under reduced pressure, the residue was further purified by column chromatography over silica gel (eluent: first with (petroleum ether: ethyl acetate = 6:1); then with (petroleum ether: ethyl acetate = 4:1); last with (petroleum ether: ethyl acetate = 3:1)) to afford **J2** as white solid powder in 58% yield (0.070 g). ^{1}H NMR (400 MHz, 293 K, $CDCl_3$): δ (ppm) phenyl: 7.40 (s, 2H), 6.85-6.72 (m, 18H); -CH_2-: 3.89 (s, 4H), 3.77 (s, 12H), 3.72 (s, 4H); -OCH_3: 3.68-3.63 (br, 48H), 3.57 (s, 6H). ^{13}C NMR (100 MHz, 293 K, $CDCl_3$): δ (ppm) phenyl: 158.11, 151.20, 151.03, 150.89, 150.82, 150.67, 150.51, 144.01, 137.76, 128.50, 128.38, 128.25, 128.19, 127.69, 126.11, 114.27, 114.12, 114.05, 113.80, 112.57; -OCH_3: 55.99, 55.95, 55.92, 55.89, 55.86, 55.79, 54.98, -CH_2-: 33.16, 29.89, 29.64. HR-MS (ESI-TOF): *m*/*z* Calcd for $[M + NH_4]^+$ $C_{88}H_{98}NO_{18}S_2$: 1520.6225; found: 1520.6176, error: -3.2 ppm.

1D NMR Spectra

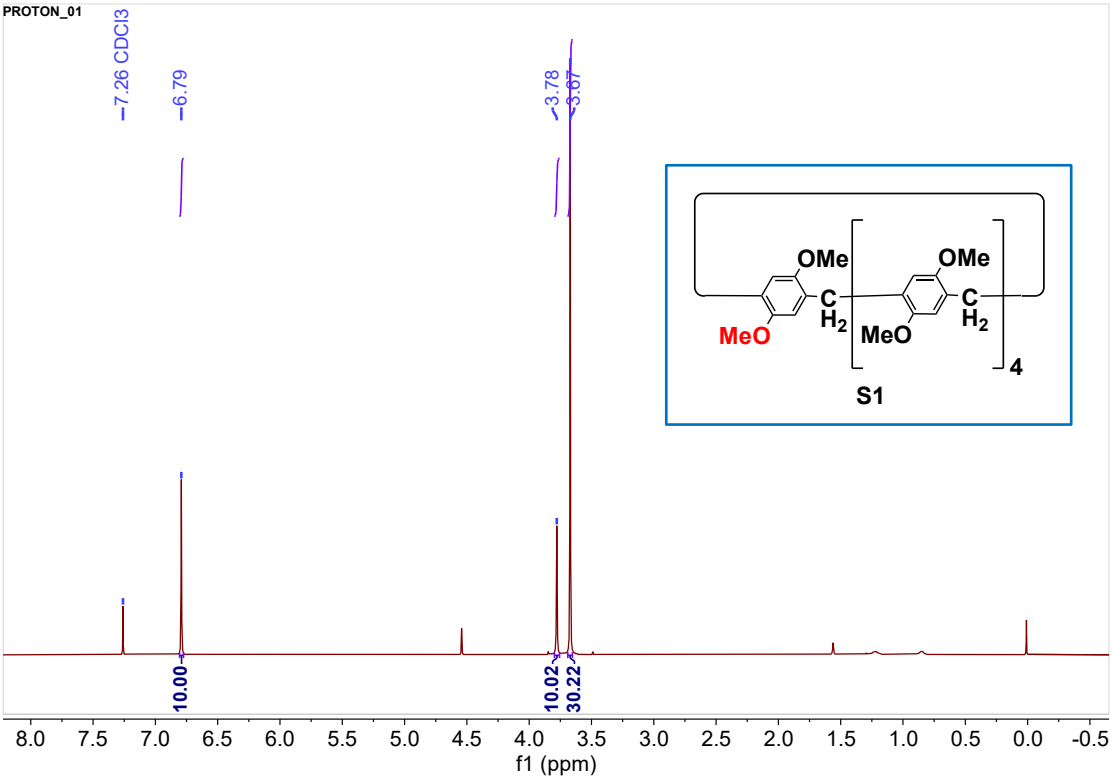

Fig. S1. ^{1}H NMR spectrum (400 MHz, $CDCl_3$, 293 K) of **S1**.

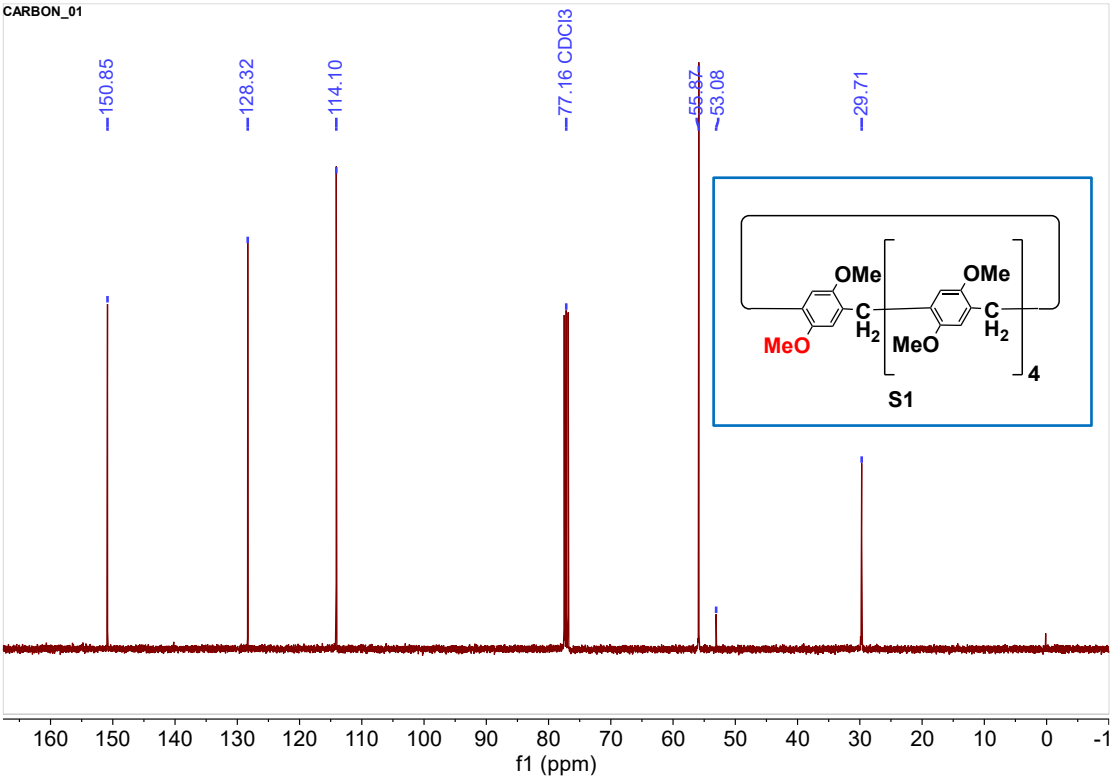

Fig. S2. ^{13}C NMR spectrum (100 MHz, $CDCl_3$, 293 K) of **S1**.

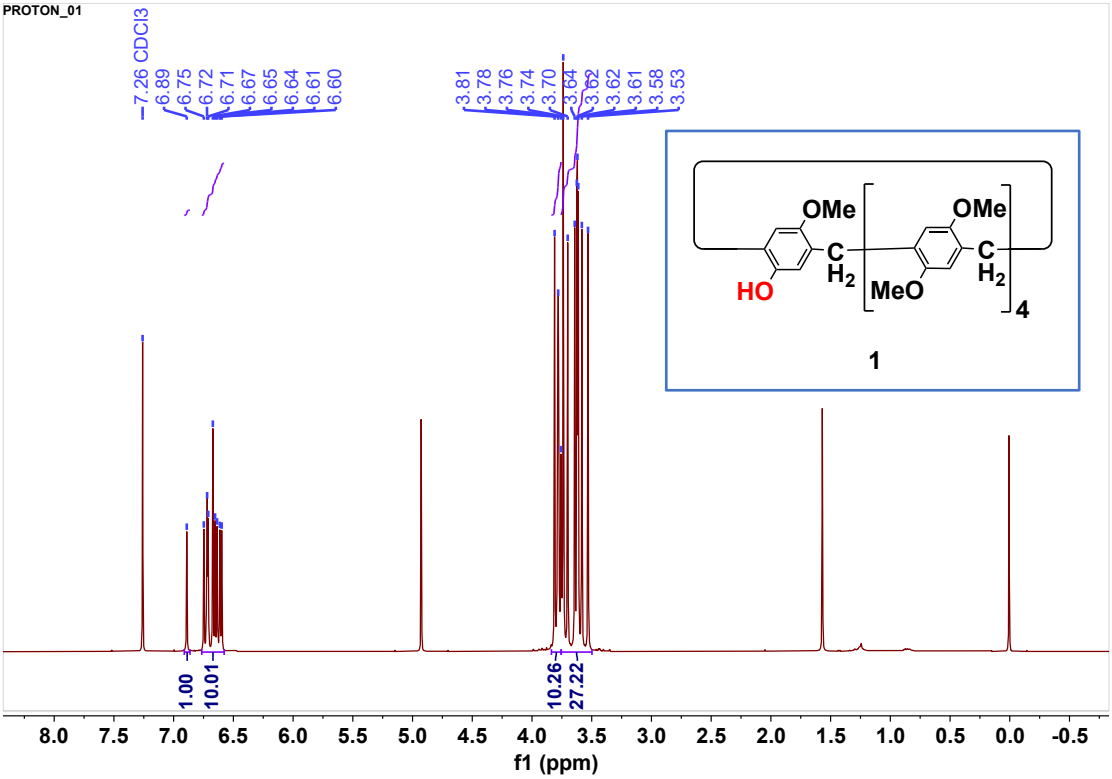

Fig. S3. ^{1}H NMR spectrum (400 MHz, $CDCl_3$, 293 K) of **1**.

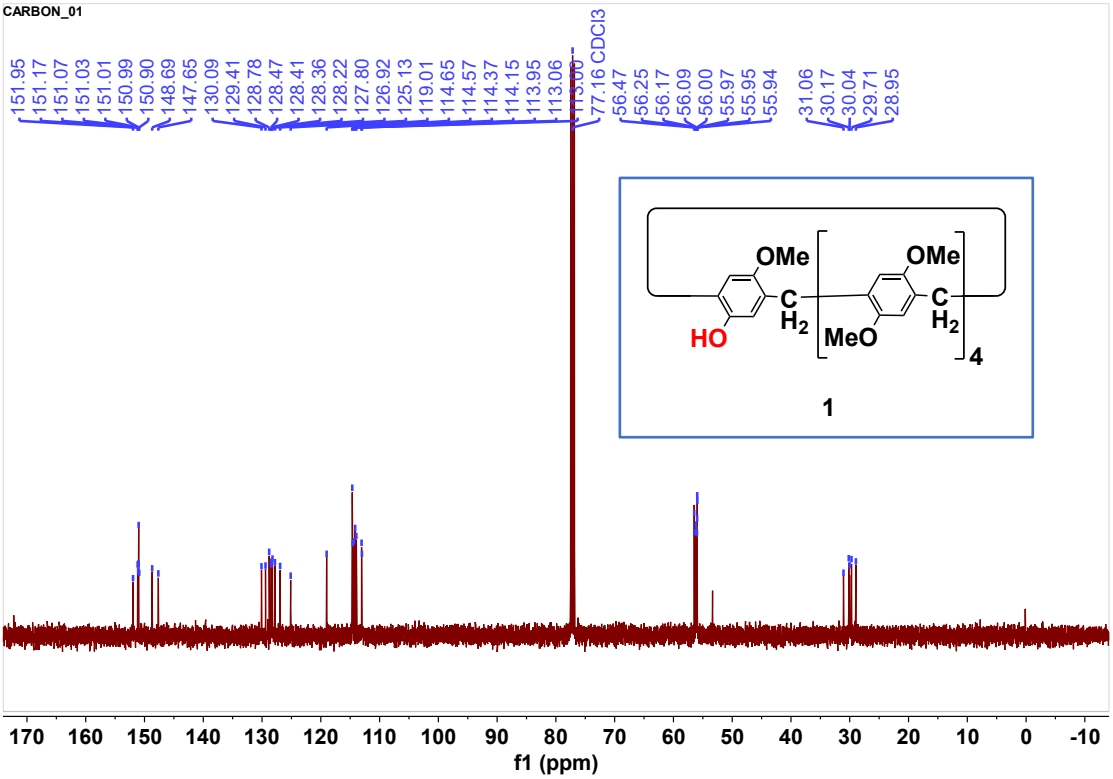

Fig. S4. ^{13}C NMR spectrum (100 MHz, $CDCl_3$, 293 K) of **1**.

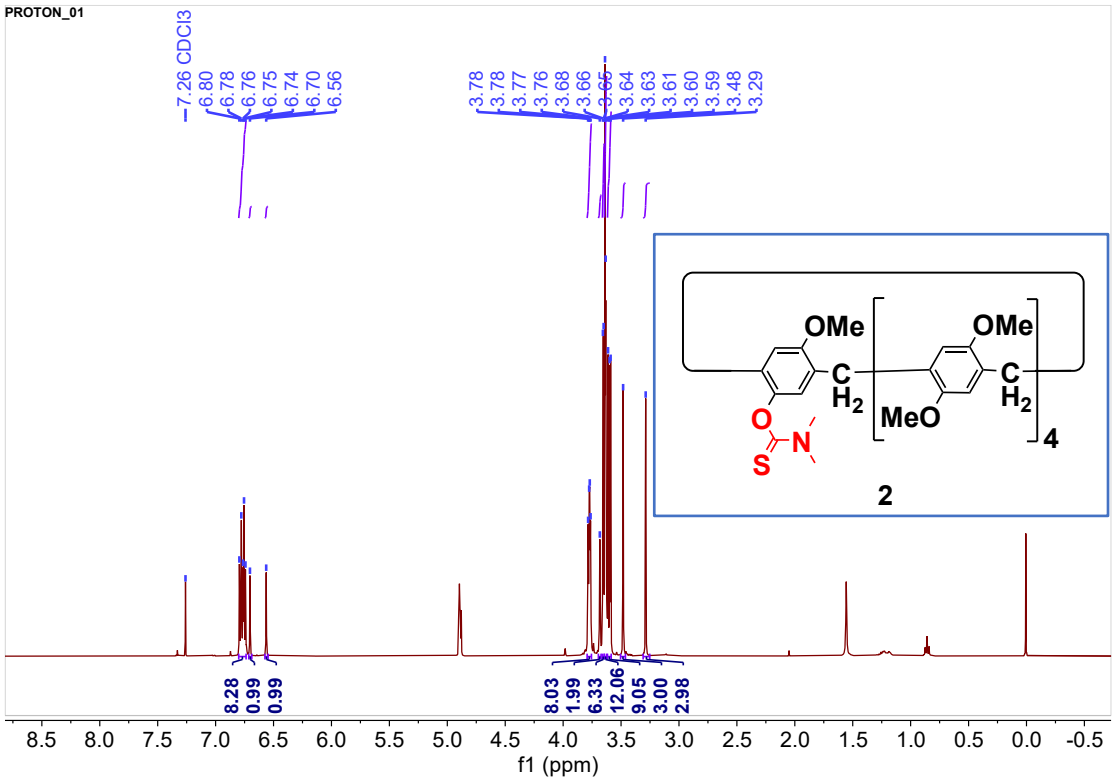

Fig. S5. ^{1}H NMR spectrum (400 MHz, $CDCl_3$, 293 K) of **2**.

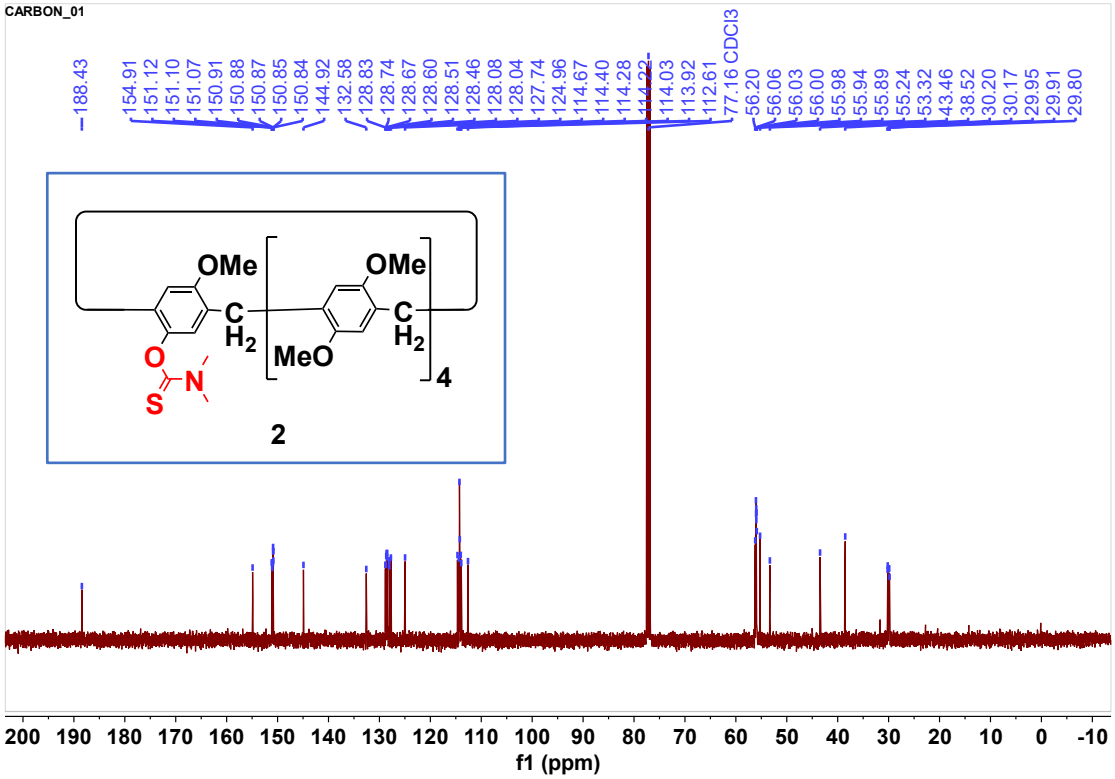

Fig. S6. ^{13}C NMR spectrum (100 MHz, $CDCl_3$, 293 K) of **2**.

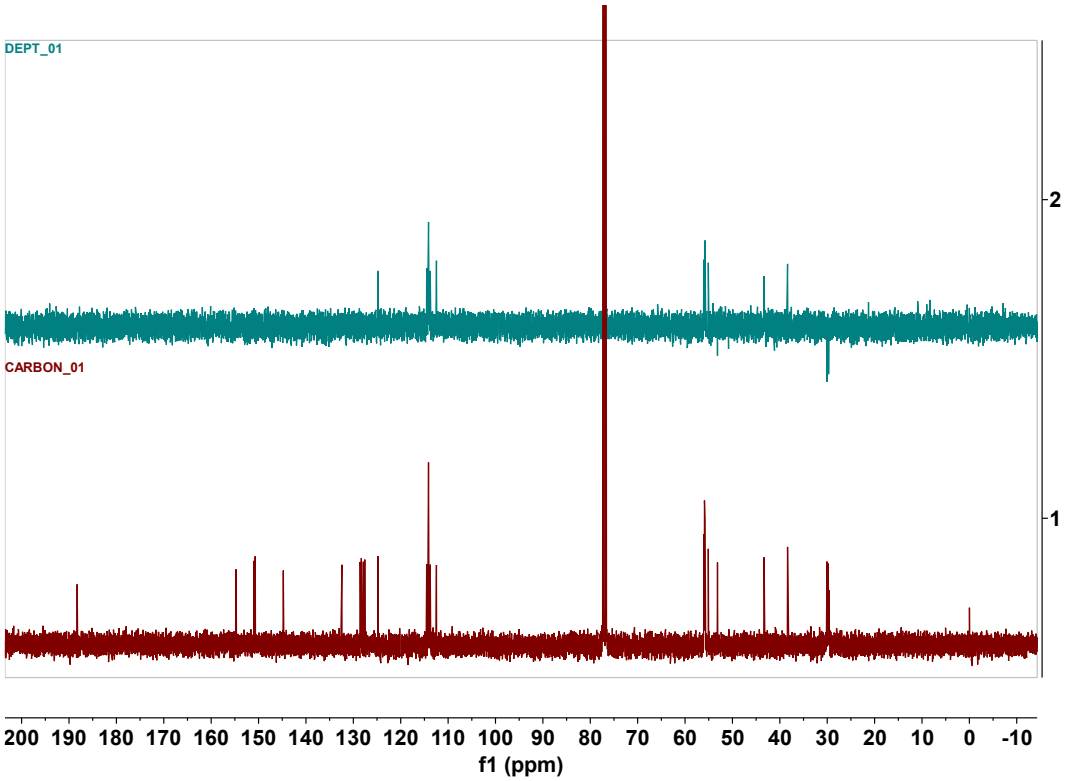

Fig. S7. DEPT (θ = 135 °) spectrum (100 MHz, $CDCl_3$, 293 K) of **2**.

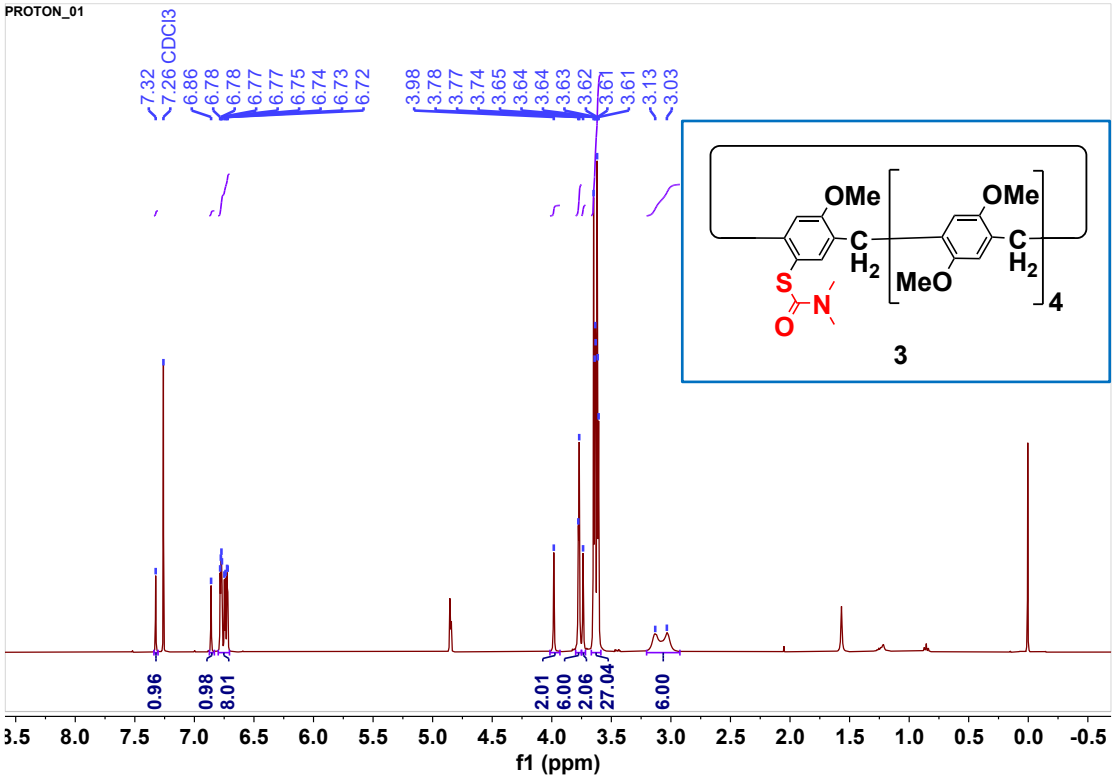

Fig. S8. ^{1}H NMR spectrum (400 MHz, $CDCl_3$, 293 K) of **3**.

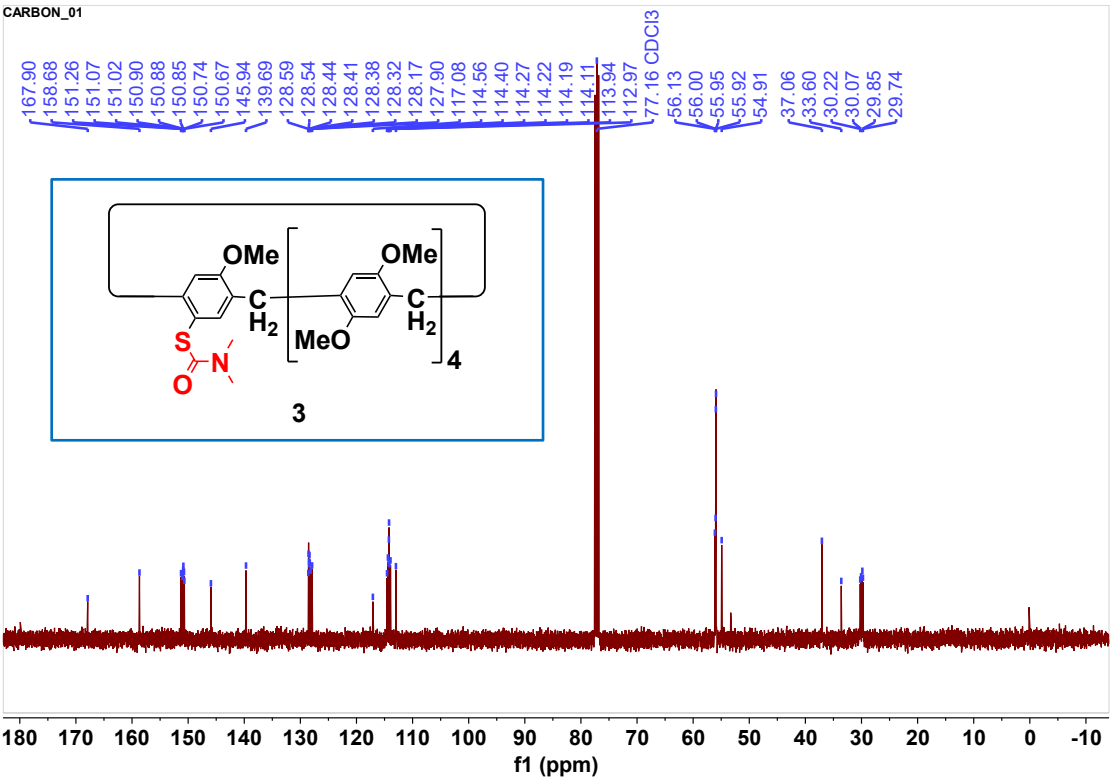

Fig. S9. ^{13}C NMR spectrum (100 MHz, $CDCl_3$, 293 K) of **3**.

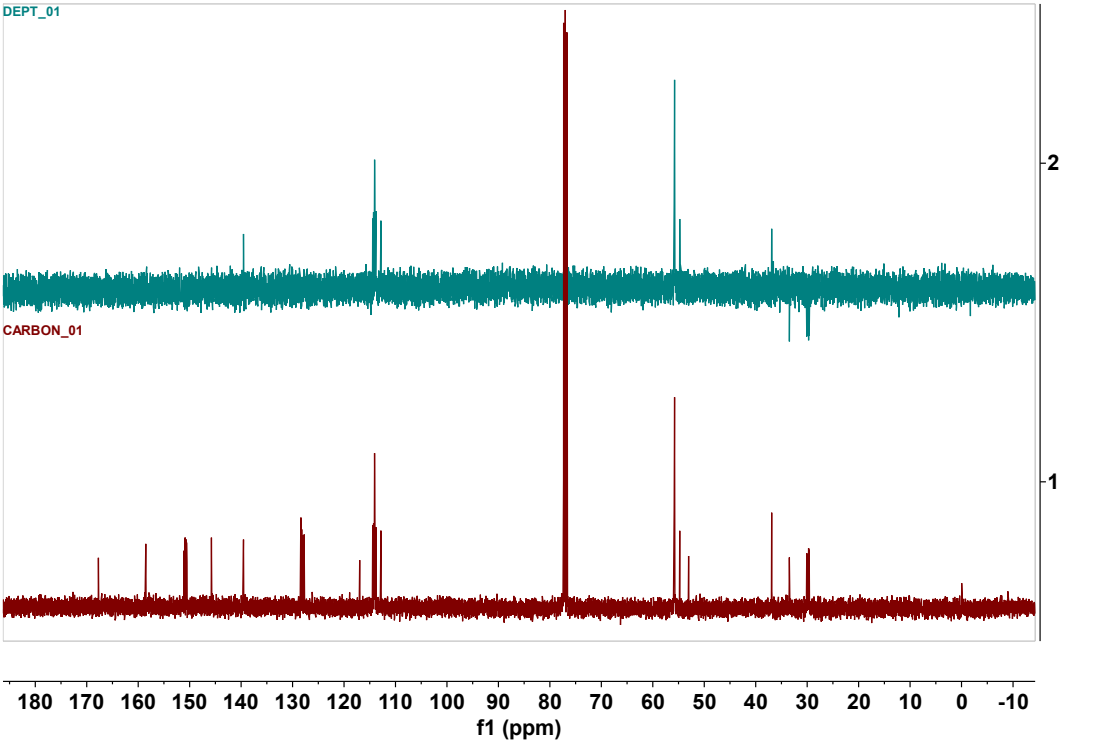

Fig. S10. DEPT (θ = 135 °) spectrum (100 MHz, $CDCl_3$, 293 K) of **3**.

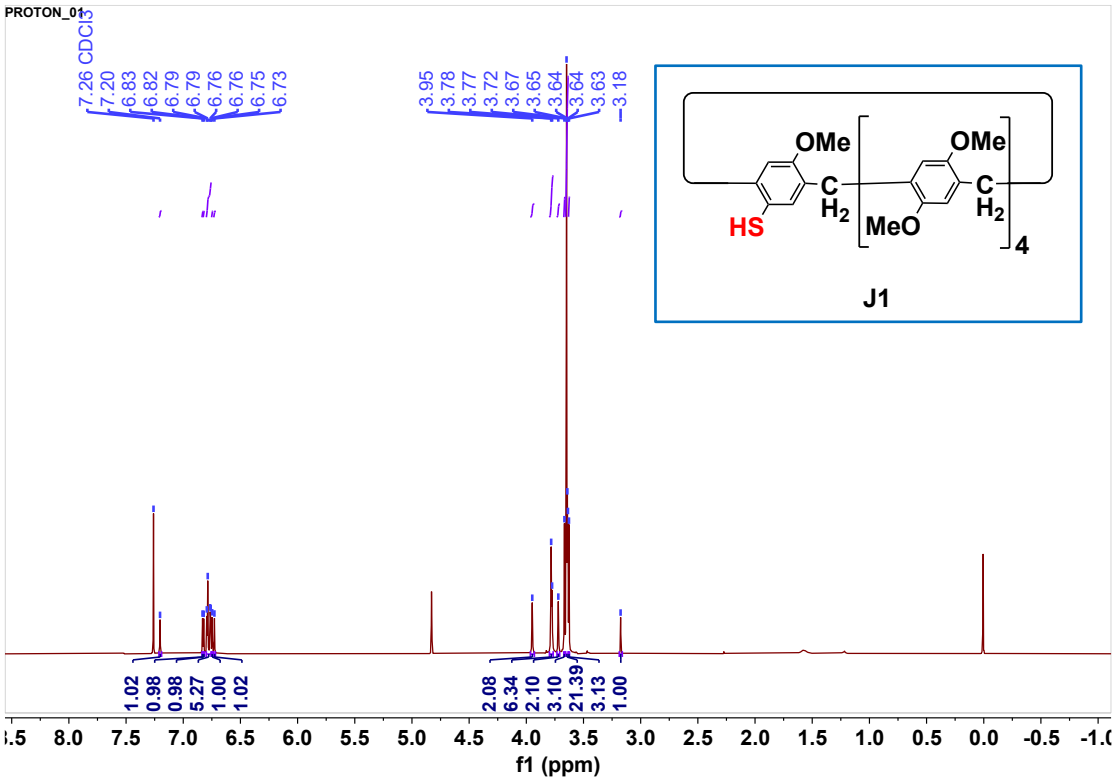

Fig. S11. ^{1}H NMR spectrum (400 MHz, $CDCl_3$, 293 K) of **J1**.

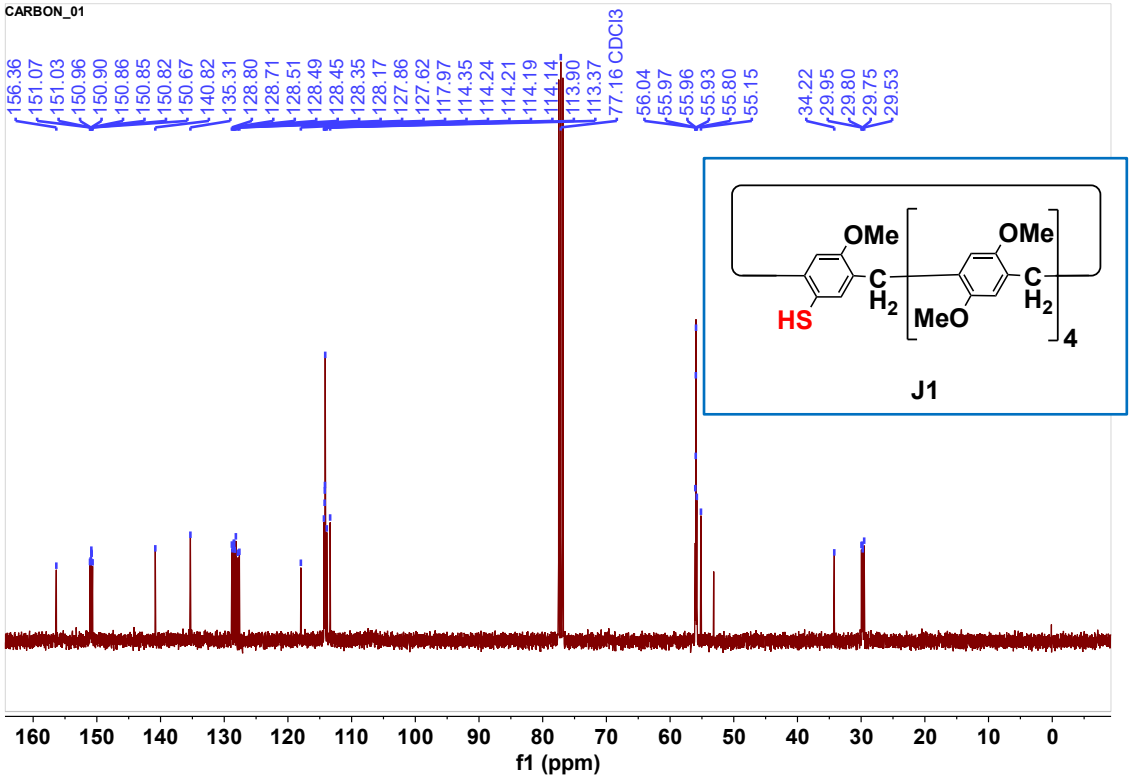

Fig. S12. ^{13}C NMR spectrum (100 MHz, $CDCl_3$, 293 K) of **J1**.

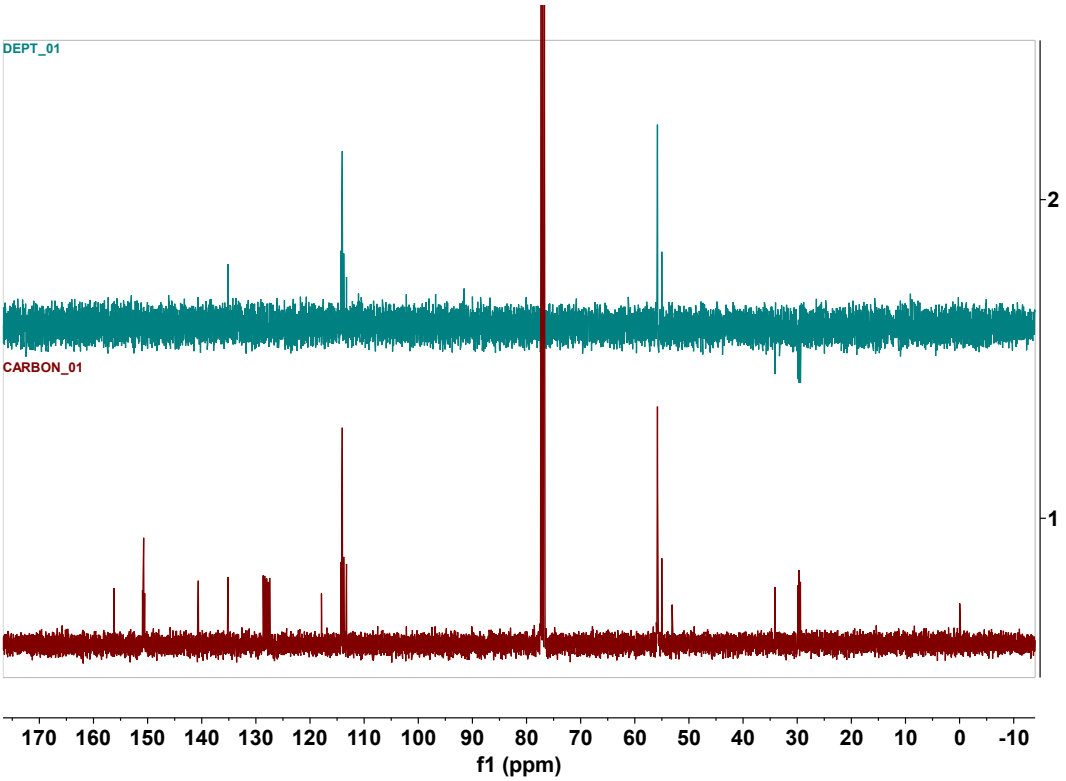

Fig. S13. DEPT (θ = 135 °) spectrum (100 MHz, $CDCl_3$, 293 K) of **J1**.

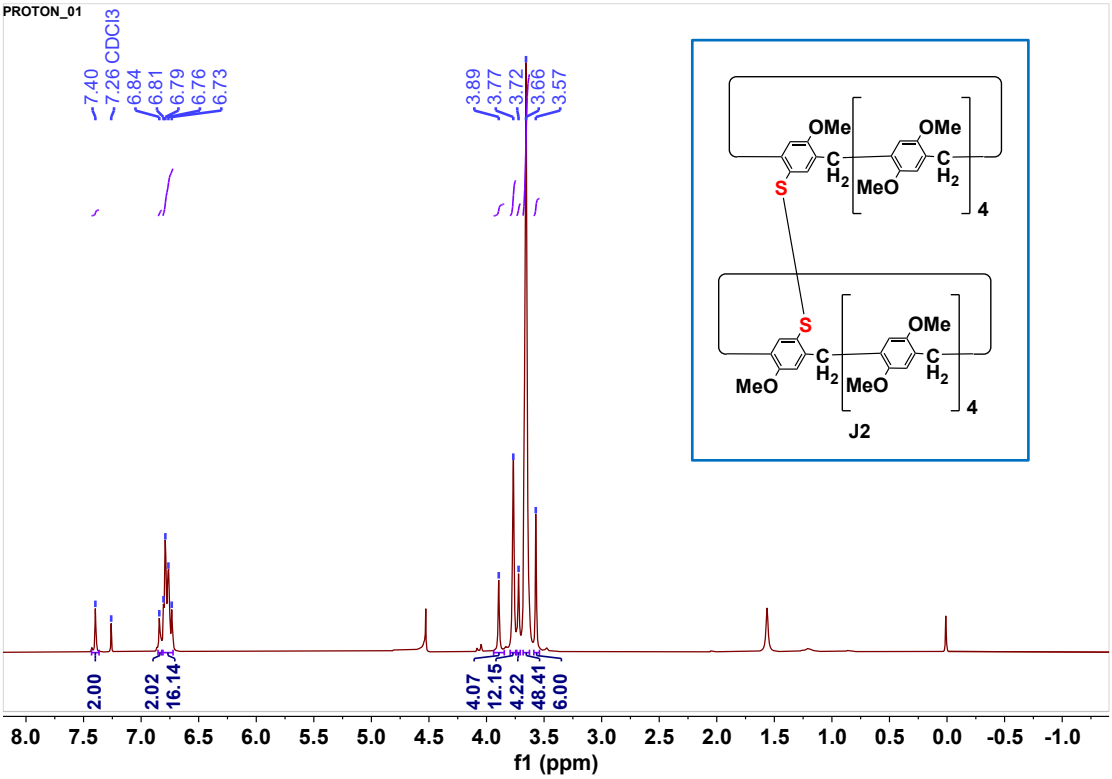

Fig. S14. ^{1}H NMR spectrum (400 MHz, $CDCl_3$, 293 K) of **J2**.

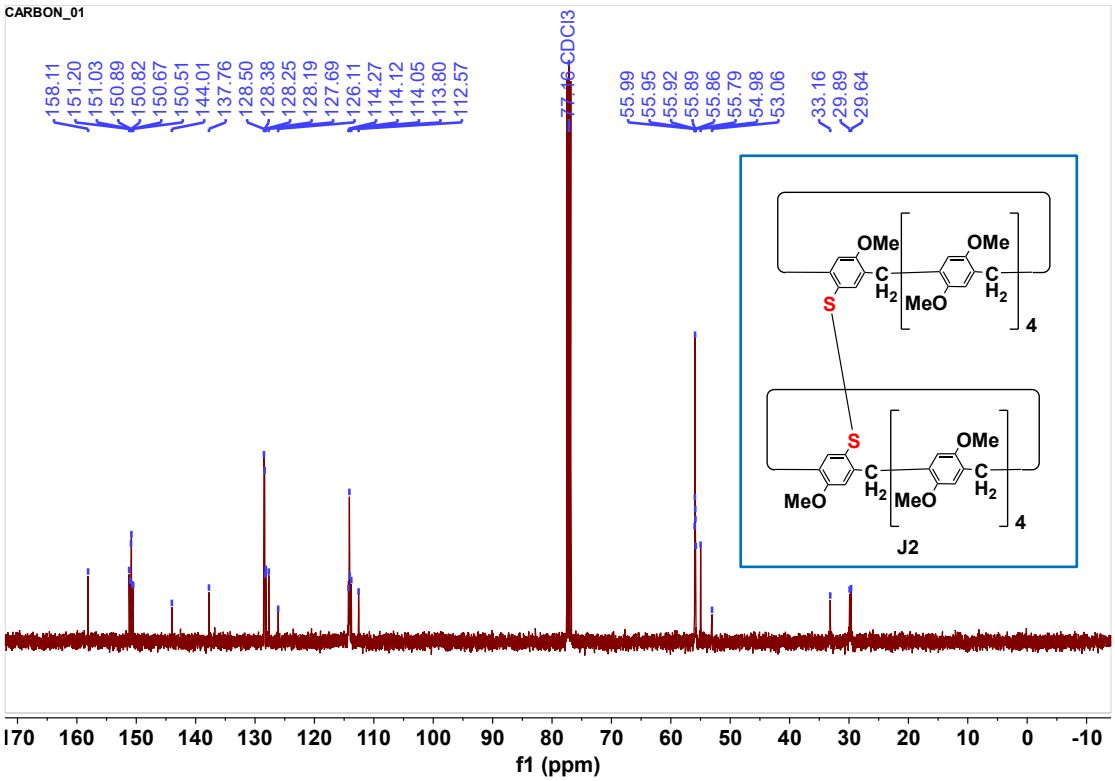

Fig. S15. ^{13}C NMR spectrum (100 MHz, $CDCl_3$, 293 K) of **J2**.

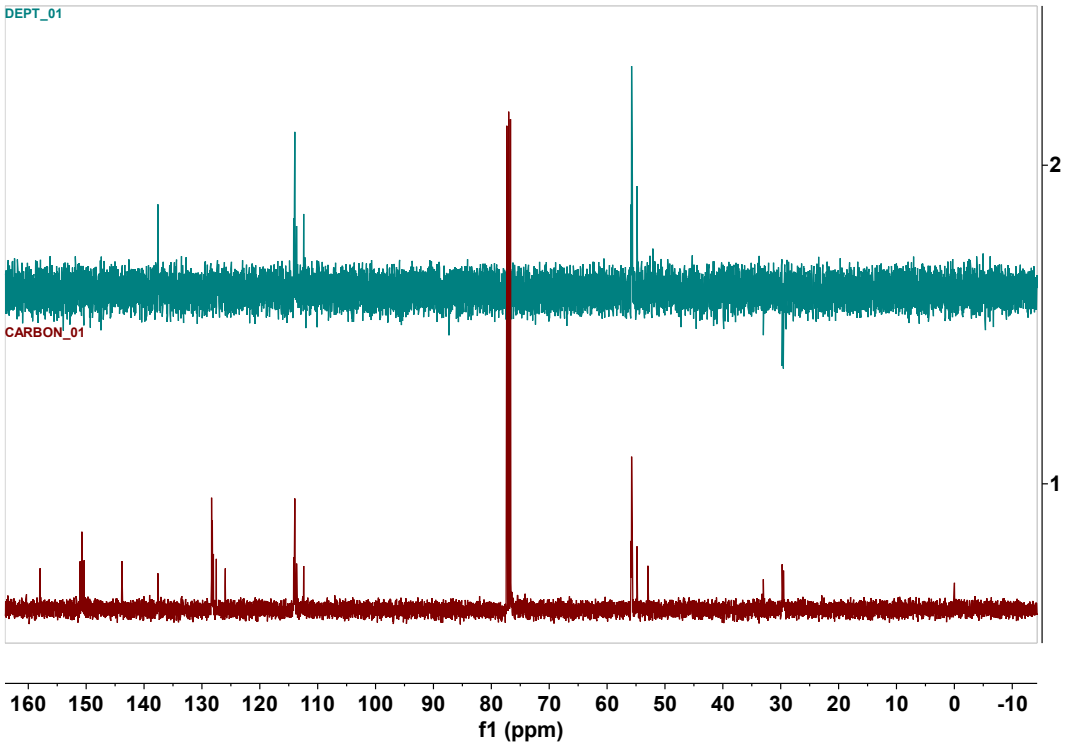

Fig. S16. DEPT (θ = 135 °) spectrum (100 MHz, $CDCl_3$, 293 K) of **J2**.

2D NMR Spectra

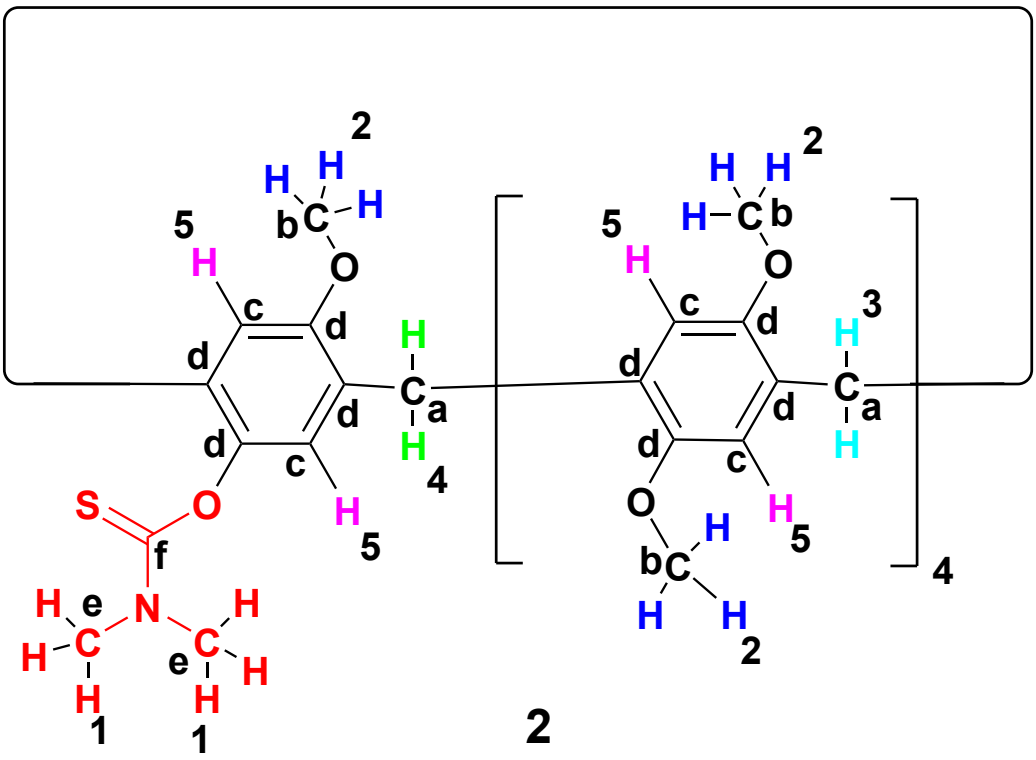

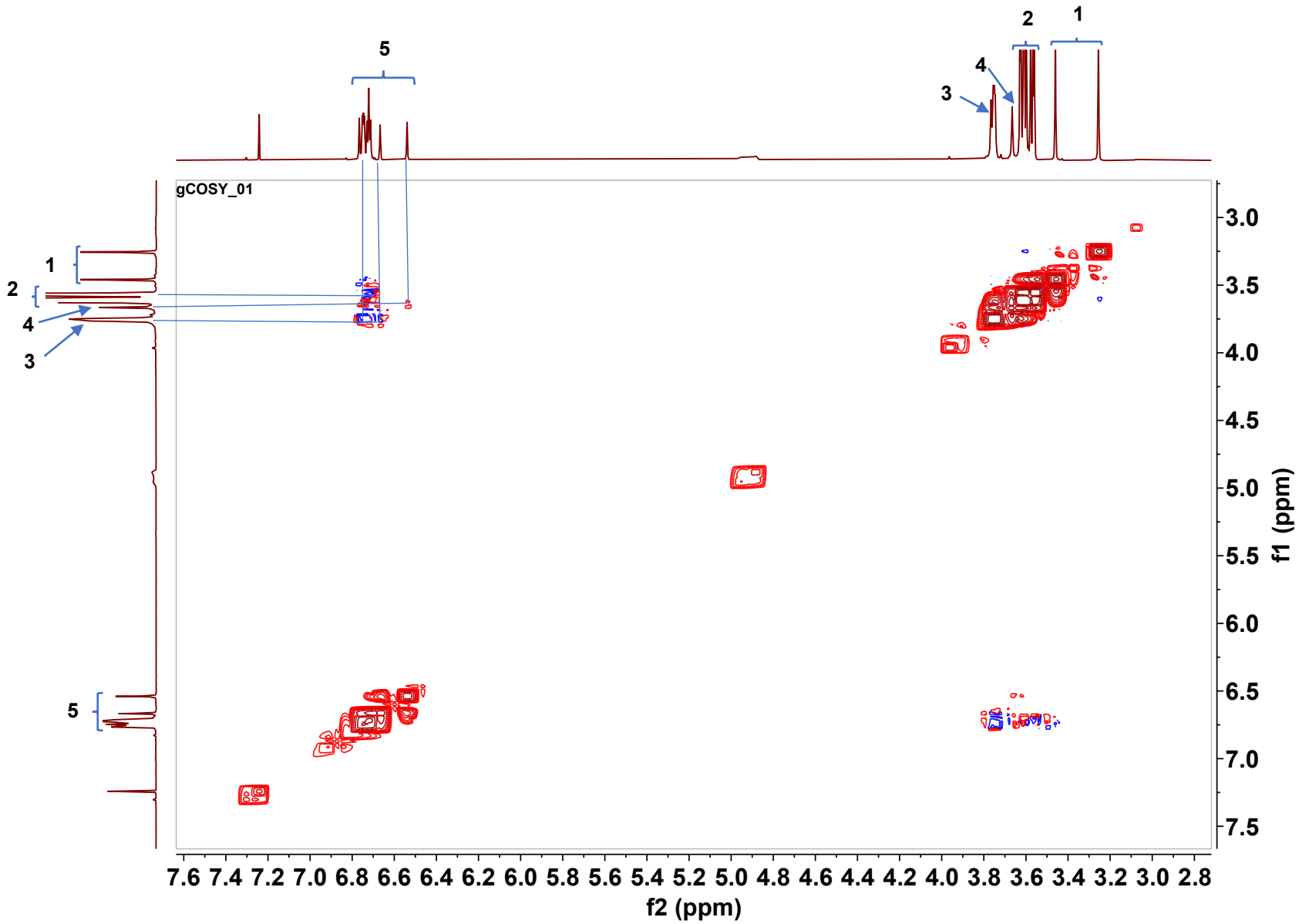

Fig. S17. Partial ^{1}H-^{1}H COSY spectra of **2** (^{1}H NMR (400 MHz, 293 K, $CDCl_3$)).

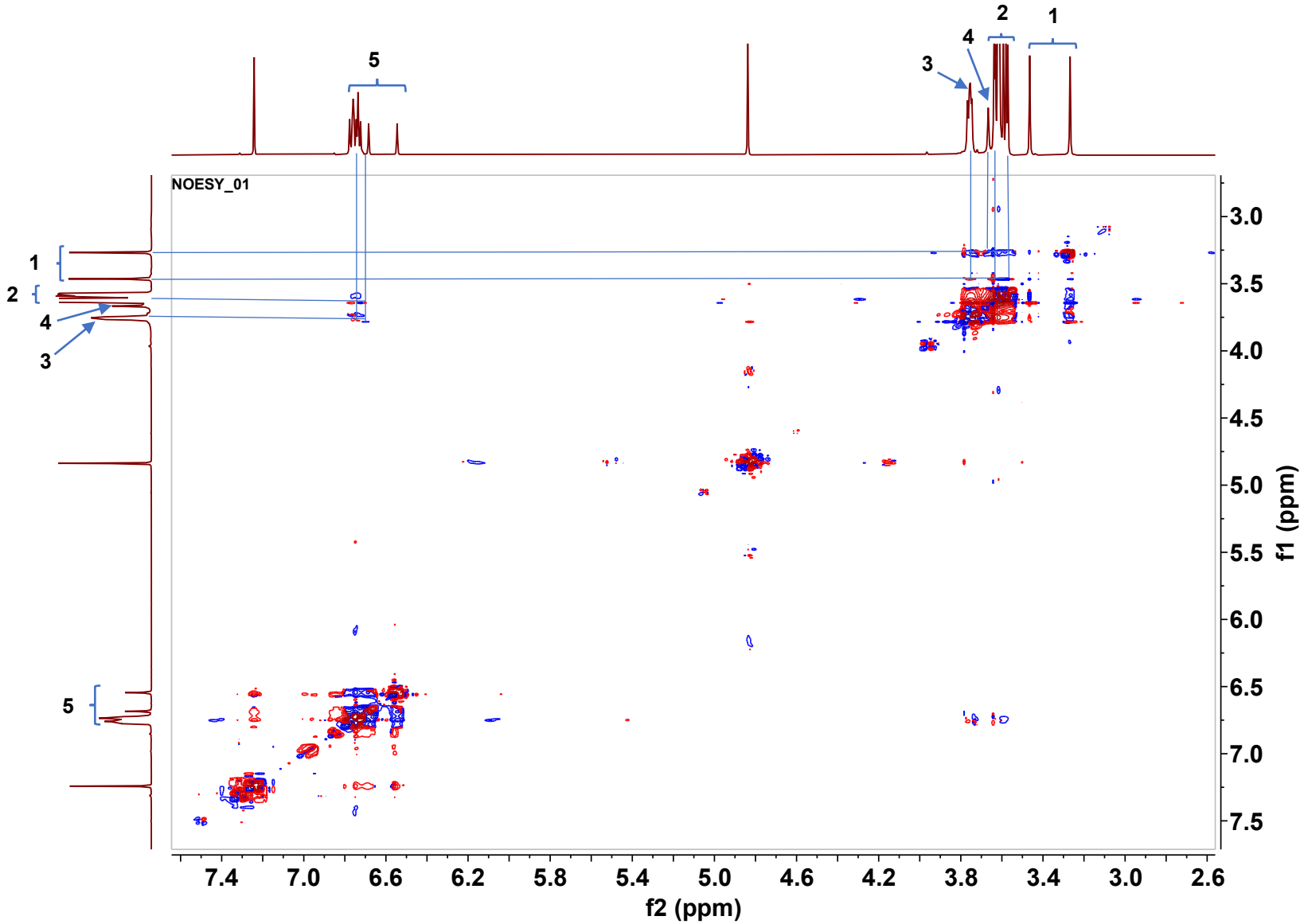

Fig. S18. Partial ^{1}H-^{1}H NOESY spectra of **2** (^{1}H NMR (400 MHz, 293 K, $CDCl_3$)).

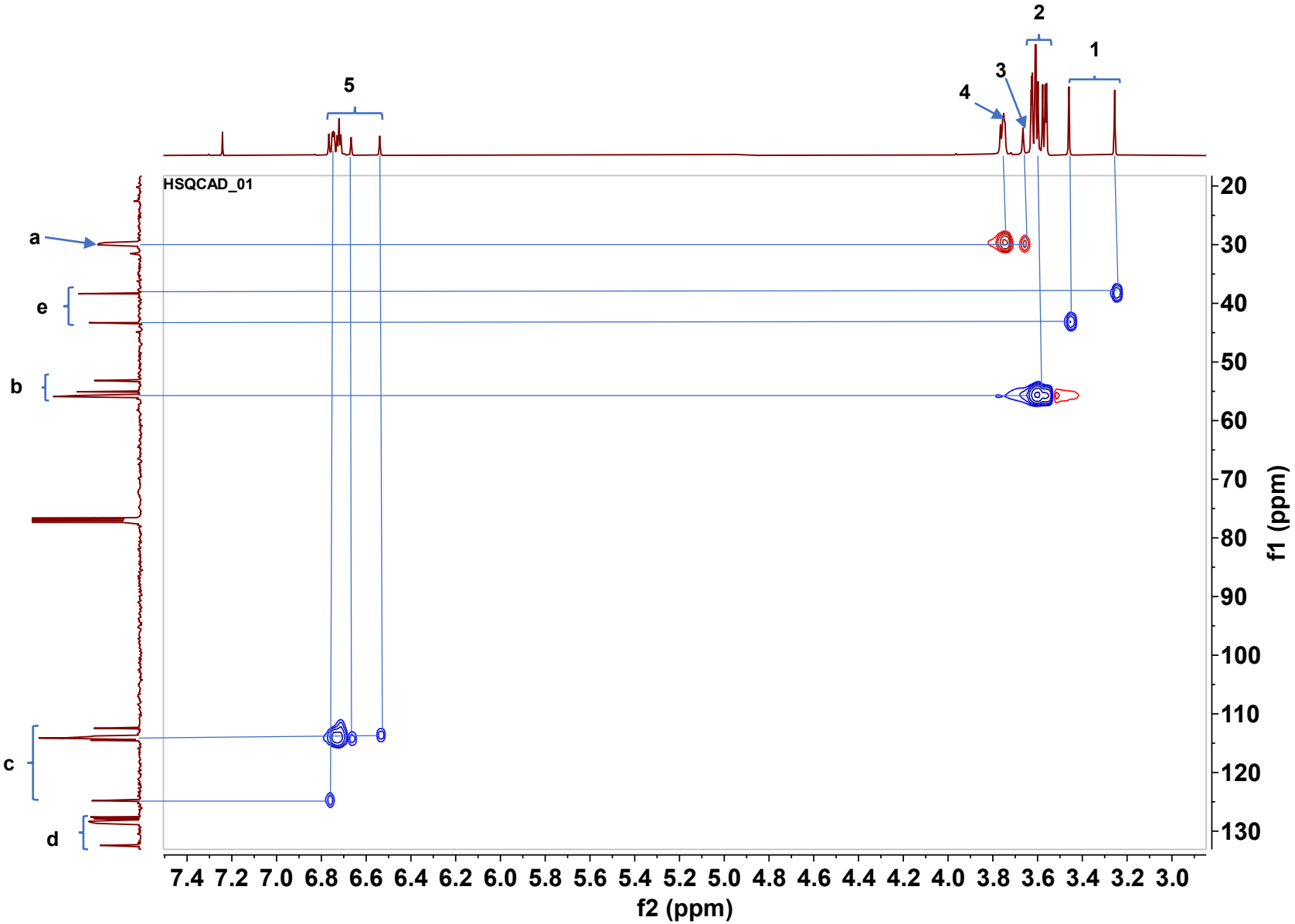

Fig. S19. Partial ^{1}H-^{13}C HSQC spectra of **2** (^{1}H NMR (400 MHz, 293 K, $CDCl_3$); ^{13}C NMR (100 MHz, 293 K, $CDCl_3$)).

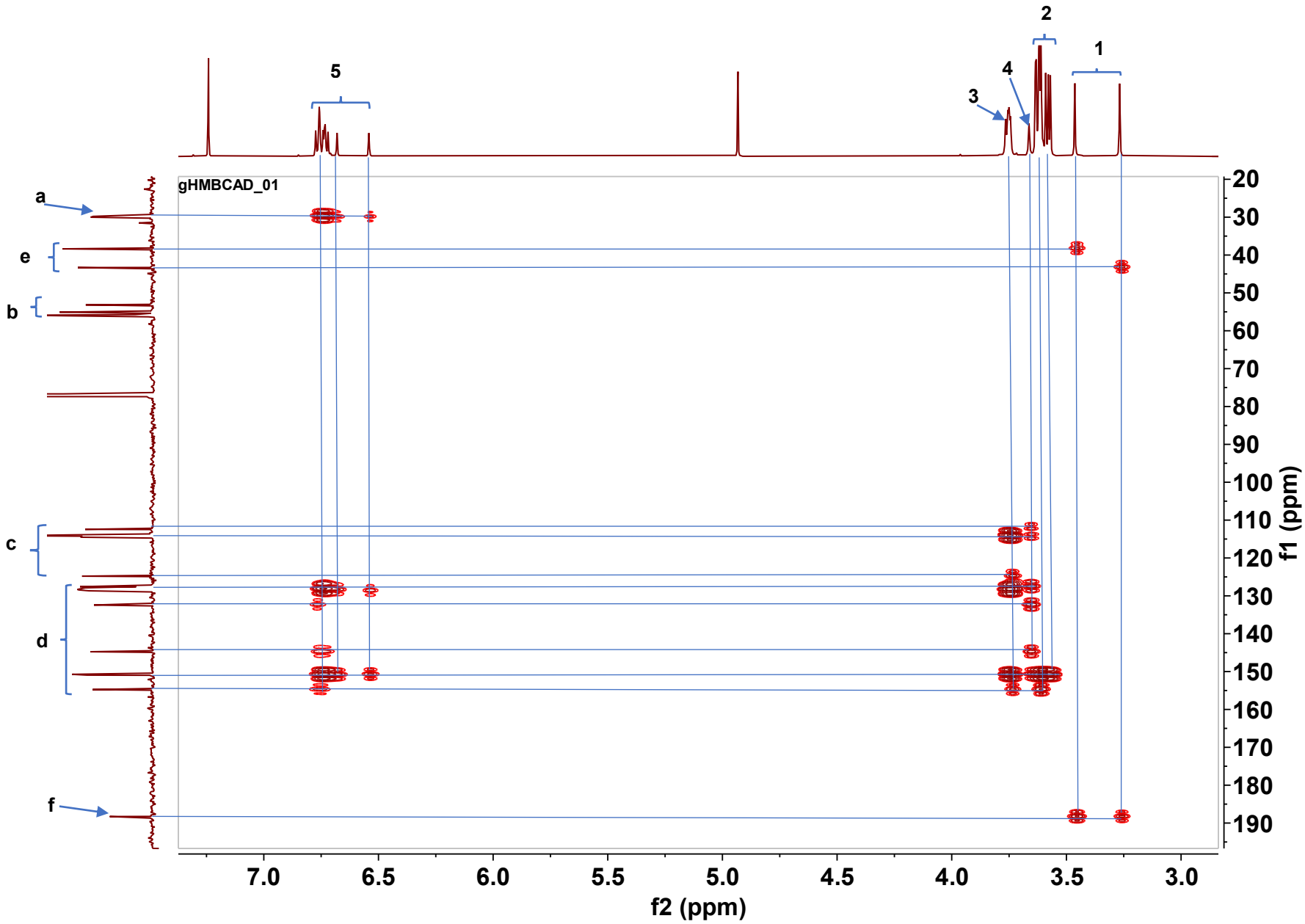

Fig. S20. Partial ^{1}H-^{13}C HMBC spectra of **2** (^{1}H NMR (400 MHz, 293 K, $CDCl_3$); ^{13}C NMR (100 MHz, 293 K, $CDCl_3$)).

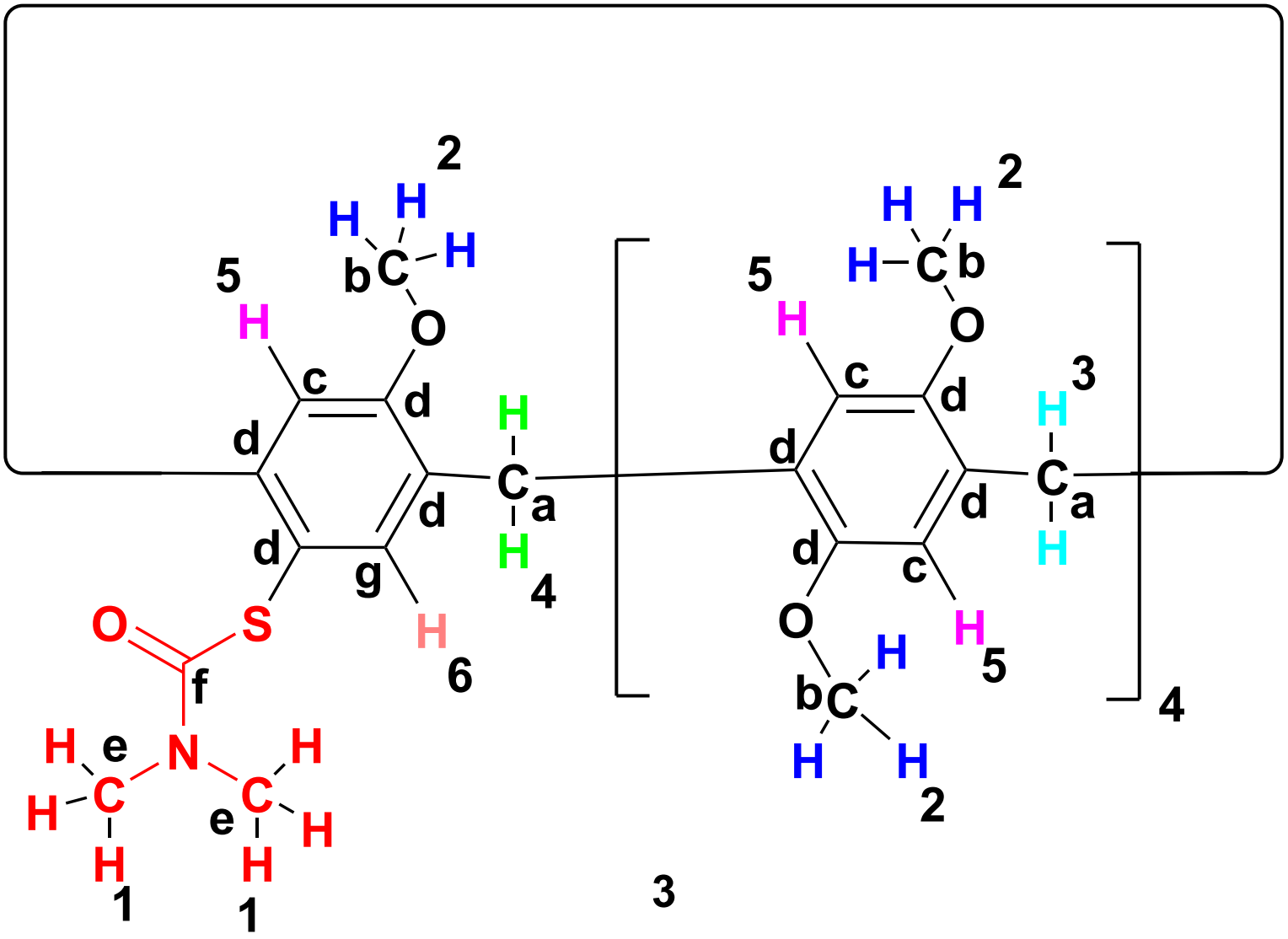
O
S
f
N
e
e
H
C
H
H
1
1
H
C
H
H
2
O
5
H
c
d
d
d
d
g
H
6
H
C
a
H
4
H
C
H
H
2
O
5
H
c
d
d
d
d
c
H
5
H
C
a
H
3
4
O
H
C
H
H
2
3

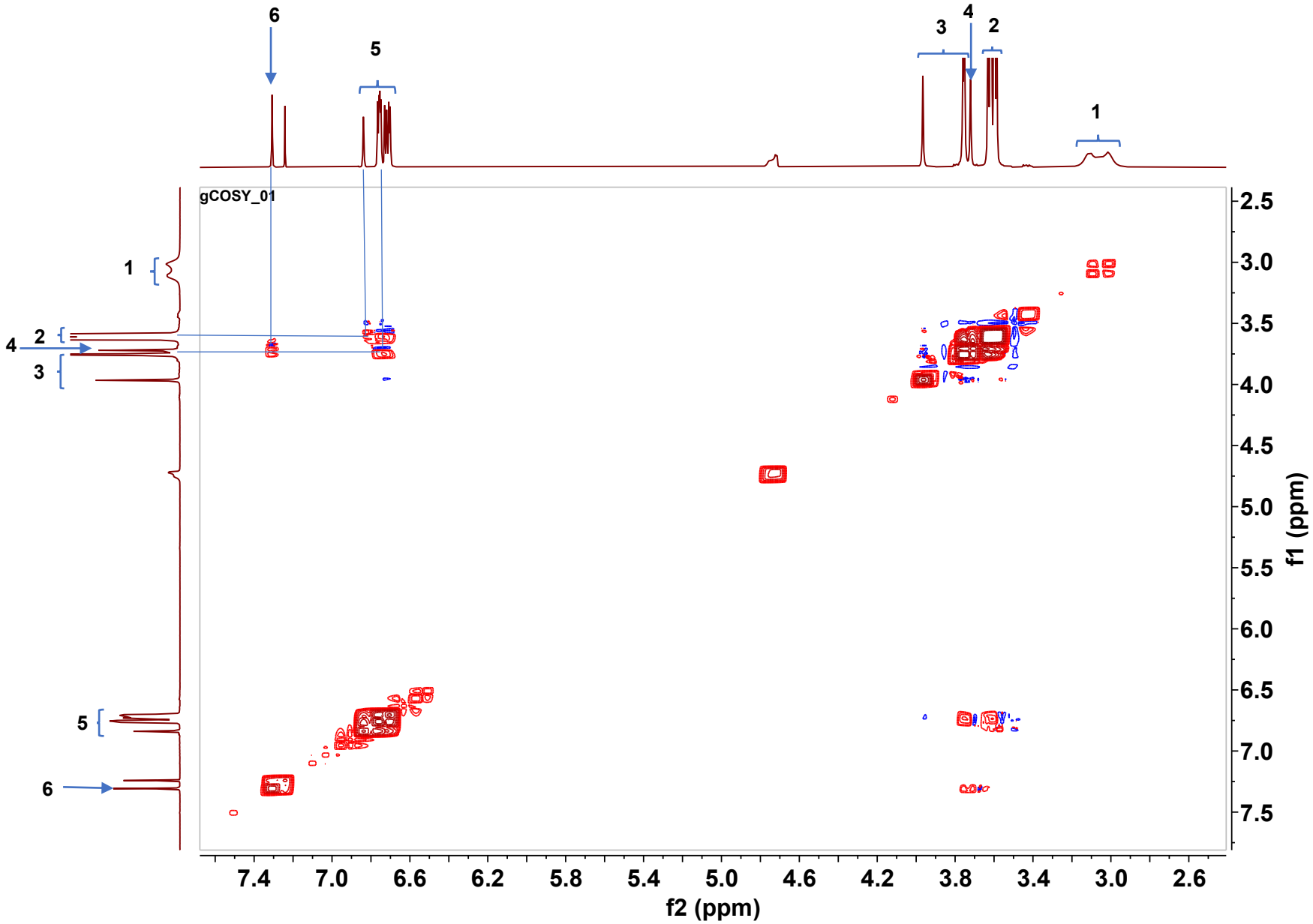

Fig. S21. Partial ^{1}H-^{1}H COSY spectra of **3** (^{1}H NMR (400 MHz, 293 K, $CDCl_3$)).

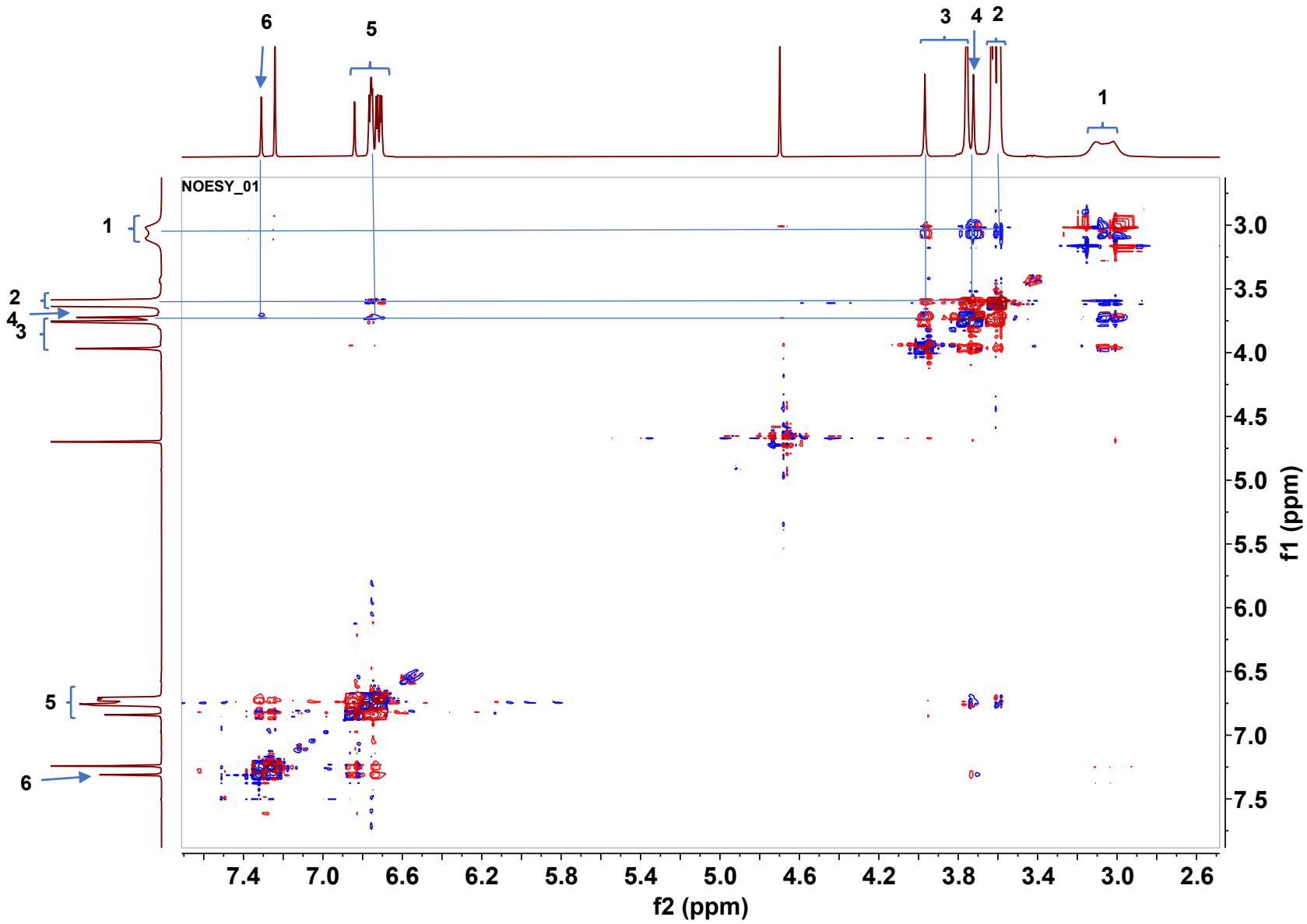

Fig. S22. Partial ^{1}H-^{1}H NOESY spectra of **3** (^{1}H NMR (400 MHz, 293 K, $CDCl_3$)).

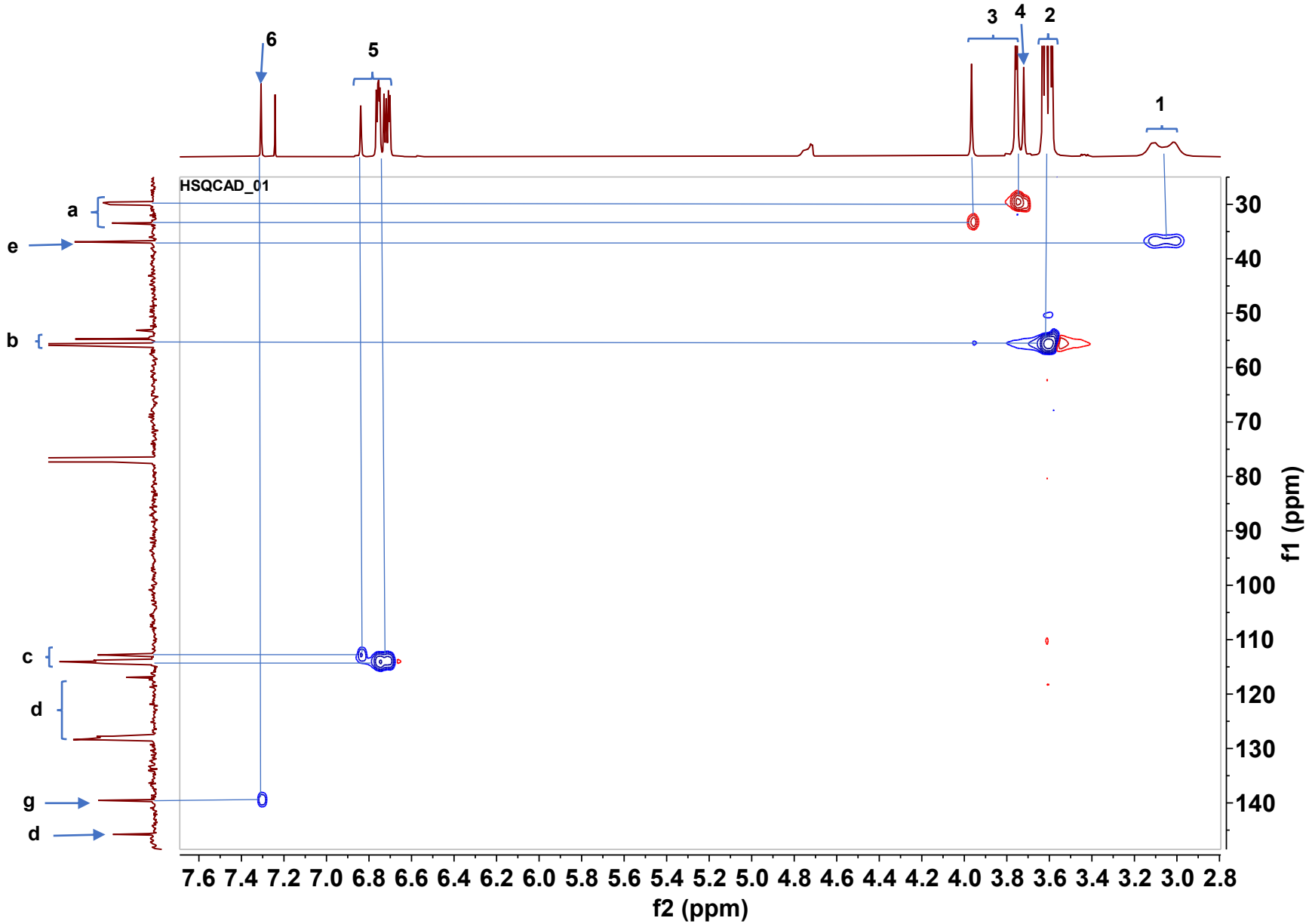

Fig. S23. Partial ^{1}H-^{13}C HSQC spectra of **3** (^{1}H NMR (400 MHz, 293 K, $CDCl_3$); ^{13}C NMR (100 MHz, 293 K, $CDCl_3$)).

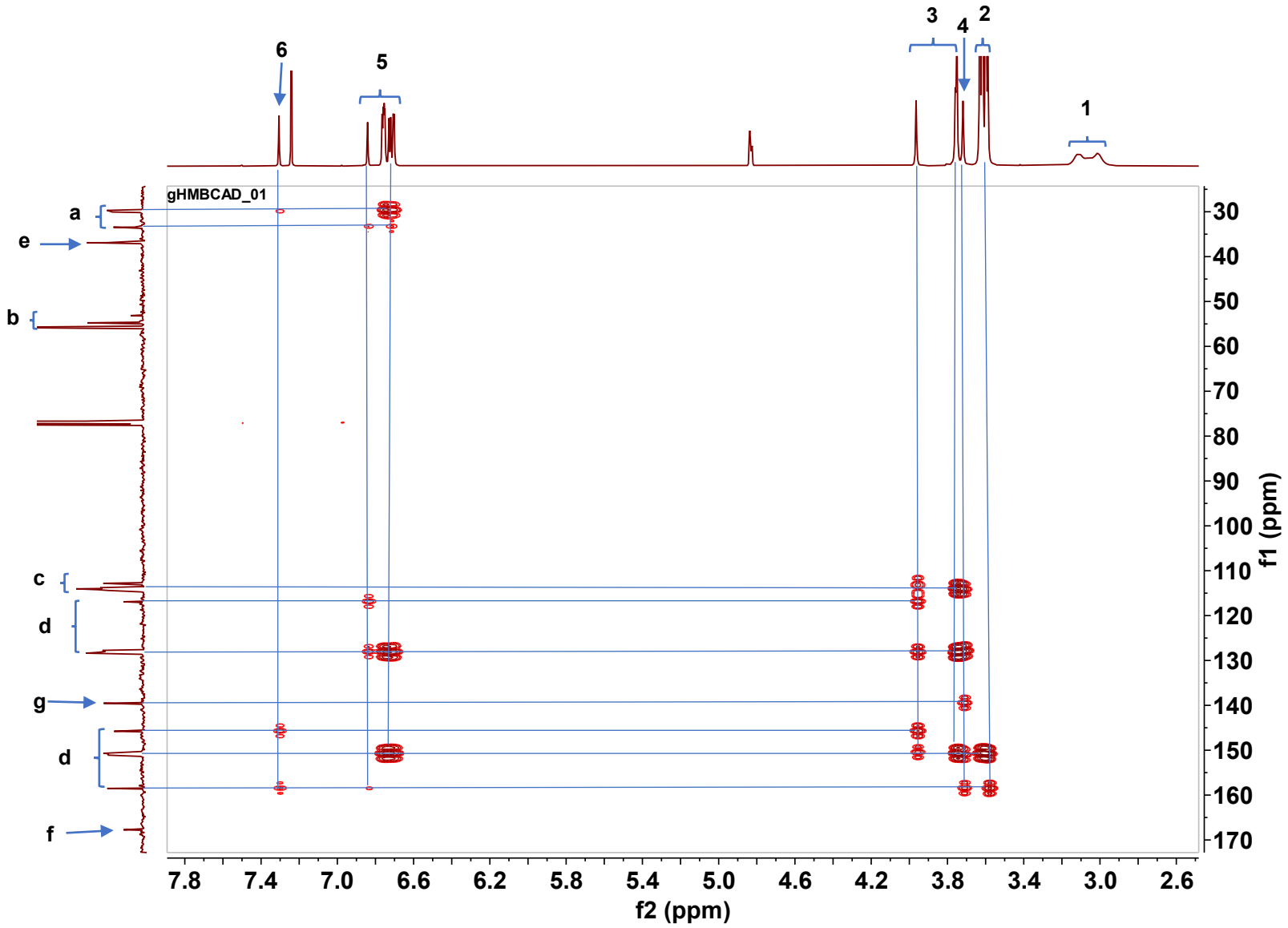

Fig. S24. Partial ^{1}H-^{13}C HMBC spectra of **3** (^{1}H NMR (400 MHz, 293 K, $CDCl_3$); ^{13}C NMR (100 MHz, 293 K, $CDCl_3$)).

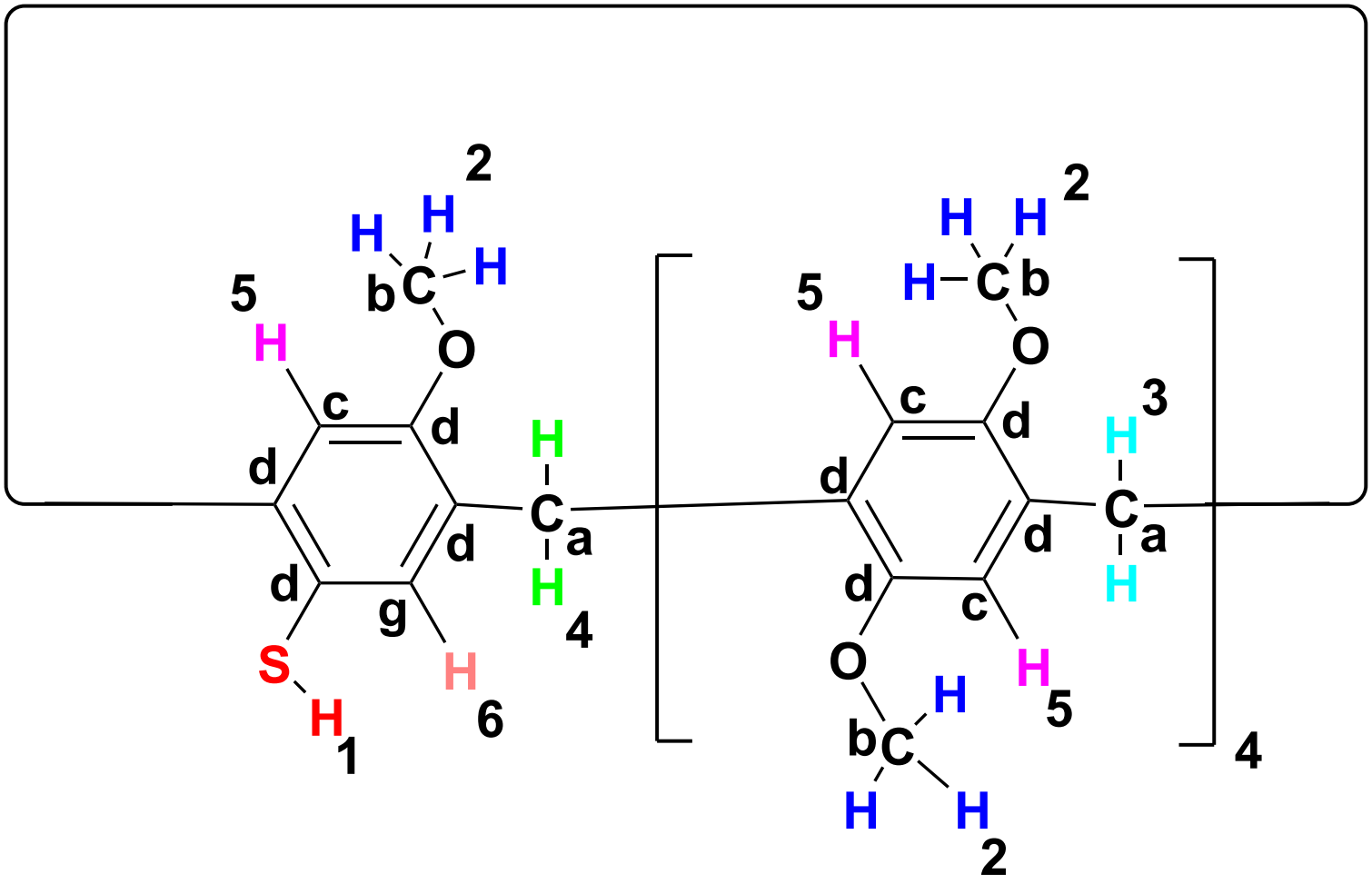
J1

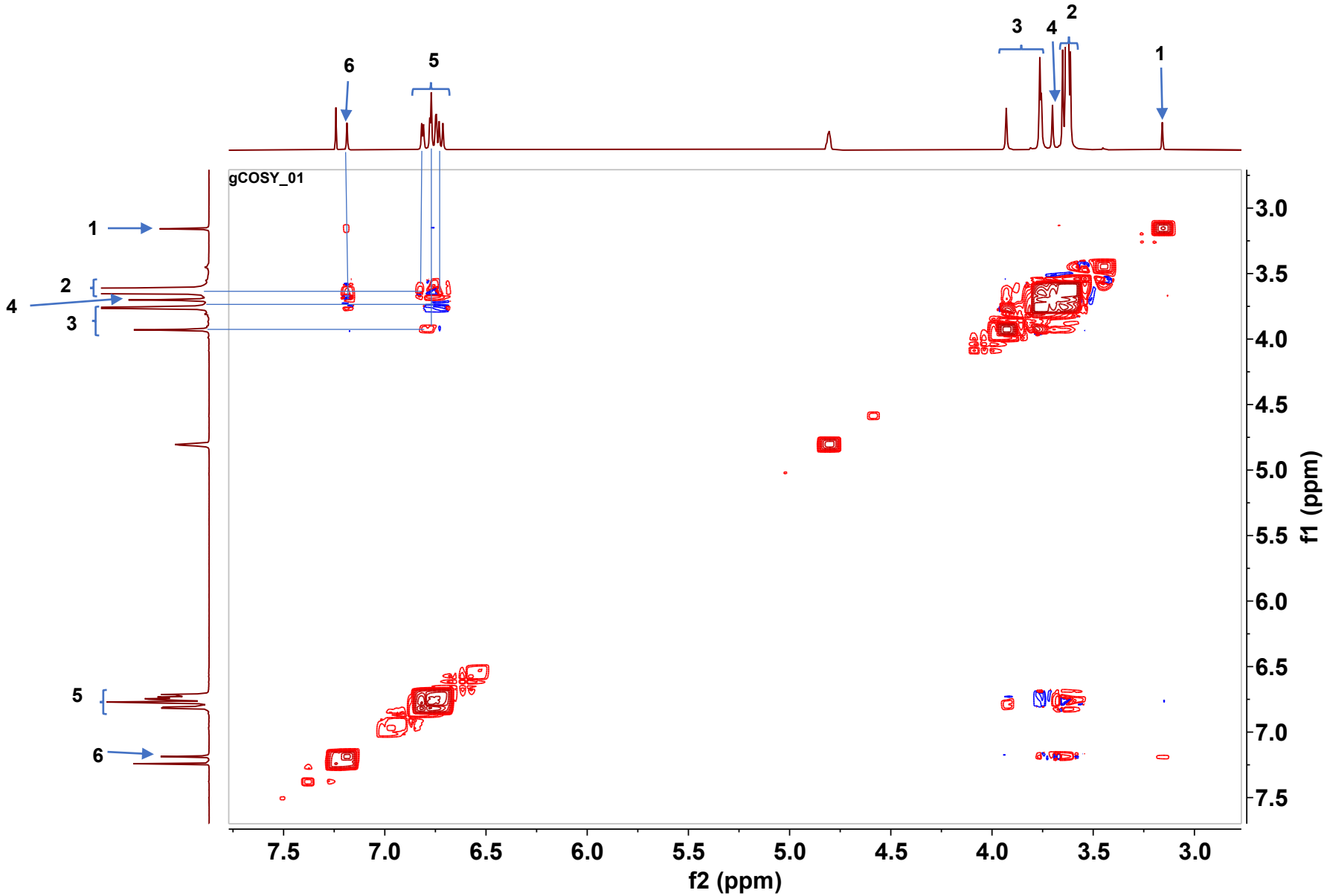

Fig. S25. Partial ^{1}H-^{1}H COSY spectra of **J1** (^{1}H NMR (400 MHz, 293 K, $CDCl_3$)).

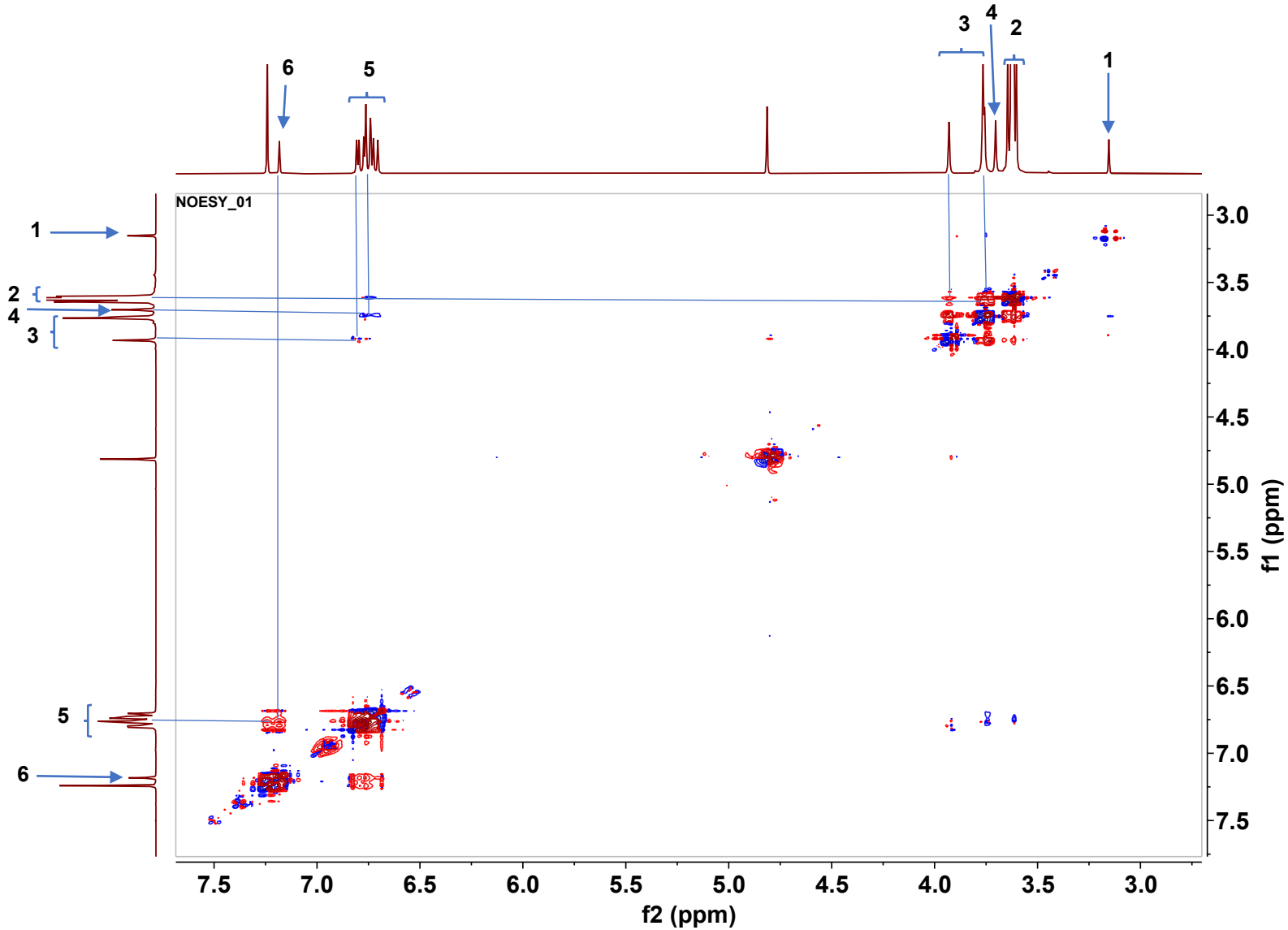

Fig. S26. Partial ^{1}H-^{1}H NOESY spectra of **J1** (^{1}H NMR (400 MHz, 293 K, $CDCl_3$)).

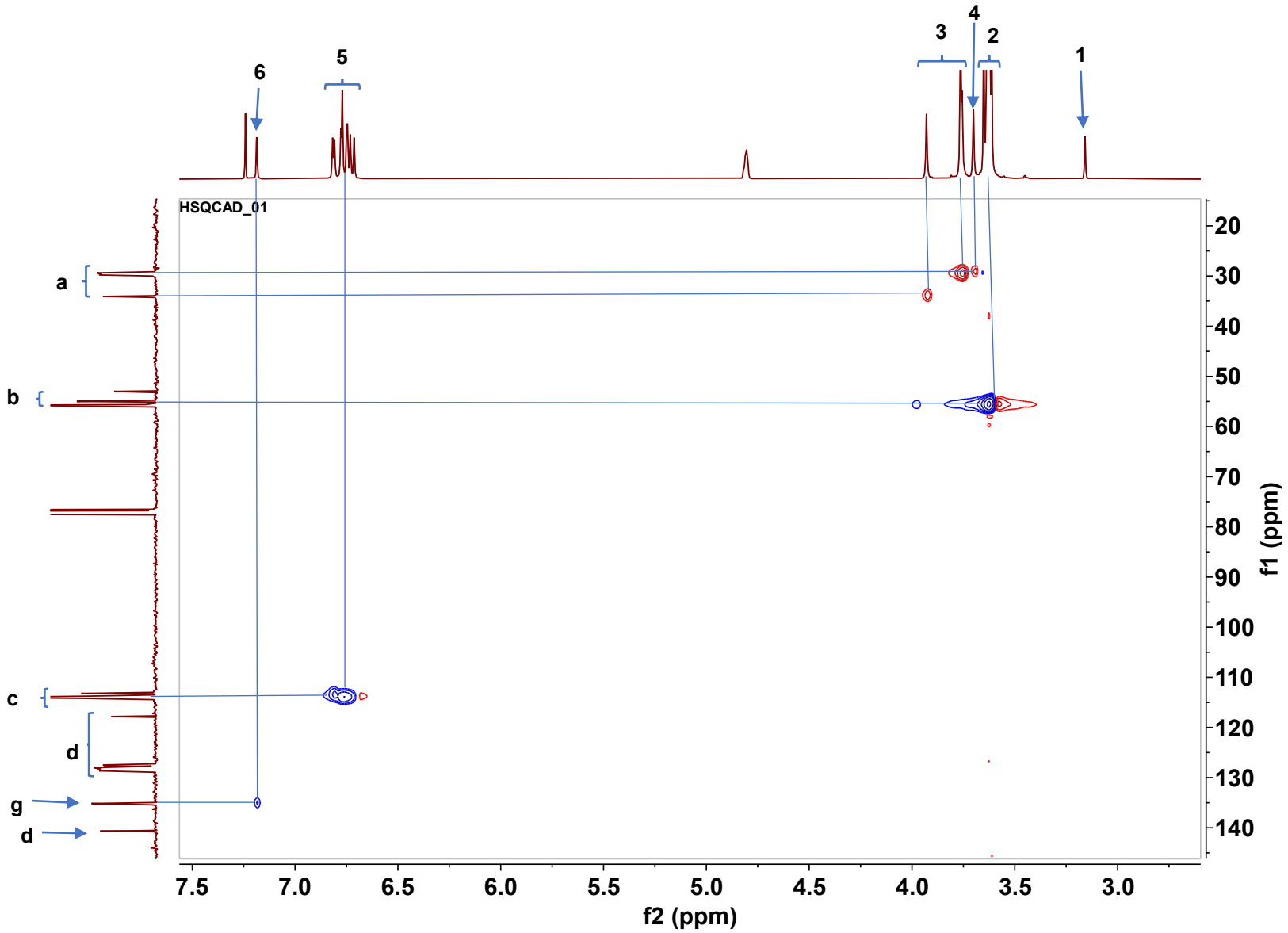

Fig. S27. Partial ^{1}H-^{13}C HSQC spectra of **J1** (^{1}H NMR (400 MHz, 293 K, $CDCl_3$); ^{13}C NMR (100 MHz, 293 K, $CDCl_3$)).

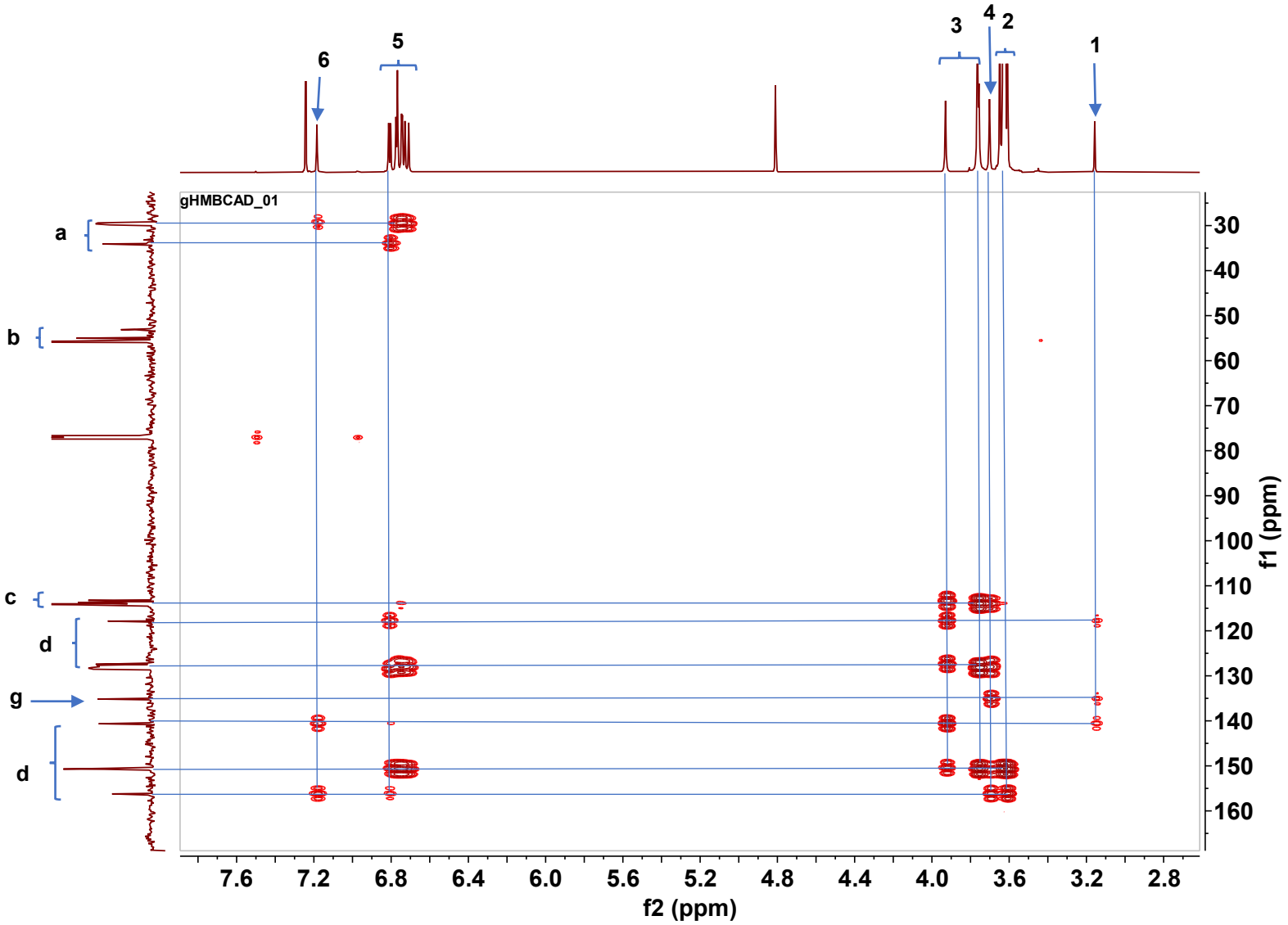

Fig. S28. Partial ^{1}H-^{13}C HMBC spectra of **J1** (^{1}H NMR (400 MHz, 293 K, $CDCl_3$); ^{13}C NMR (100 MHz, 293 K, $CDCl_3$)).

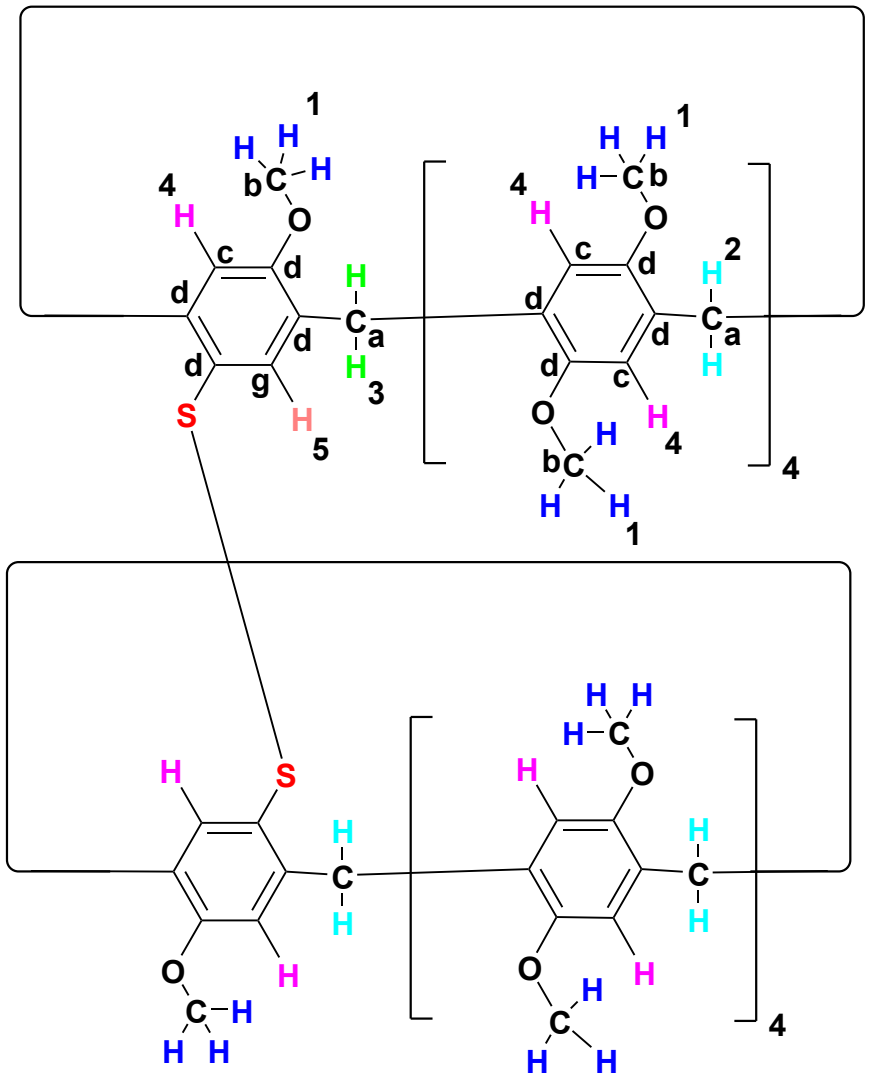

J2

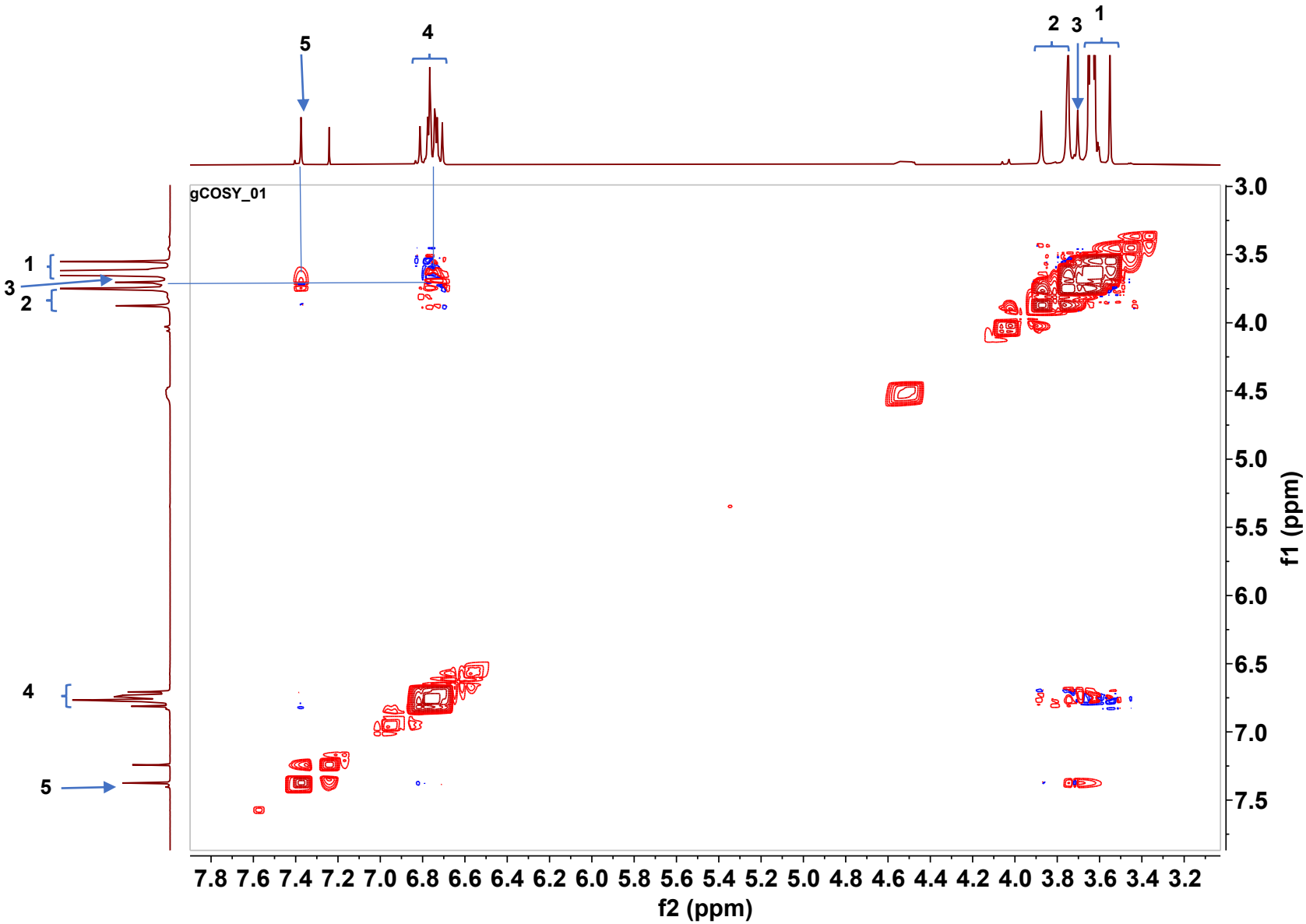

Fig. S29. Partial ^{1}H-^{1}H COSY spectra of **J2** (^{1}H NMR (400 MHz, 293 K, $CDCl_3$)).

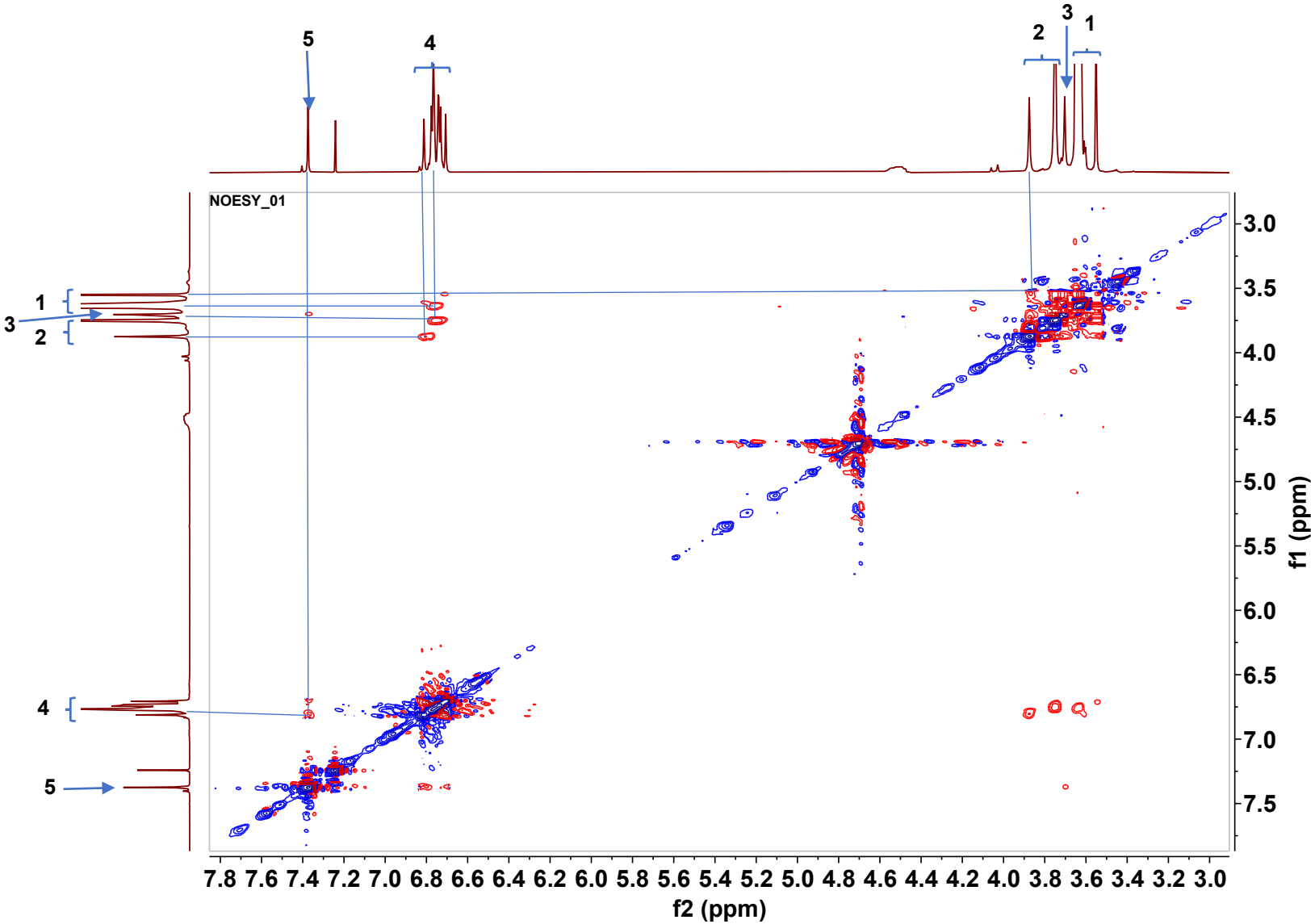

Fig. S30. Partial ^{1}H-^{1}H NOESY spectra of **J2** (^{1}H NMR (400 MHz, 293 K, $CDCl_3$)).

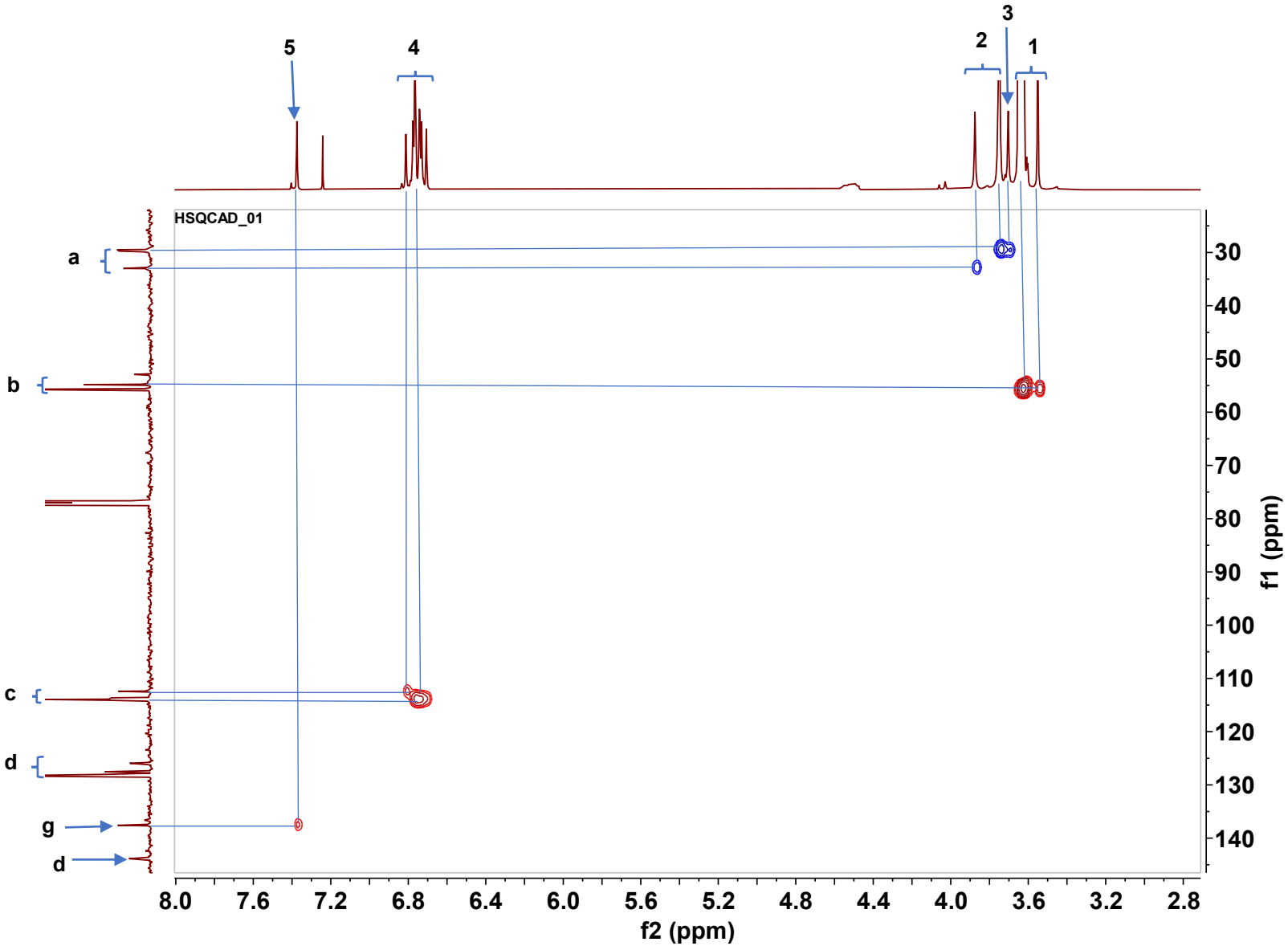

Fig. S31. Partial ^{1}H-^{13}C HSQC spectra of **J2** (^{1}H NMR (400 MHz, 293 K, $CDCl_3$); ^{13}C NMR (100 MHz, 293 K, $CDCl_3$)).

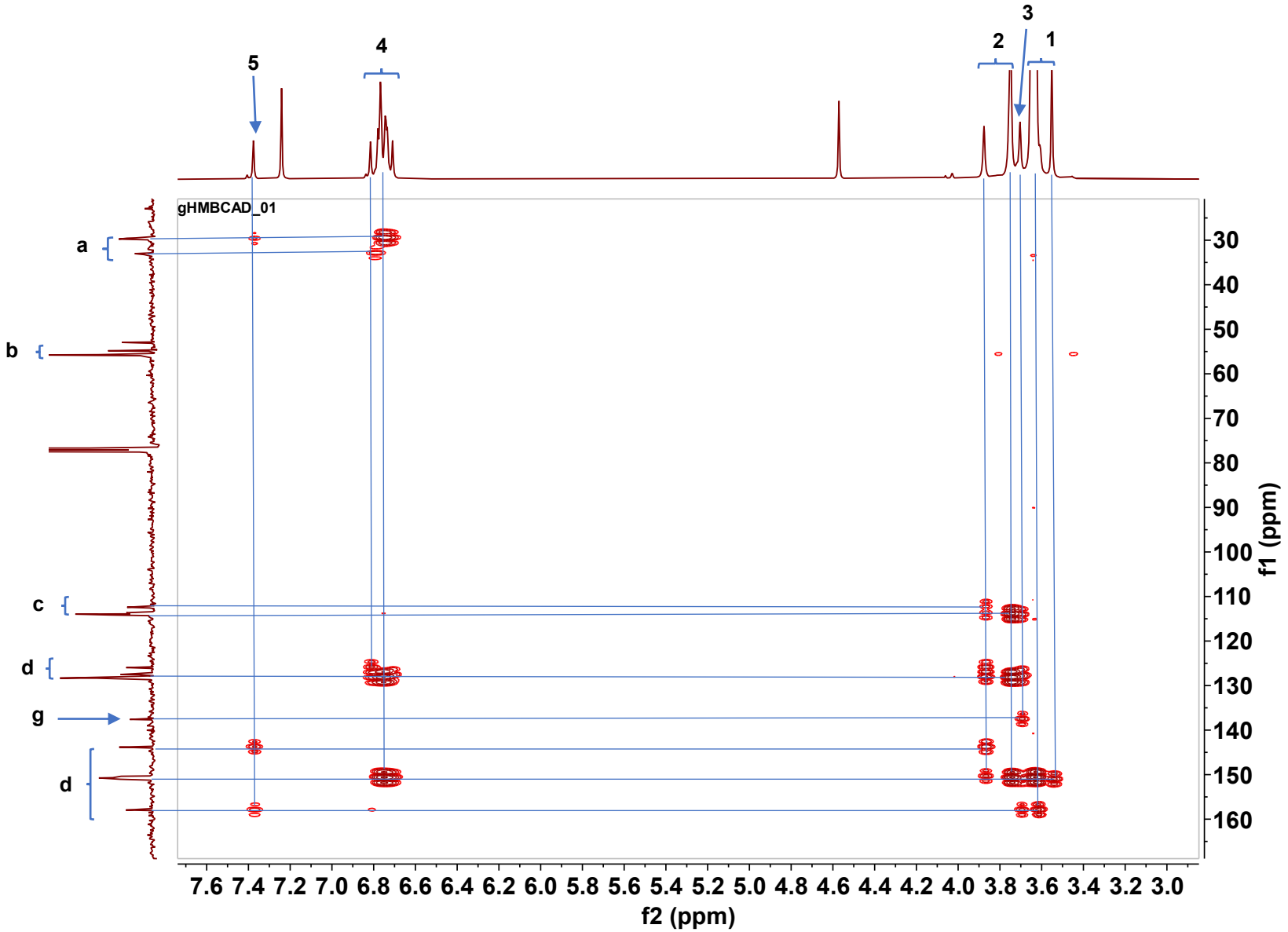

Fig. S32. Partial ^{1}H-^{13}C HMBC spectra of **J2** (^{1}H NMR (400 MHz, 293 K, $CDCl_3$); ^{13}C NMR (100 MHz, 293 K, $CDCl_3$)).

HR-MS (ESI-TOF) Spectra

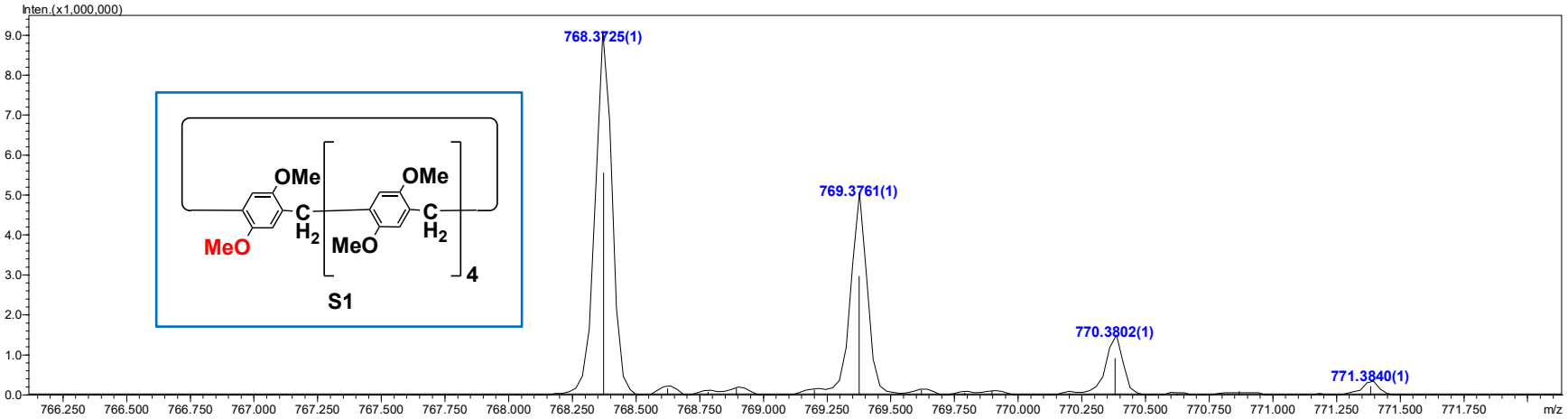

Fig. S33. HR-MS (ESI-TOF) spectra of [**S1**+NH_4]$^+$.

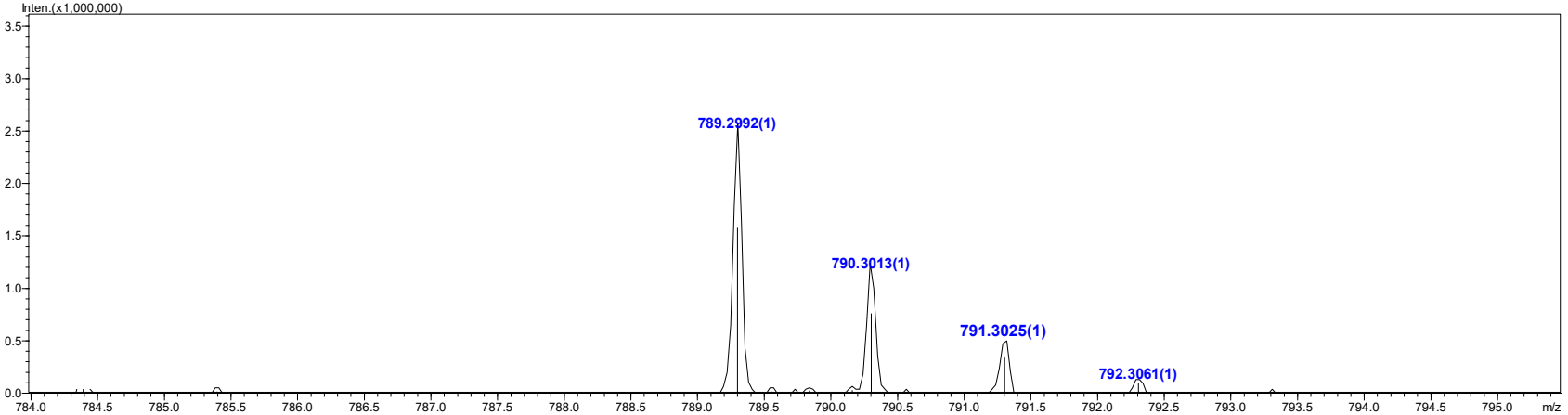

Fig. S34. HR-MS (ESI-TOF) spectra of [**S1**+K]$^+$

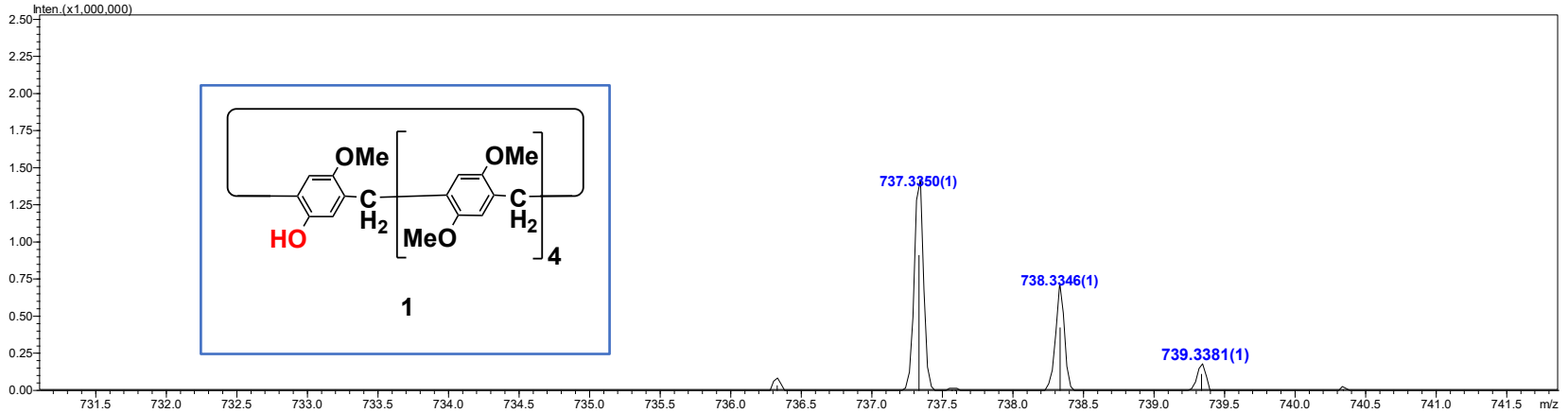

Fig. S35. HR-MS (ESI-TOF) spectra of [**1** + H]$^+$

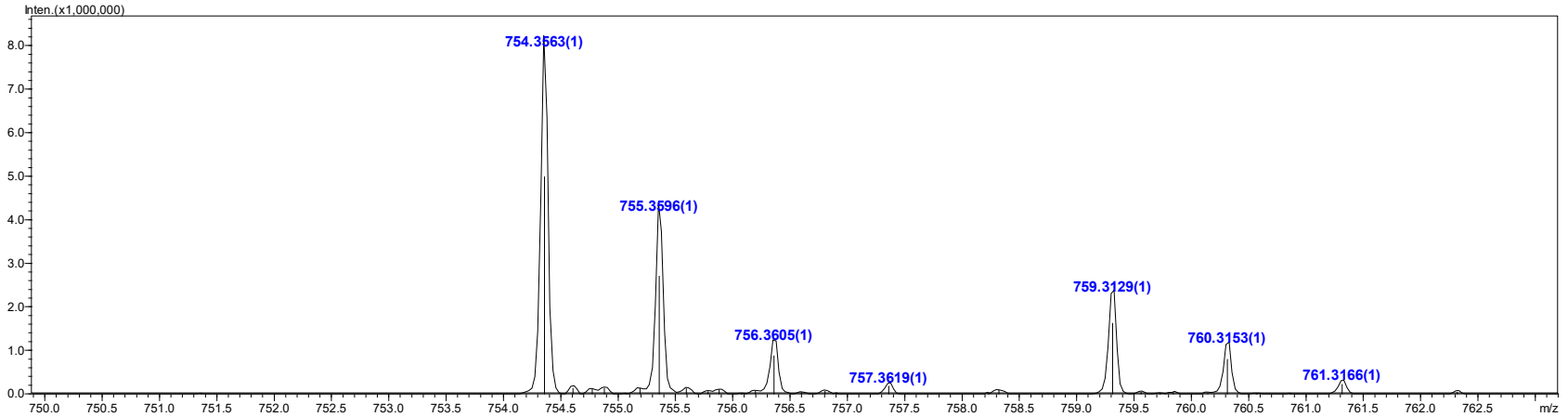

Fig. S36. HR-MS (ESI-TOF) spectra of [**1** + NH_4]$^+$ and [**1** + Na]$^+$

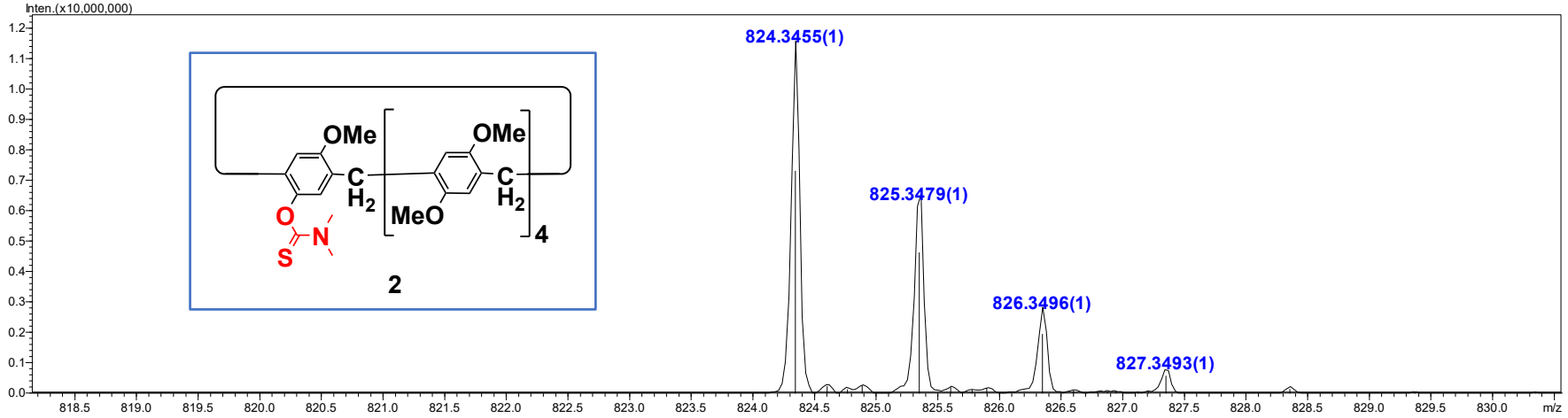

Fig. S37. HR-MS (ESI-TOF) spectra of [**2** + H]$^+$

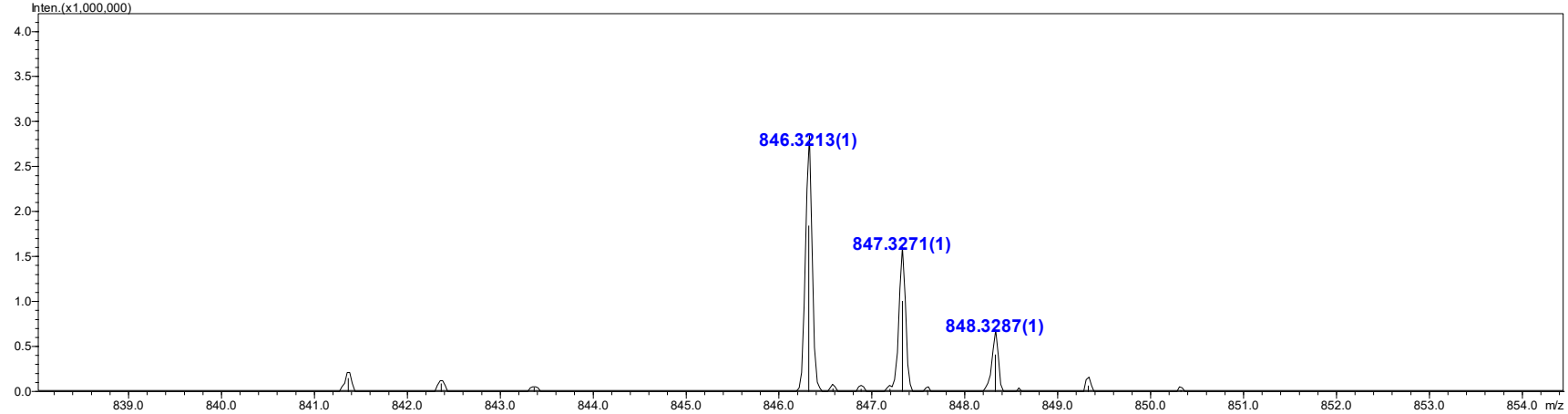

Fig. S38. HR-MS (ESI-TOF) spectra of [**2** + Na]$^+$

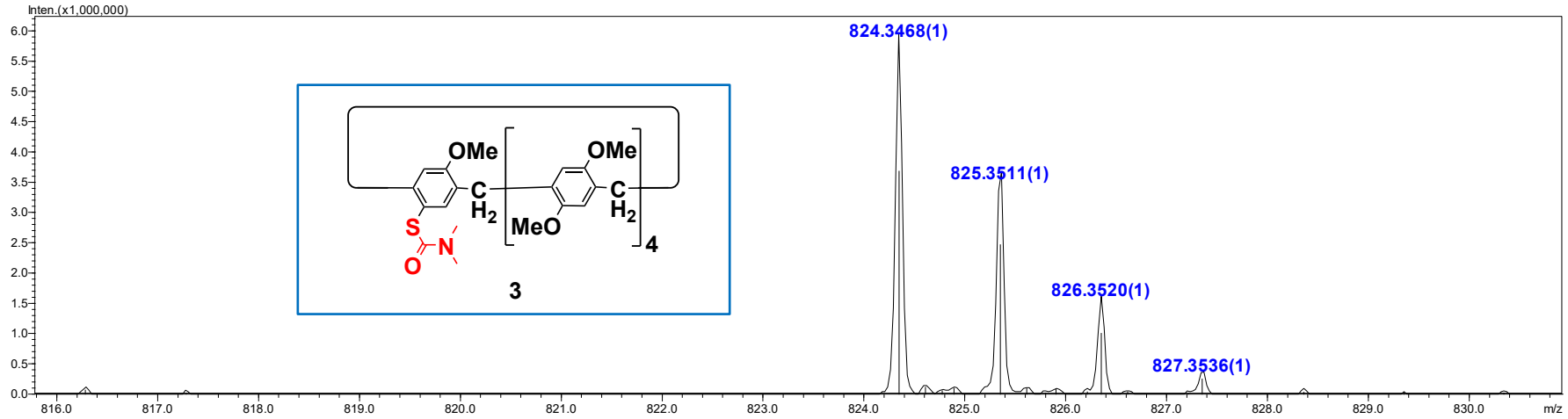

Fig. S39. HR-MS (ESI-TOF) spectra of [**3** + H]$^+$

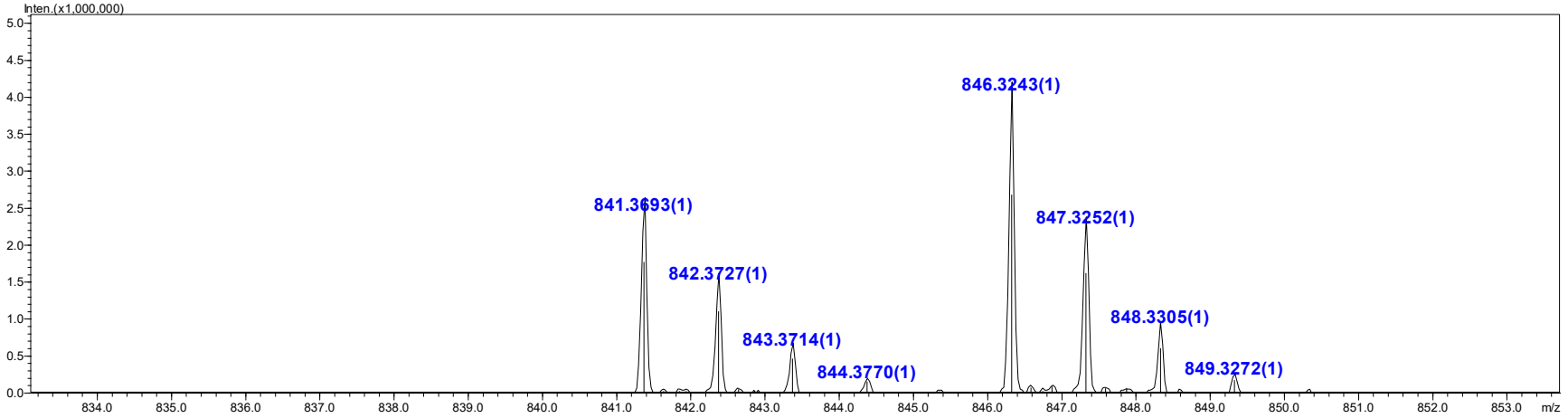

Fig. S40. HR-MS (ESI-TOF) spectra of [**3** + NH_4]$^+$ and [**3** + Na]$^+$

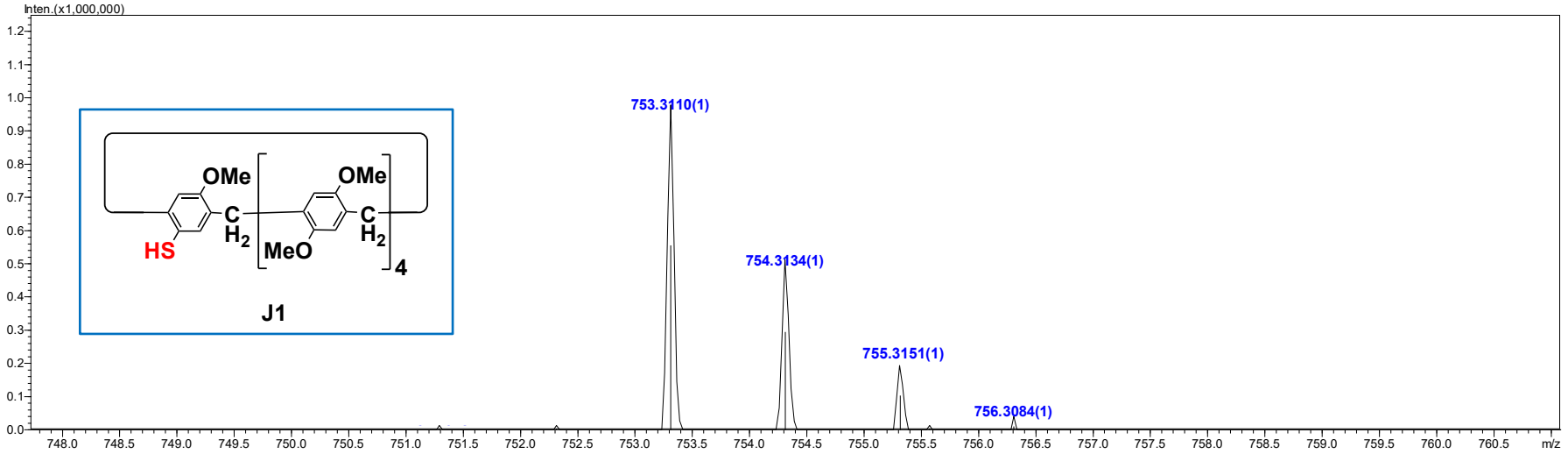

Fig. S41. HR-MS (ESI-TOF) spectra of [**J1** + H]$^+$

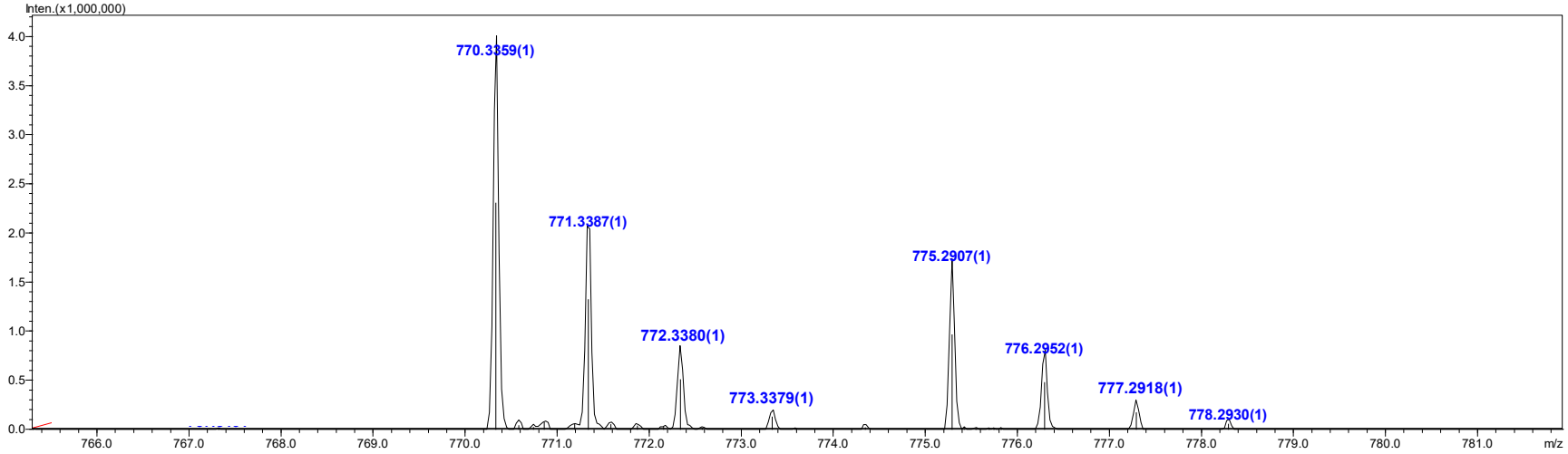

Fig. S42. HR-MS (ESI-TOF) spectra of [**J1** + NH_4]$^+$ and [**J1** + Na]$^+$

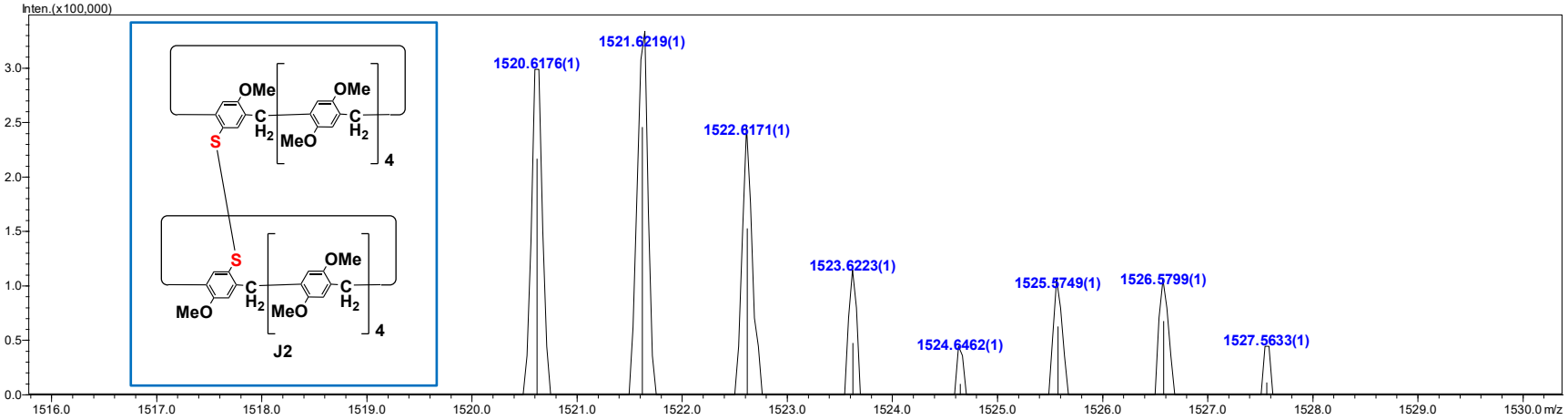

Fig. S43. HR-MS (ESI-TOF) spectra of [**J2** + NH_4]$^+$ and [**J2** + Na]$^+$

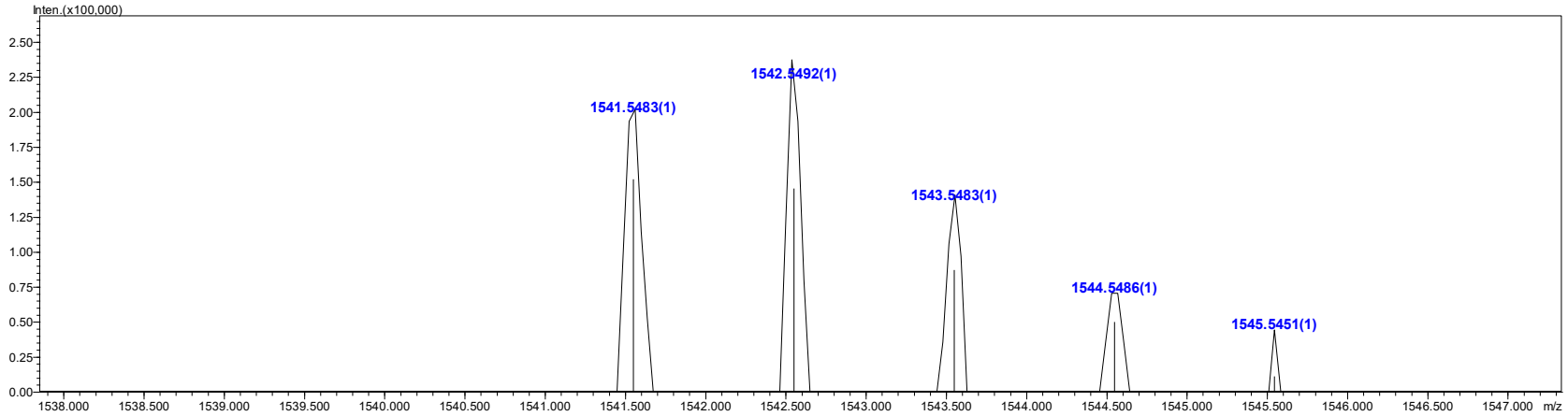

Fig. S44. HR-MS (ESI-TOF) spectra of [**J2** + K]$^+$

3. Reversible Redox Conversion between J1 and J2

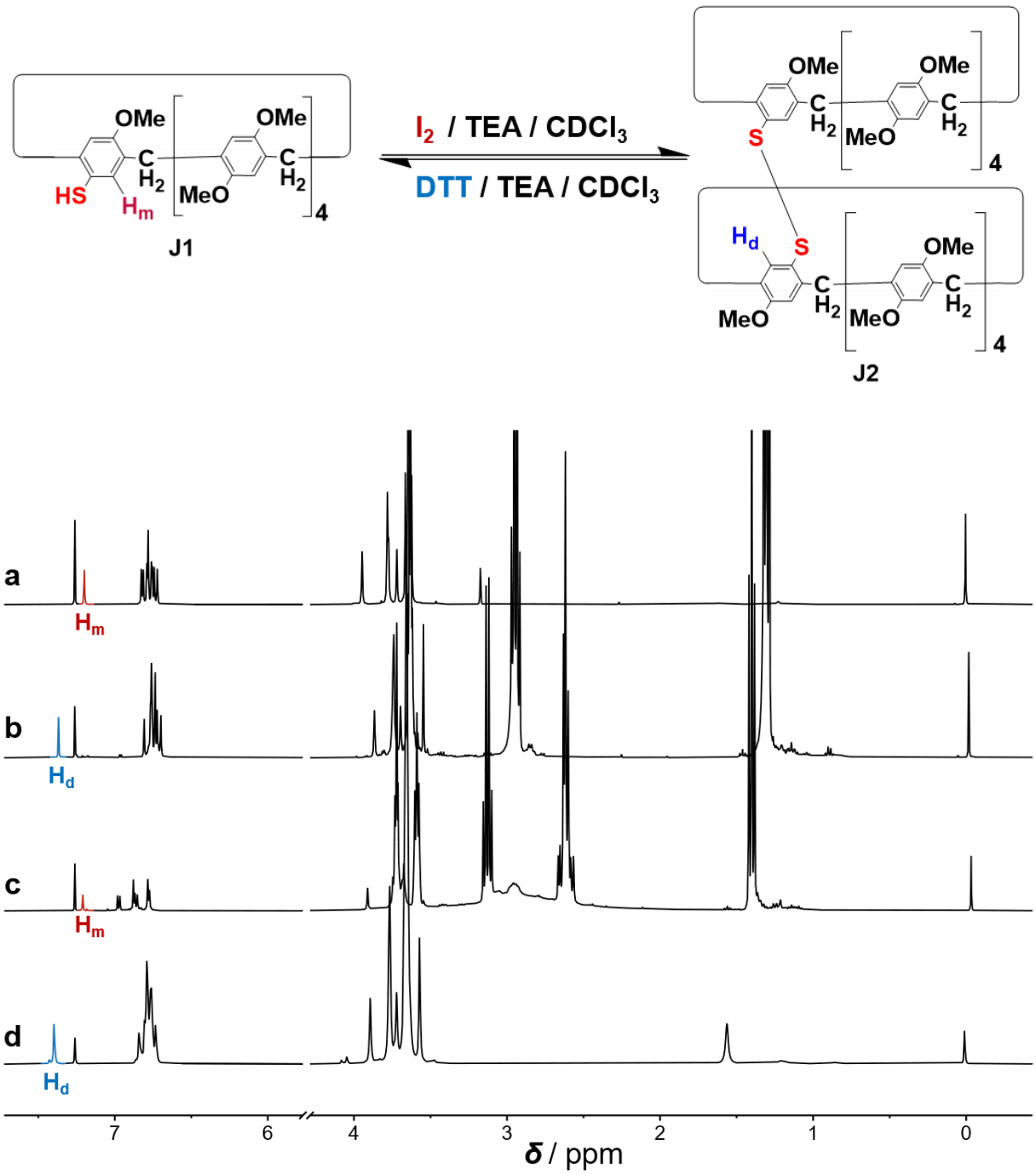

Fig. S45. ^{1}H NMR spectroscopic analysis of reversible redox conversion of **J1** and **J2** using I_2 as oxidant and DTT as reductant. Partial ^{1}H NMR spectra (400 MHz, $CDCl_3$, 293 K) of (a) **J1**, (b) a reaction mixture of **J1** and I_2 after reacting for 100 min, (b) a reaction mixture from (c) adding DTT (dithiothreitol) for 5 h 40 min, (d) **J2**. The chemical shifts assigned to phenyl of **J1** (**Fig. S45-c**) are not completely consistent with pure **J1** (**Fig. S45-a**) probably due to the existence of host-guest

complexation among DTT, the oxidized product of DTT, **J1**. Peaks are highlighted in red and blue for **J1** (H_m) and **J2** (H_d), respectively.

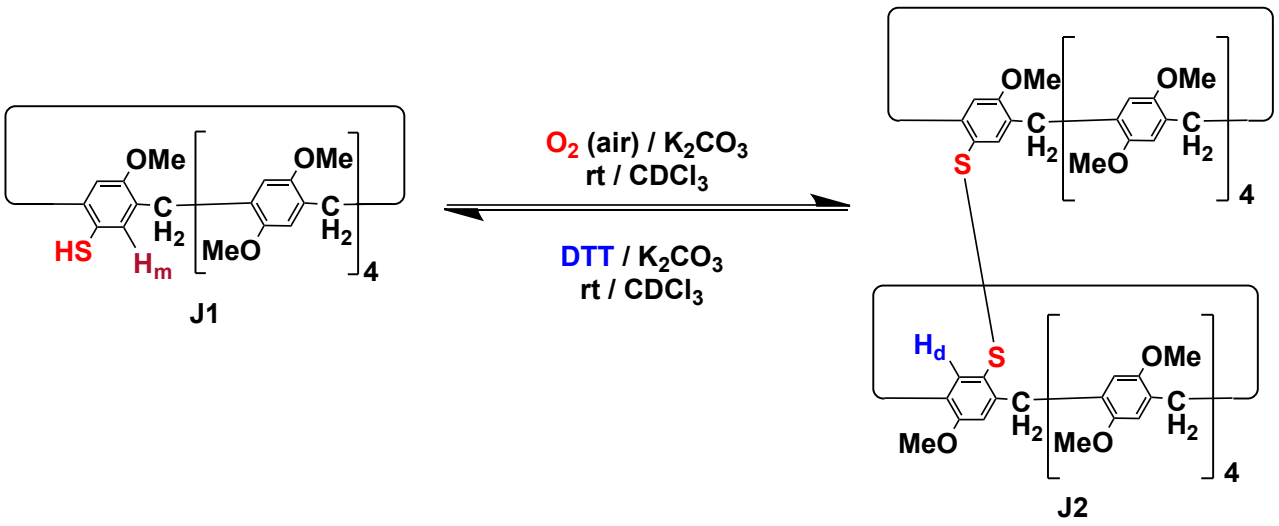

Fig. S46. The reversible redox conversion in the presence of oxidant O_2 and reductant **DTT (dithiothreitol)** between **J1** and **J2**.

The oxidative self-dimerization of J1 in the presence of O_2 and K_2CO_3

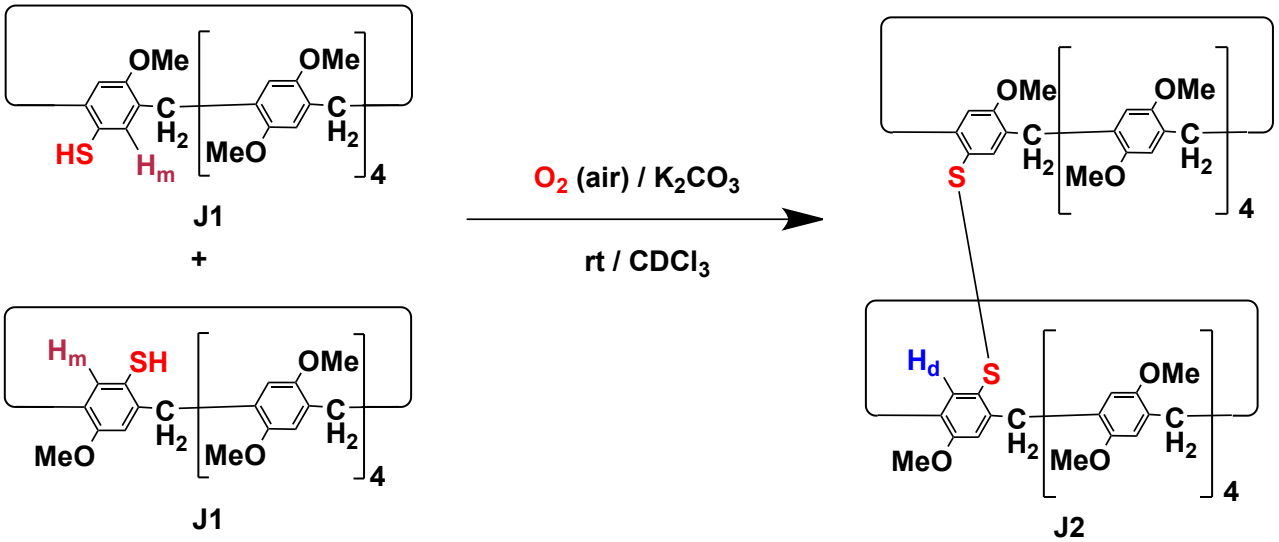

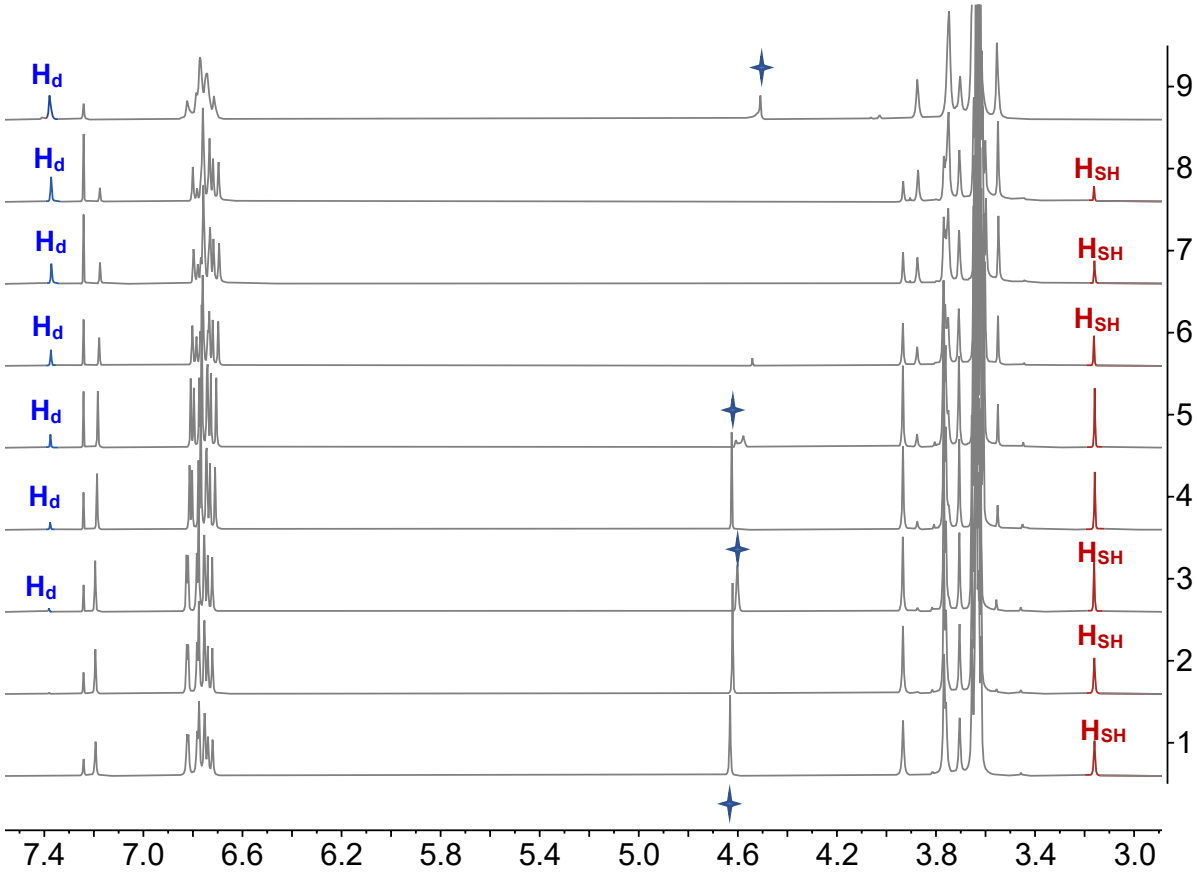

Fig. S47. The partial ^{1}H NMR (400 MHz, $CDCl_3$, 293 K) spectra changes of **J1** in the presence of O_2 and K_2CO_3(1: **J1**; 2: 0 d; 3: 1 d; 4: 2 d; 5: 5 d; 6: 16 d; 7: 30 d; 8: 47 d; 9: **J2**). Asterisk represents dichloromethane.

The reduction of J2 in the presence of DTT and K_2CO_3

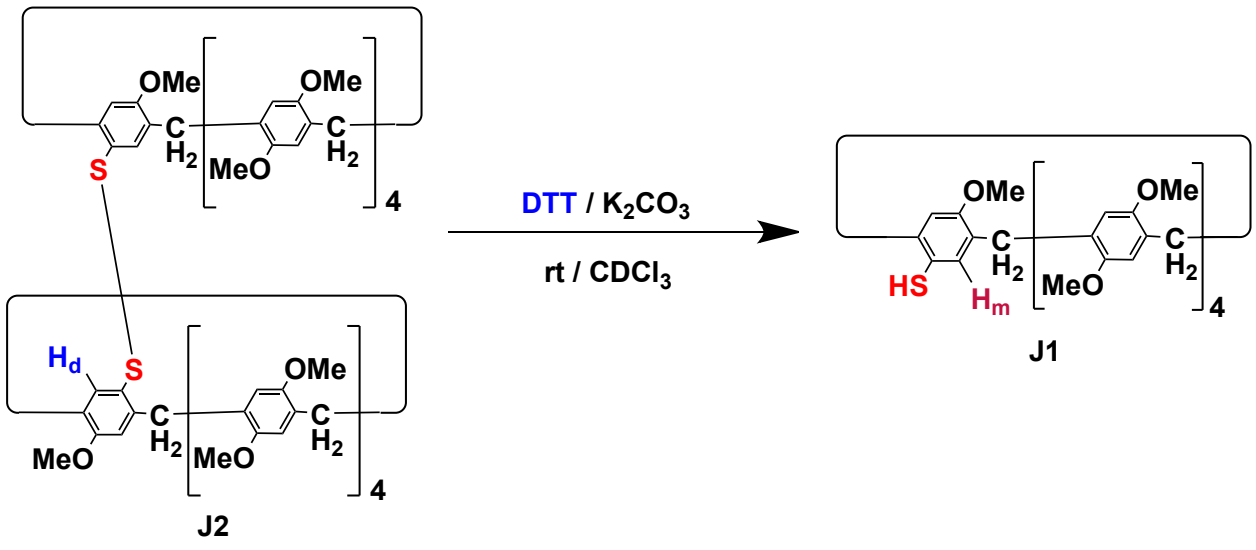

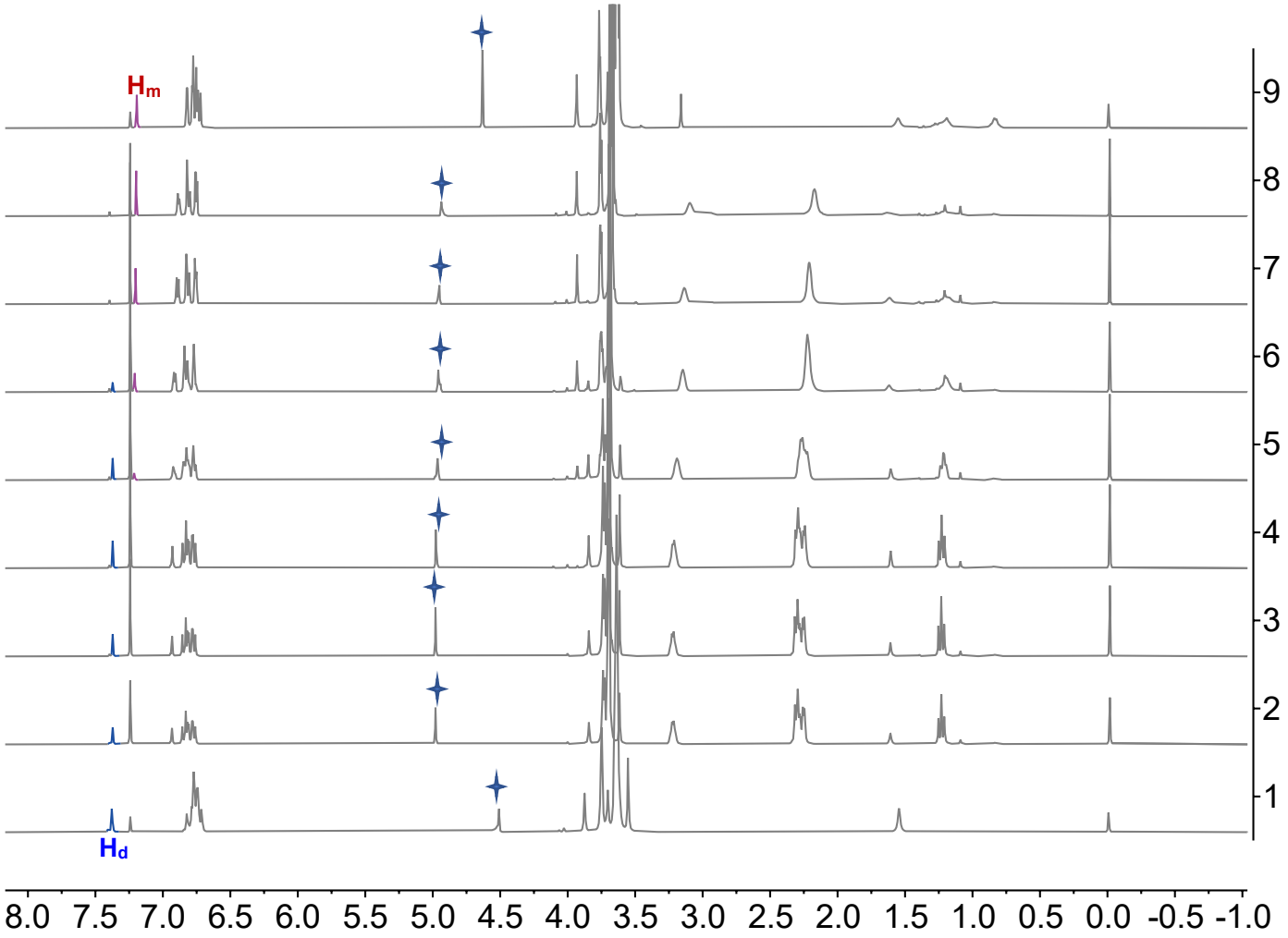

Fig. S48. The full ^{1}H NMR spectra (400 MHz, $CDCl_3$, 293 K) changes of **J2** in the presence of **DTT** and K_2CO_3(1: **J2**; 2: 10 min; 3: 40 min; 4: 163 min; 5: 590 min; 6: 23 h 43 min; 7: 34 h 10 min; 8: 47 h; 9: **J1**). Asterisk represents dichloromethane.

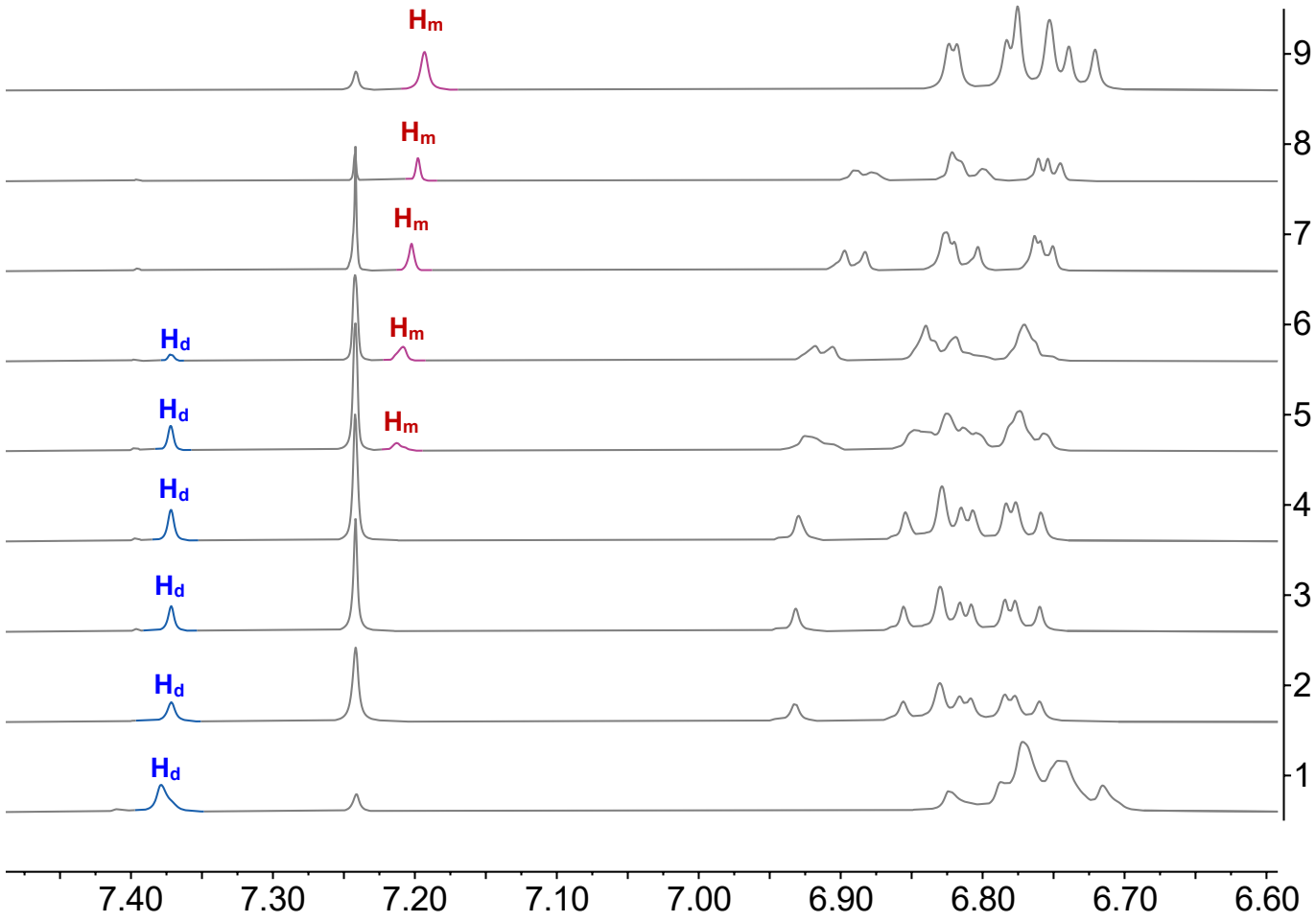

Fig. S49. The partial ^{1}H NMR spectra (400 MHz, $CDCl_3$, 293 K) changes of **J2** in the presence of **DTT** and K_2CO_3(1: **J2**; 2: 10 min; 3: 40 min; 4: 163 min; 5: 590 min; 6: 23 h 43min; 7: 34 h 10 min; 8: 47 h; 9: **J1**). Asterisk represents dichloromethane.

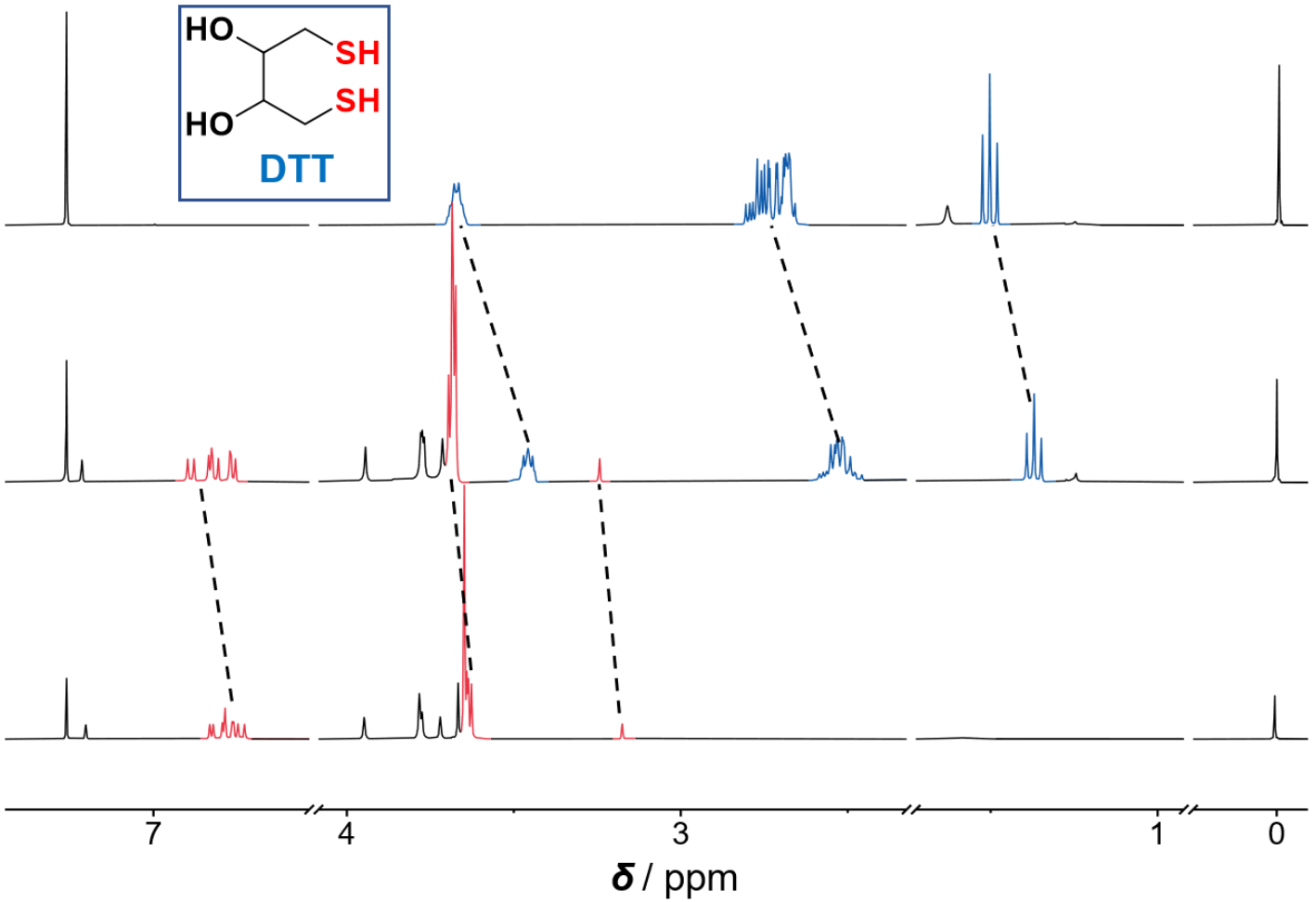

Fig. S50. ^{1}H NMR spectra (400 MHz, $CDCl_3$, 293 K) of (a) **DTT**, (b) **J1** in the presence of **DTT**, (c) **J1**.

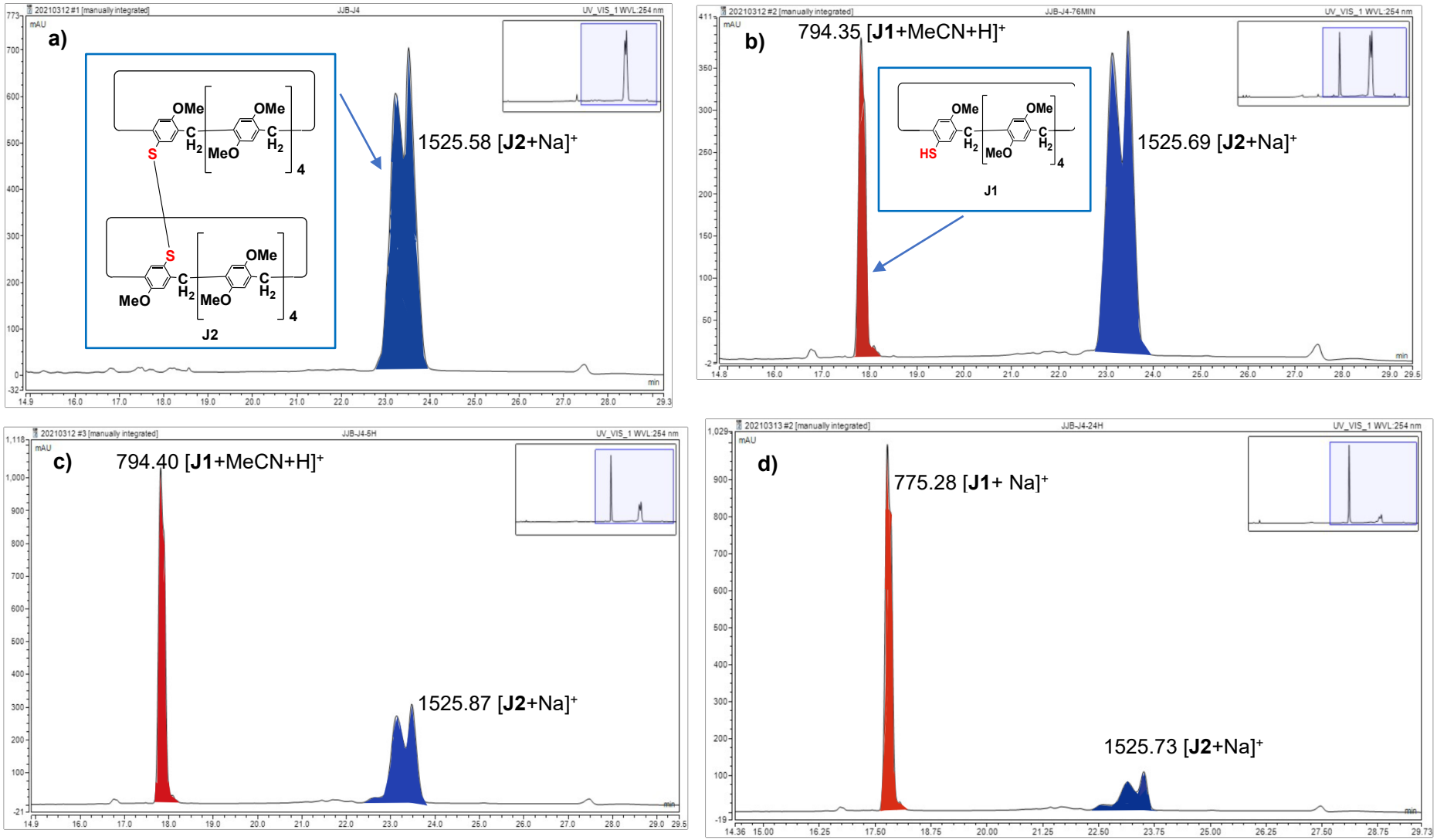

Fig. S51. The UPLC chromatogram changes of **J2** in the presence of **DTT** and K_2CO_3 (blue: **J2**; red: **J1**) (a: **J2**; b: 76 min; c: 5 h; d: 24 h).

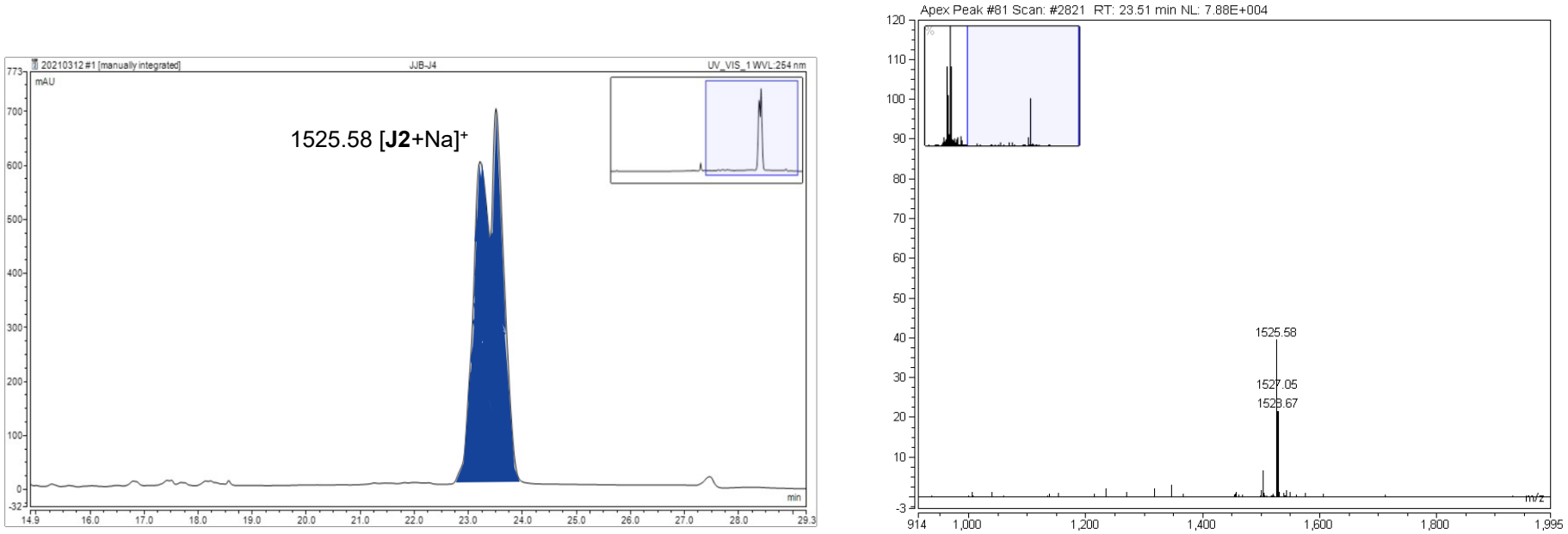

Fig. S52. The UPLC chromatogram (left) and the corresponding mass spectra of **J2** (right). The split peak is ascribed to the nonoptimal separation conditions including stationary phase, mobile phase, separation column temperature, solvent effect, etc.

Determination of oxidative self-dimerization rate constant of J1 by linear fitting

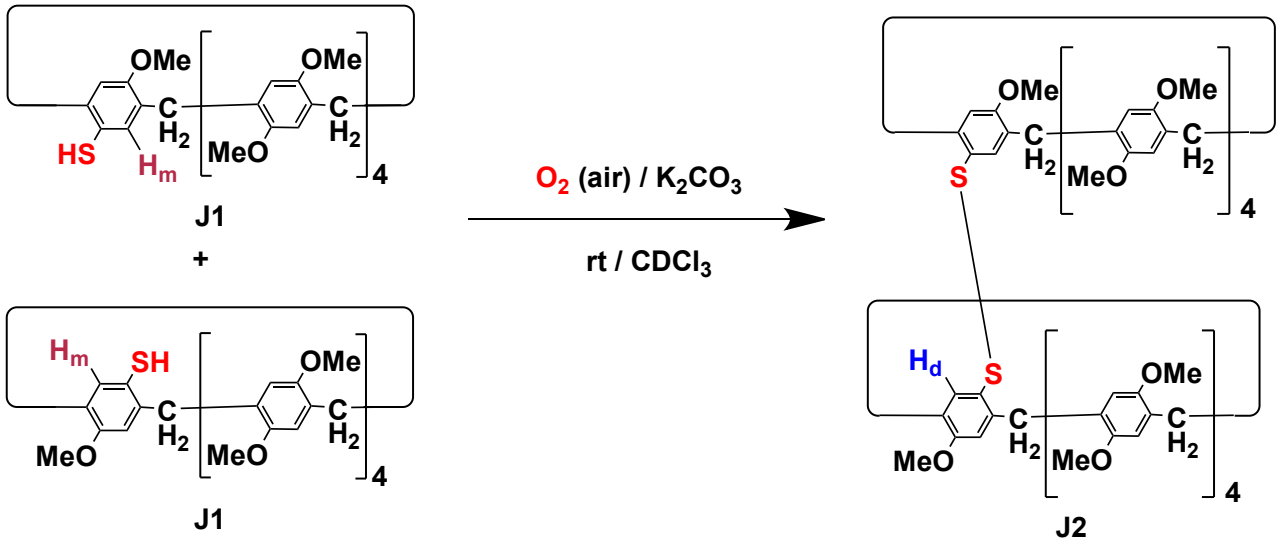

Fig. S53. The oxidative self-dimerization of **J1**.

The oxidative self-dimerization rate constant of **J1** was determined by linear fitting. A linear fitting method was applied to calculate the oxidative self-dimerization rate constant for **J1**, which was based on the second order reaction equation as follows:

$$\frac{1}{c} - \frac{1}{c_0} = k_2 t \qquad \text{(eq-1)}$$

Where c_0 is the fixed initial concentration of **J1** (c_0 = 42 mM), c obtained by calculation from relative proportion of H_{SH} and H_d in ^{1}H NMR spectra is the concentration of **J1** when reaction time is t, t is reaction time of the oxidative self-dimerization of **J1**.

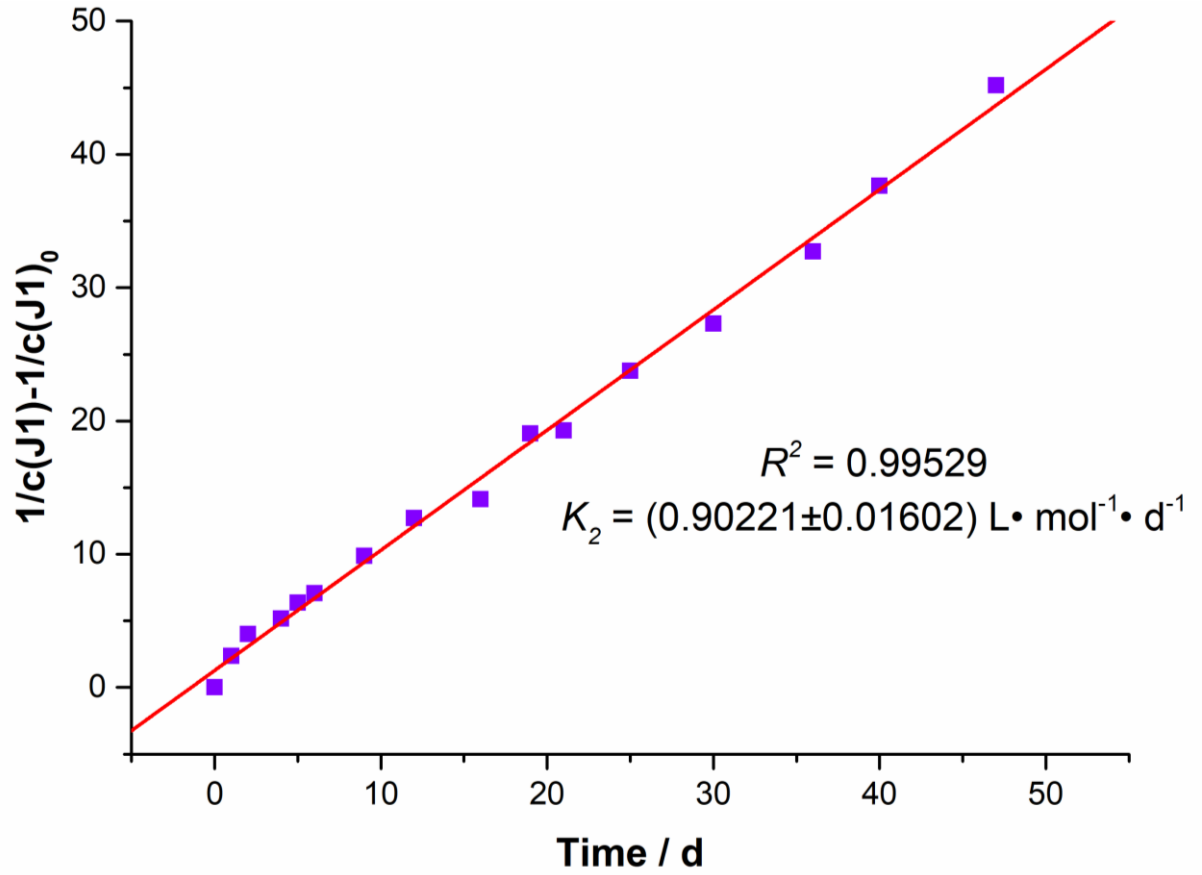

Fig. S54. The linear fitting plot of oxidative self-dimerization rate constant of **J1**.

The changes of oxidative self-dimerization conversion ratio of J1 by nonlinear curve-fitting

The oxidative self-dimerization is a kind of second order reaction according to the result of **Fig. S63**. For oxidative self-dimerization conversion ratio of **J1** α, its expression is obtained as follows:

$$\alpha = \frac{n_0 - n}{n_0}$$

$$n = cV_0,\ n_0 = c_0V_0$$

$$\frac{1}{c} - \frac{1}{c_0} = k_2t$$

$$c = \frac{c_0}{c_0k_2t + 1}$$

$$\alpha = \frac{c_0k_2t}{c_0k_2t+1} = \frac{At}{At+1} = \frac{1}{1+\frac{1}{At}} \qquad \text{(eq-2)}$$

Where c_0 is the fixed initial concentration of **J1** (c_0 = 42 mM);

c: the concentration of **J1** obtained by calculation from relative proportion of H_{SH} and H_d in ^{1}H NMR spectra when reaction time is t;

t: reaction time of the oxidative self-dimerization of **J1**;

α: oxidative self-dimerization conversion ratio of **J1**;

n: the amount of substance of **J1** obtained by calculation from relative proportion of H_{SH} and H_d in ^{1}H NMR spectra when reaction time is t;

n_0: the fixed initial amount of substance of **J1** (n_0 = 0.021 mmol);

k_2: the oxidative self-dimerization rate constant of **J1** (k_2 = (0.902±0.016) L• mol^{-1}•d^{-1});

$A = c_0k_2$.

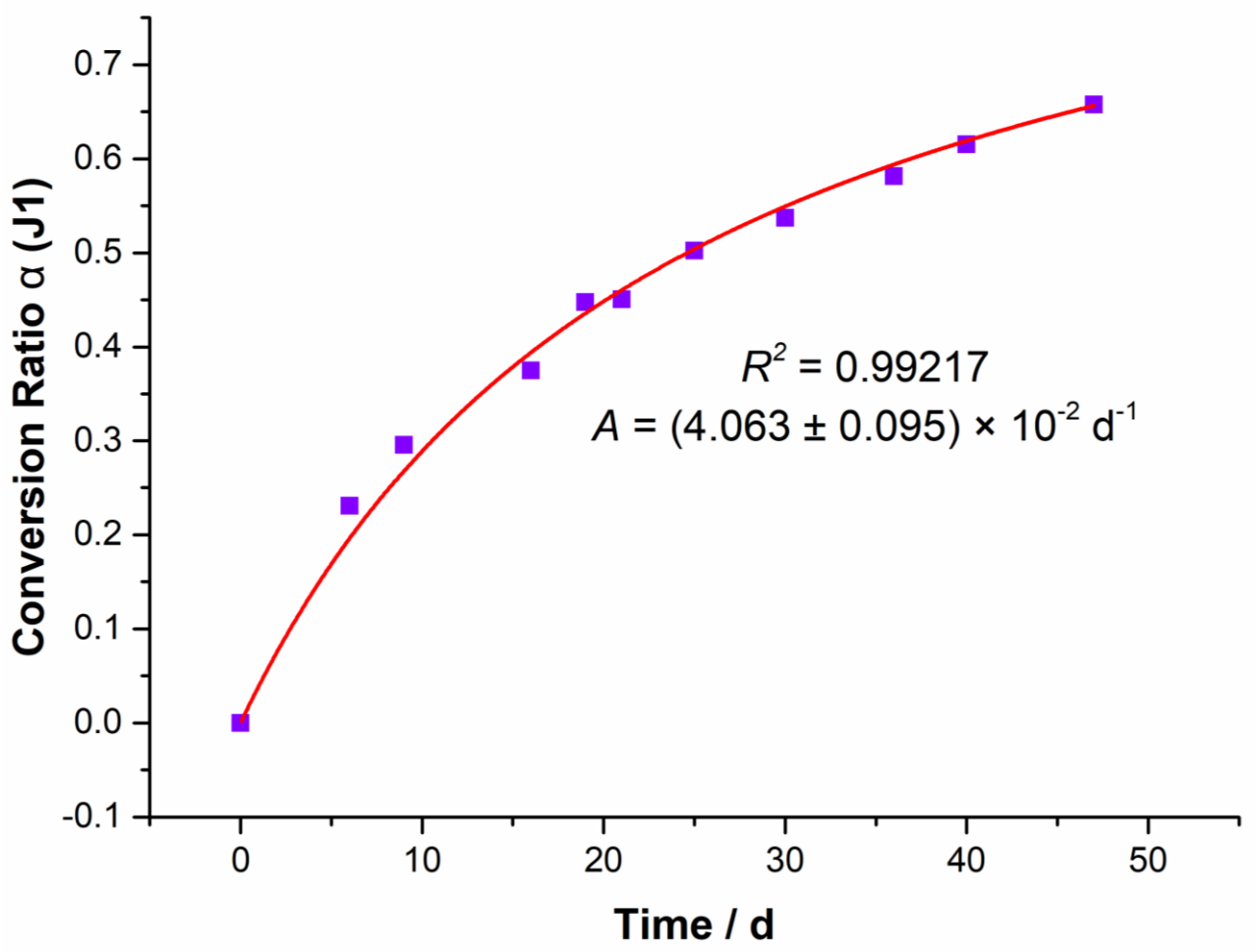

Fig. S55. The changes of oxidative self-dimerization conversion ratio of **J1** α by nonlinear curve-fitting.

4. Host-guest Complexation

NMR spectra of HDPB (1-hexadecylpyridinium bromide) in the absence and presence of J1

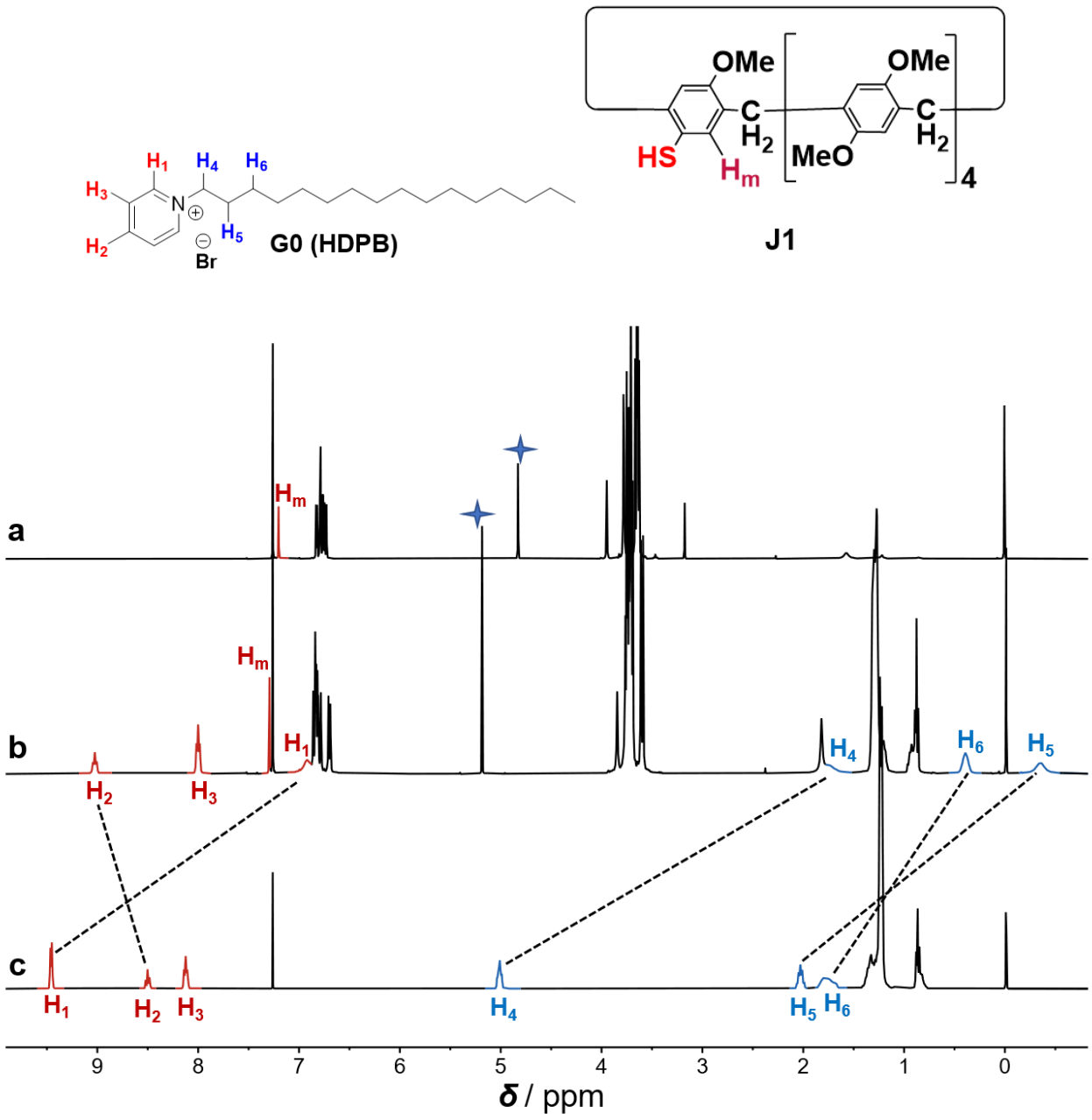

Fig. S56. ^{1}H NMR spectra (400 MHz, $CDCl_3$, 293 K) of (a) **J1**, (b) **HDPB** in the presence of **J1**, (c) **HDPB**. [**J1**] = [**HDPB**] = 44.8 mM. Asterisk represents dichloromethane.

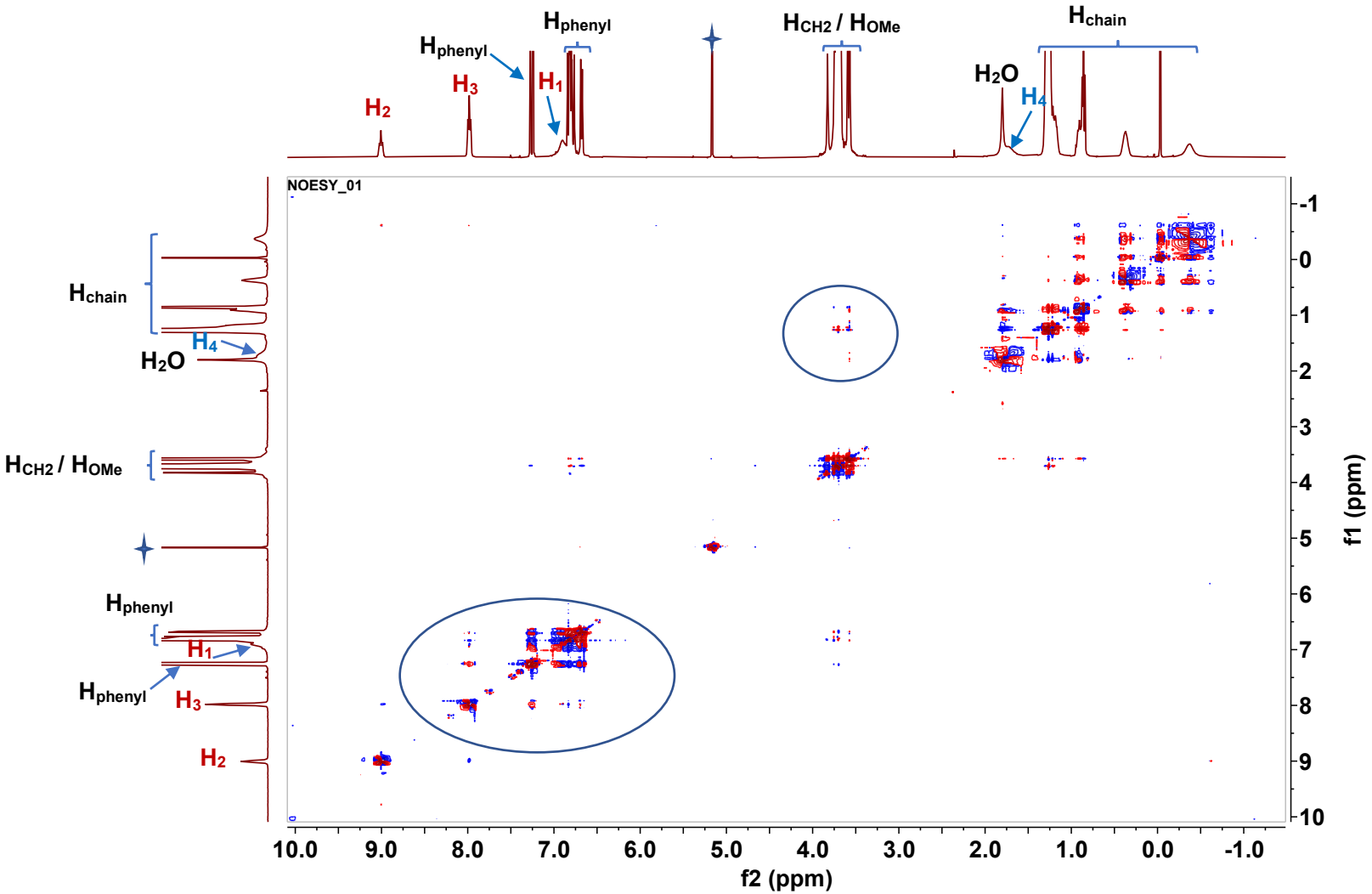

Fig. S57. Full ^{1}H-^{1}H NOESY spectra of **HDPB** in the presence of **J1** (^{1}H NMR (400 MHz, 293 K, $CDCl_3$)). [**J1**] = [**HDPB**] = 44.8 mM. Asterisk represents dichloromethane.

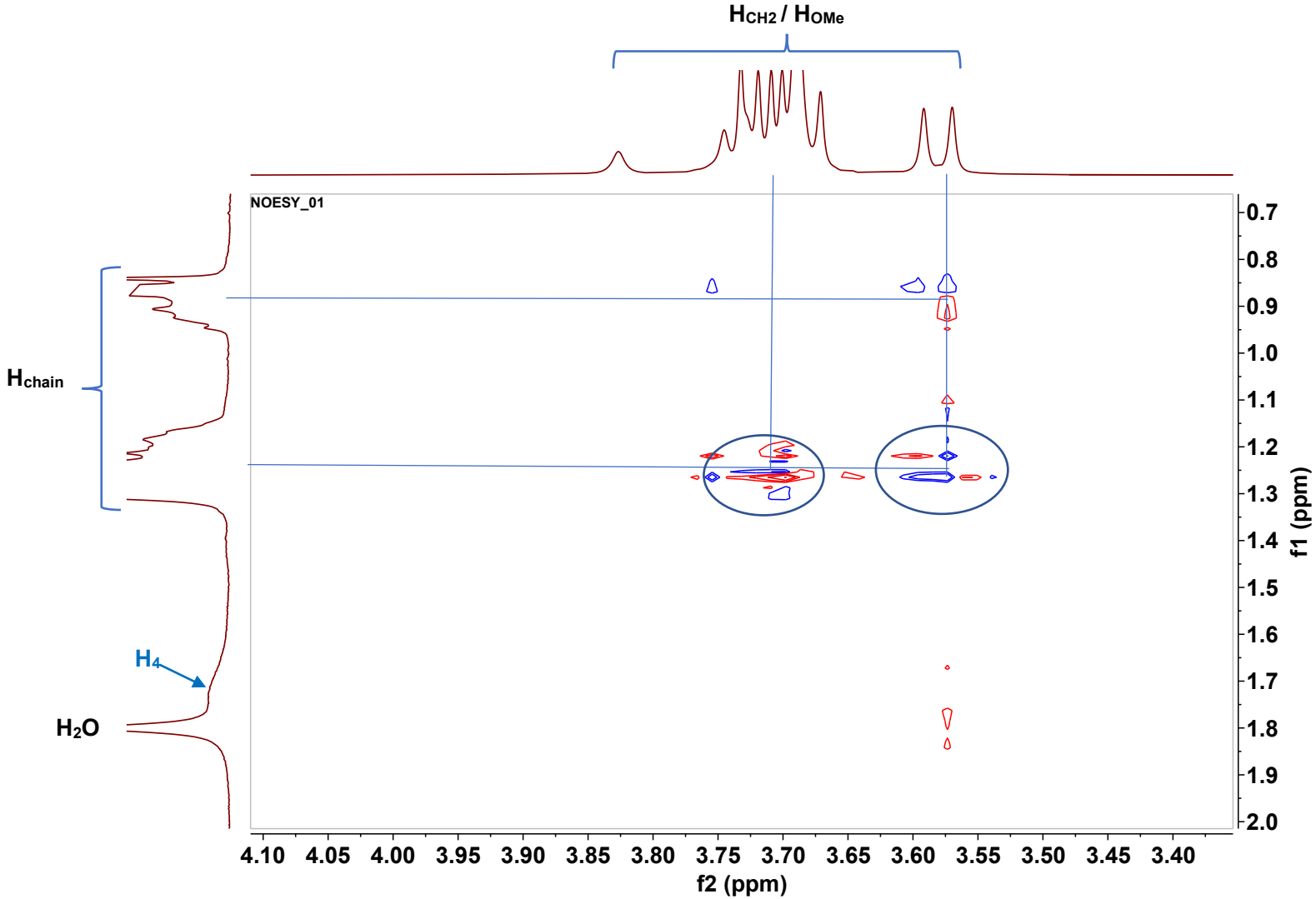

Fig. S58. Partial ^{1}H-^{1}H NOESY spectra of **HDPB** in the presence of **J1** (^{1}H NMR (400 MHz, 293 K, $CDCl_3$)). [**J1**] = [**HDPB**] = 44.8 mM.

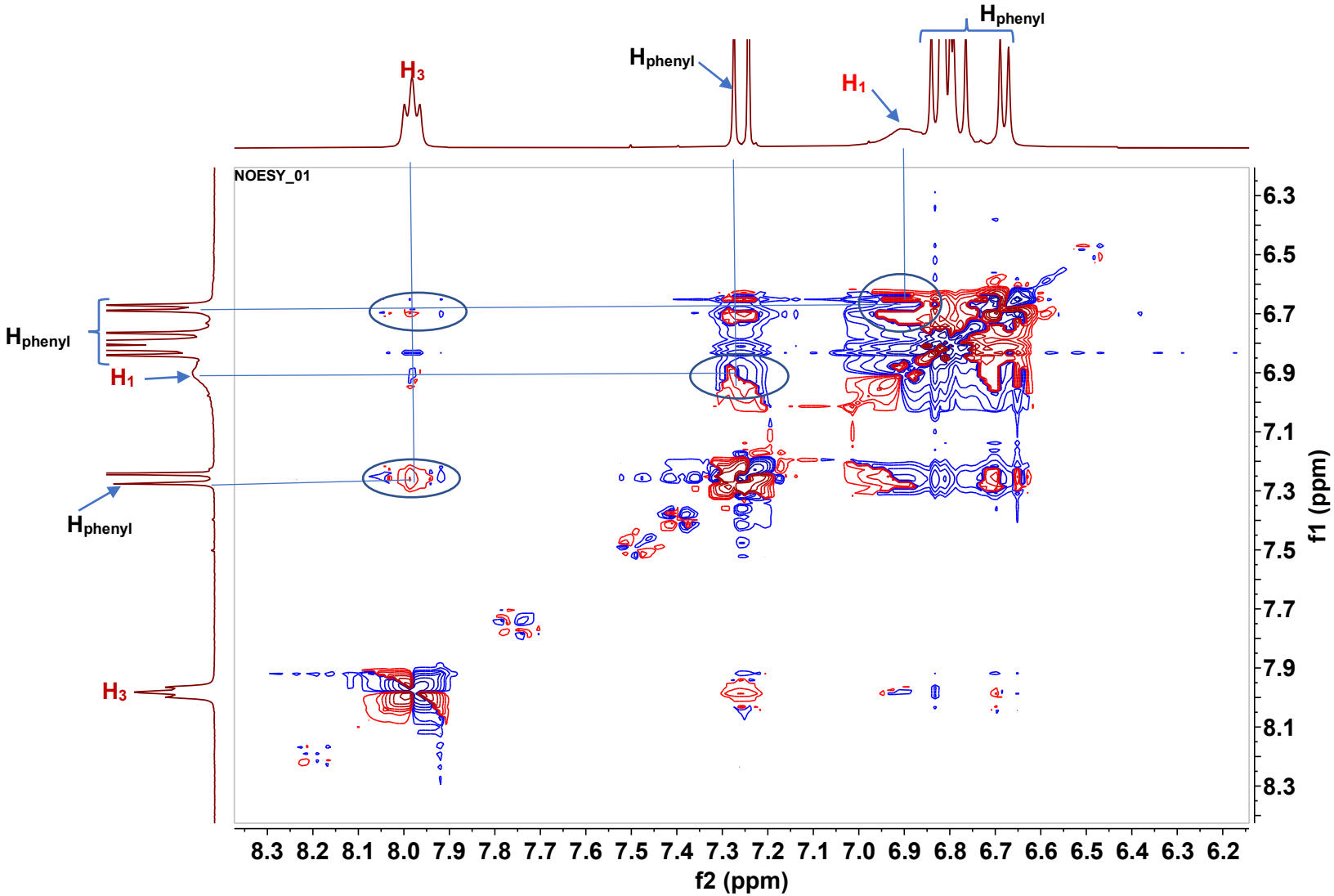

Fig. S59. Partial ^{1}H-^{1}H NOESY spectra of **HDPB** in the presence of **J1** (^{1}H NMR (400 MHz, 293 K, $CDCl_3$)). [**J1**] = [**HDPB**] = 44.8 mM.

NMR spectra of HDPB (1-hexadecylpyridinium bromide) in the absence and presence of J2

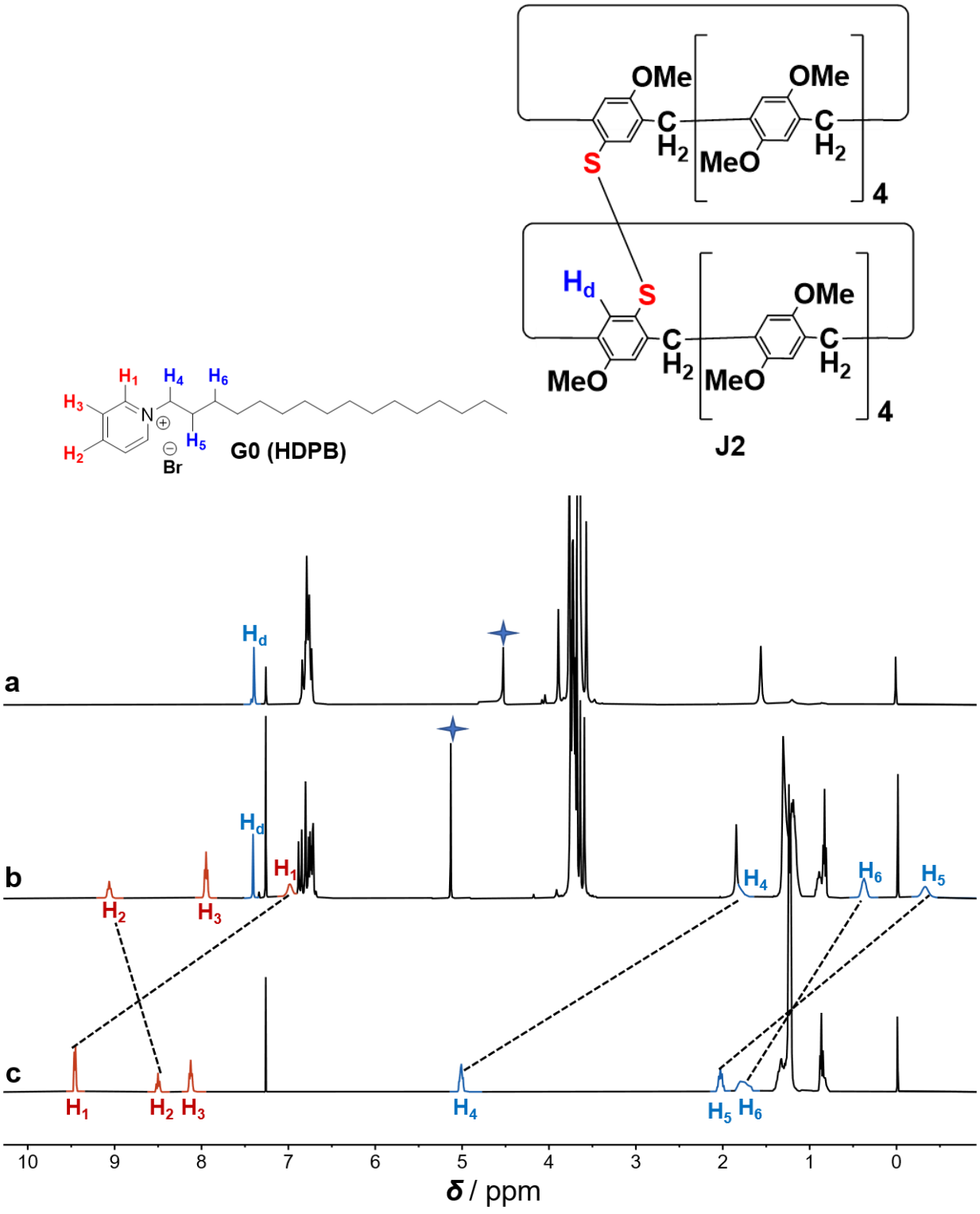

Fig. S60. ^{1}H NMR spectra (400 MHz, $CDCl_3$, 293 K) of (a) **J2**, (b) **HDPB** in the presence of **J2**, (c) **HDPB**. [**HDPB**] = 2[**J2**] = 40.0 mM. Asterisk represents dichloromethane.

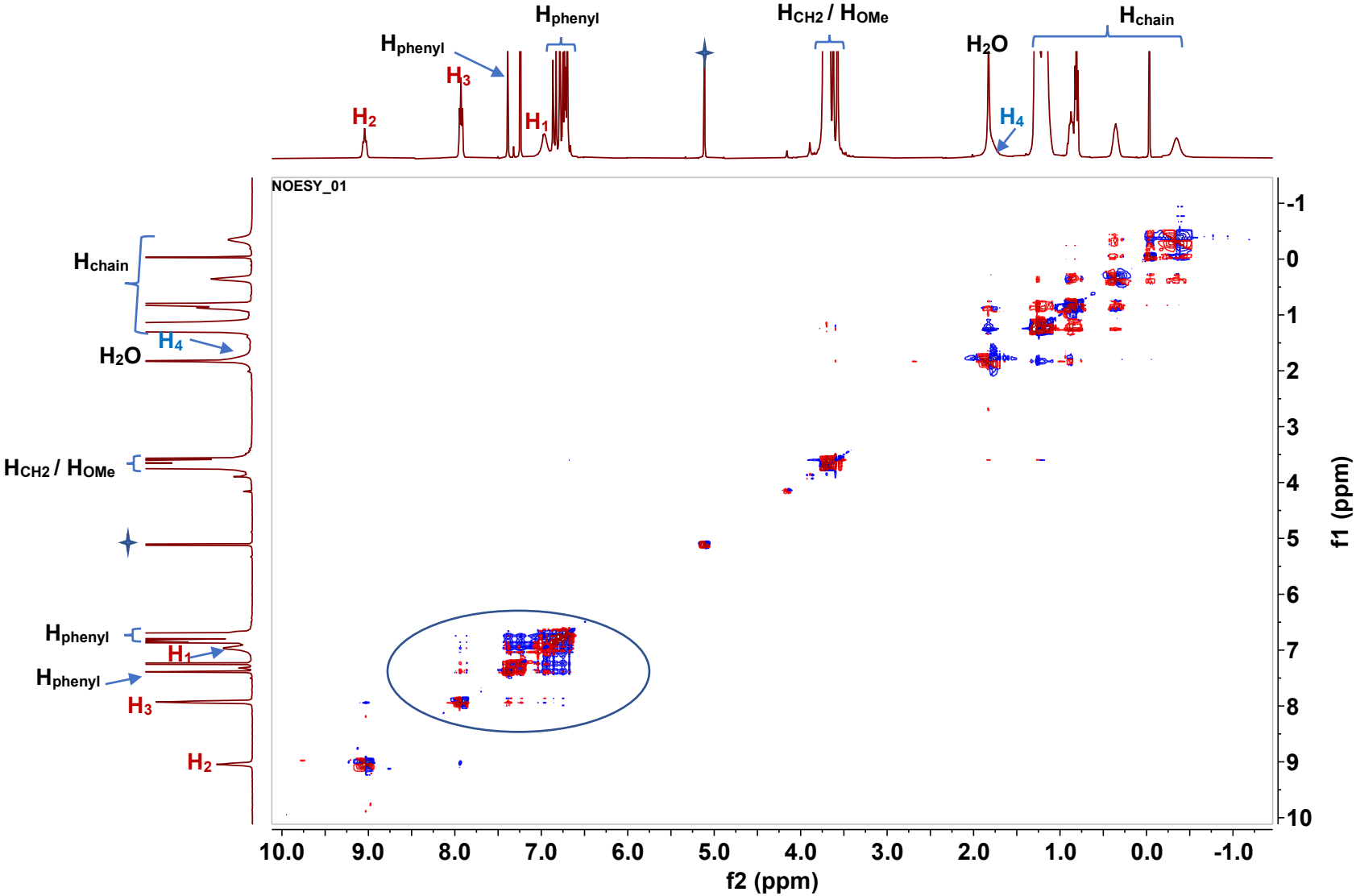

Fig. S61. Full ^{1}H-^{1}H NOESY spectra of **HDPB** in the presence of **J2** (^{1}H NMR (400 MHz, 293 K, $CDCl_3$)). [**HDPB**] = 2[**J2**] = 40.0 mM. Asterisk represents dichloromethane.

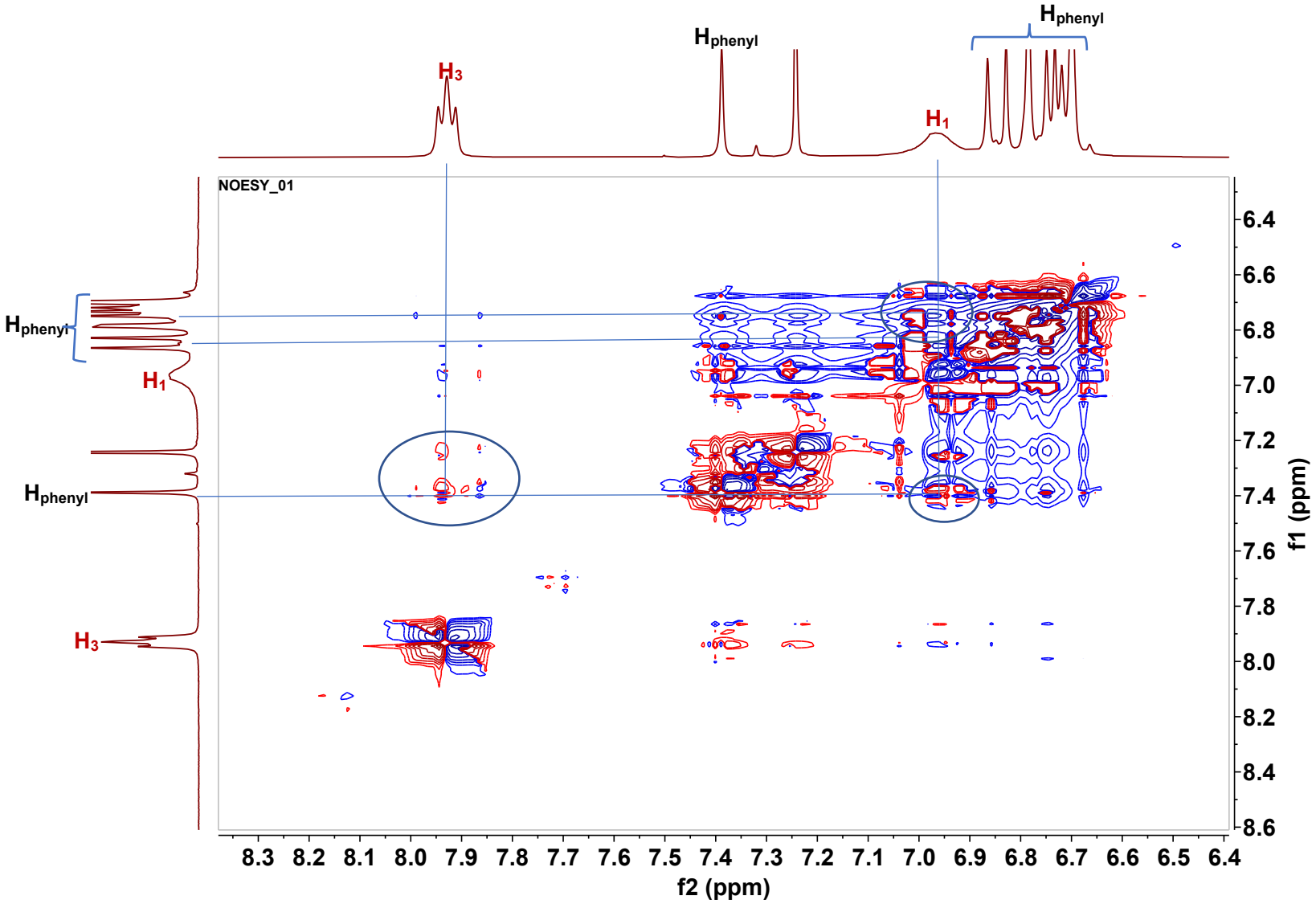

Fig. S62. Partial ^{1}H-^{1}H NOESY spectra of **HDPB** in the presence of **J2** (^{1}H NMR (400 MHz, 293 K, $CDCl_3$)). [**HDPB**] = 2[**J2**] = 40.0 mM.

NMR spectra of titration

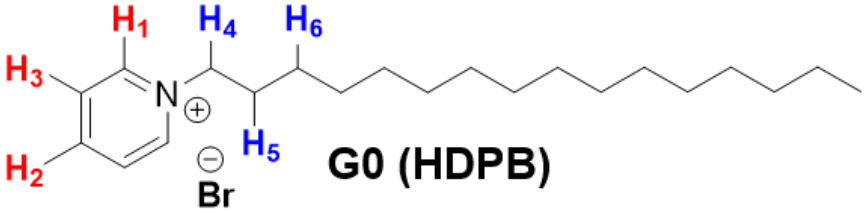

G0 (HDPB)

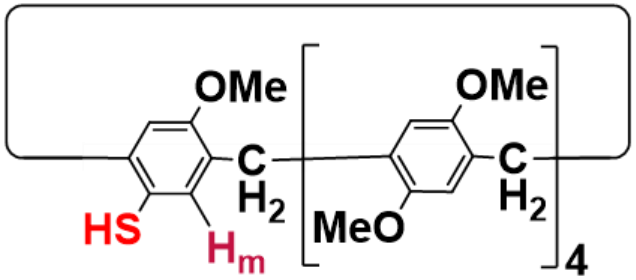

J1

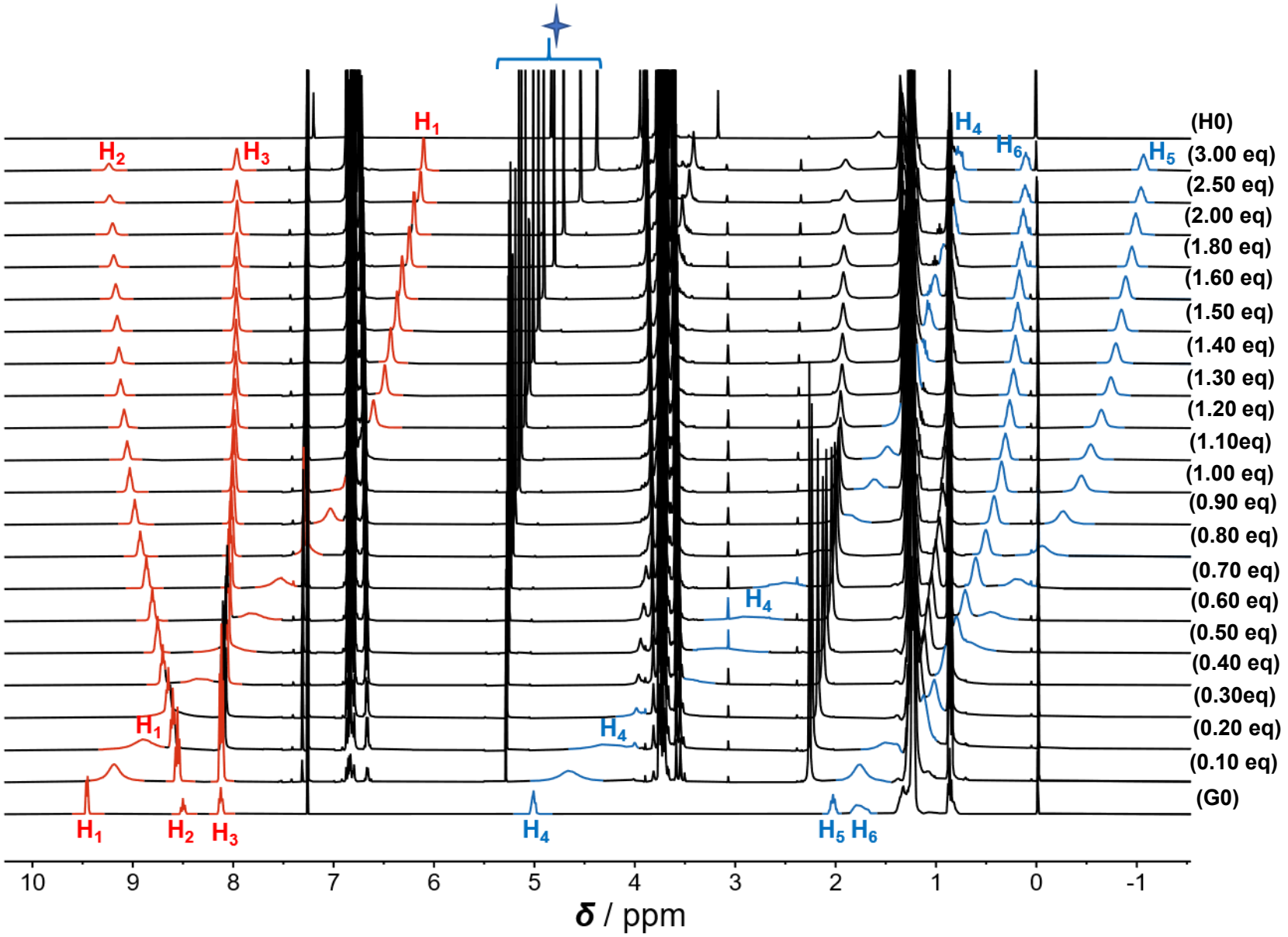
H1
H2
H3
H4
H6
H5
(H0)
(3.00 eq)
(2.50 eq)
(2.00 eq)
(1.80 eq)
(1.60 eq)
(1.50 eq)
(1.40 eq)
(1.30 eq)
(1.20 eq)
(1.10eq)
(1.00 eq)
(0.90 eq)
(0.80 eq)
(0.70 eq)
(0.60 eq)
(0.50 eq)
(0.40 eq)
(0.30eq)
(0.20 eq)
(0.10 eq)
(G0)
H1 H2 H3
H4
H5 H6
10 9 8 7 6 5 4 3 2 1 0 -1
δ / ppm

Fig. S63. The ^{1}H NMR spectra of titration of **G0** (**HDPB**) and **H0** (**J1**), **G0** in the presence of **H0** (0.1-3.0 eq) (^{1}H NMR (400 MHz, 293 K, $CDCl_3$)). Asterisk represents dichloromethane.

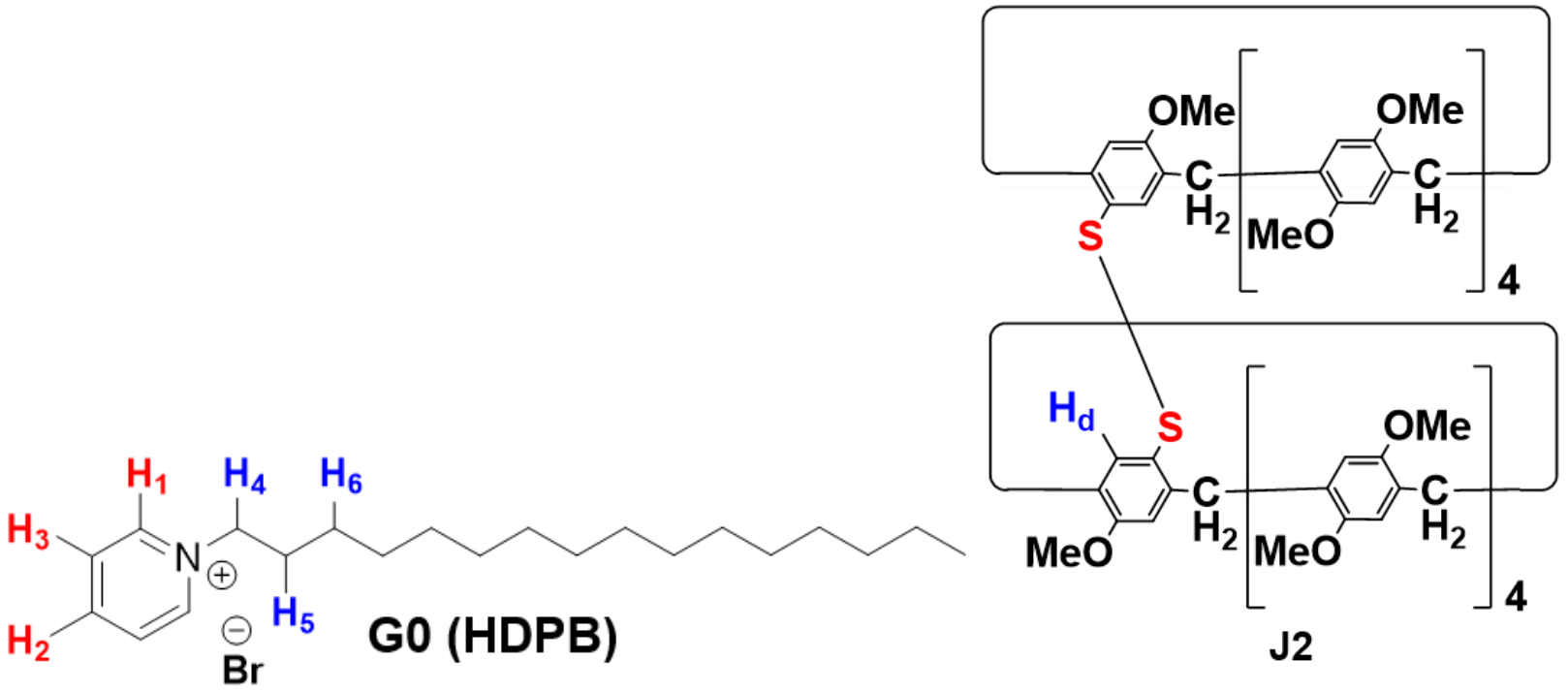

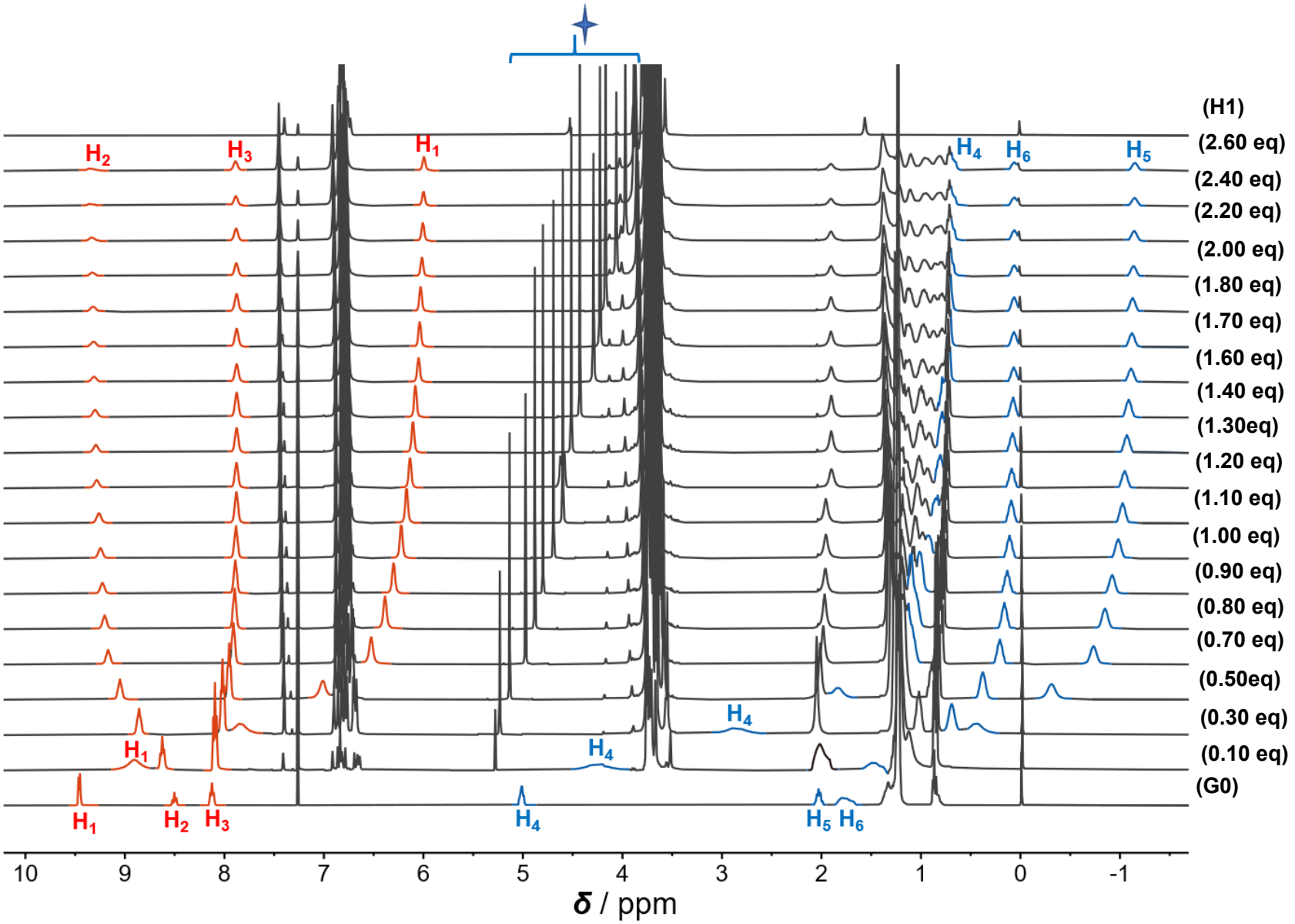
(H1)
(2.60 eq)
(2.40 eq)
(2.20 eq)
(2.00 eq)
(1.80 eq)
(1.70 eq)
(1.60 eq)
(1.40 eq)
(1.30eq)
(1.20 eq)
(1.10 eq)
(1.00 eq)
(0.90 eq)
(0.80 eq)
(0.70 eq)
(0.50eq)
(0.30 eq)
(0.10 eq)
(G0)
H2
H3
H1
H4
H6
H5
H1
H2
H3
H4
H4
H4
H5
H6
10
9
8
7
6
5
4
3
2
1
0
-1
δ / ppm

Fig. S64. The ^{1}H NMR spectra of titration of **G0** (**HDPB**) and **H1** (**J2**), **G0** in the presence of **H1** (0.1-2.6 eq) (^{1}H NMR (400 MHz, 293 K, $CDCl_3$)). Asterisk represents dichloromethane.

Molar ratio plot for the complexation by ^{1}H NMR titration

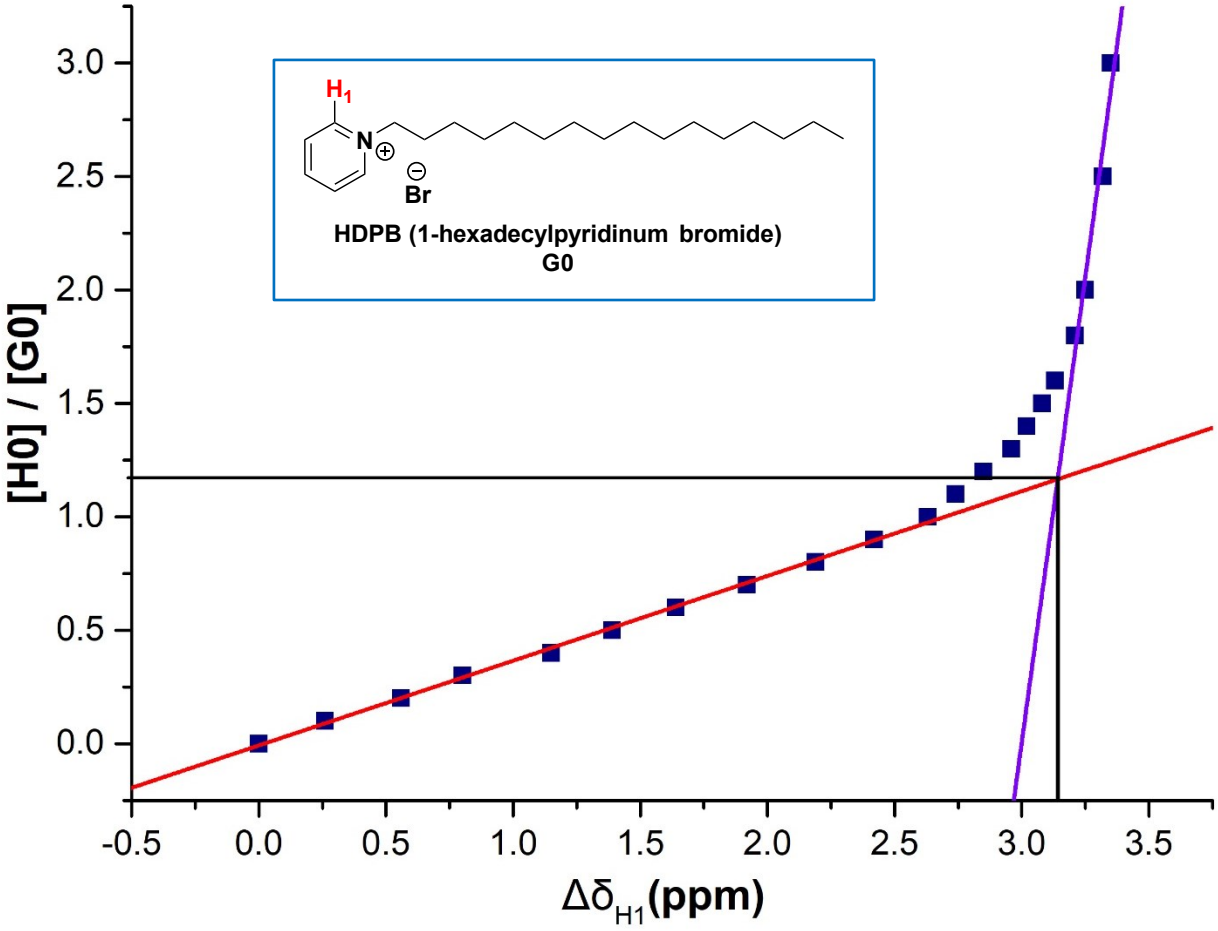

Fig. S65. Molar ratio plot for the complexation between **G0** (**HDPB**) and **H0** (**J1**), indicating a 1:1 stoichiometry.

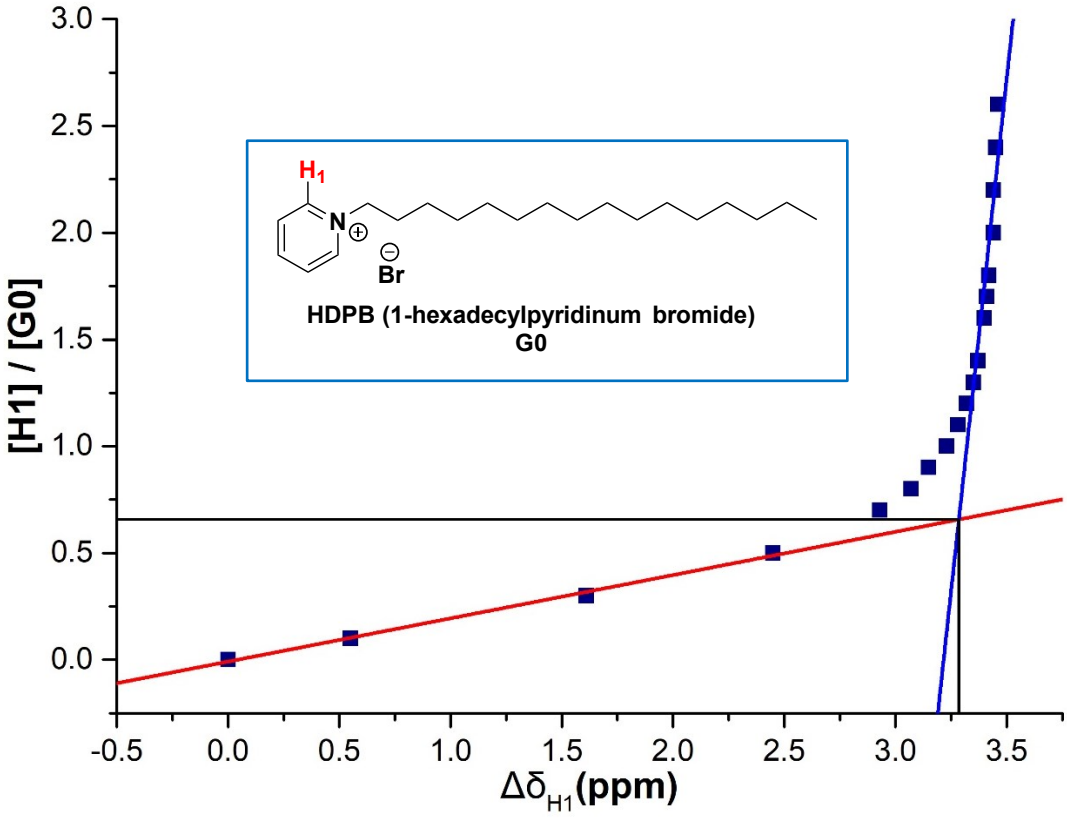

Fig. S66. Molar ratio plot for the complexation between **G0** (**HDPB**) and **H1** (**J2**), indicating a 2:1 stoichiometry.

Determination of association constants by ^{1}H NMR titration

The association constant between the host **H0** (**J1**) and the guest **G0** (**HDPB**) was determined by ^{1}H NMR titration. A nonlinear curve-fitting method (Fitter: NMR 1:1; Method: Nelder-Mead; Flavour: None (Full))[7] was applied to calculate the association constant for complexation between **H0** and **G0**, which was based on the online tools for supramolecular chemistry research and analysis (http://supramolecular.org).

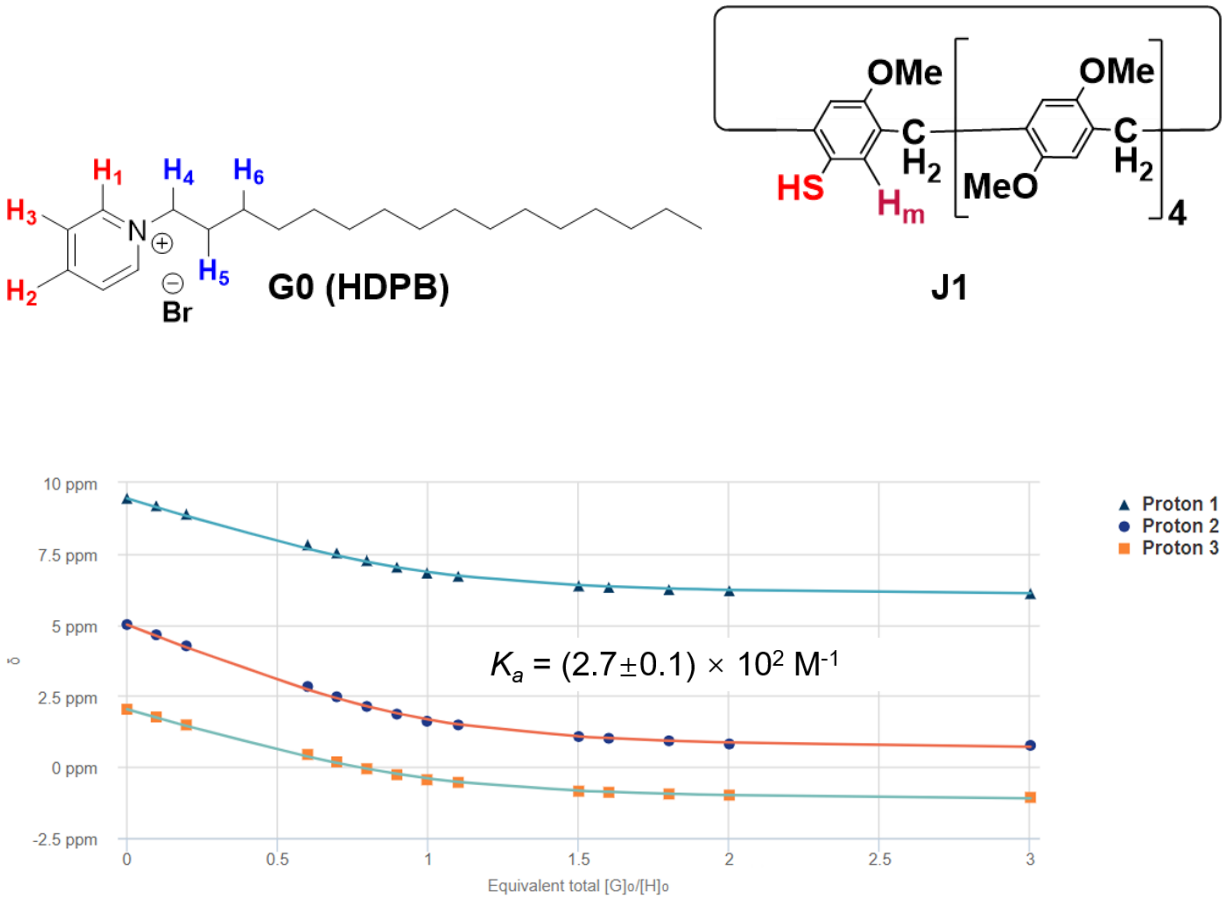

Fig. S67. The chemical shift changes and the nonlinear-fitting curves by BindFit v0.5 of $\mathbf{H_1}$ (Proton 1), $\mathbf{H_4}$ (Proton 2) and $\mathbf{H_5}$ (Proton 3) of **G0** (42 mM) upon the addition of **H0** (0–3.00 eq).

The association constant between the host **H1** (**J2**) and the guest **G0** (**HDPB**) was determined by ^{1}H NMR titration. A nonlinear curve-fitting method (Fitter: NMR 2:1; Method: Nelder-Mead; Flavour: None (Full))[8] was applied to calculate the association constant for complexation between **H1** and **G0**, which was based on the online tools for supramolecular chemistry research and analysis (http://supramolecular.org).

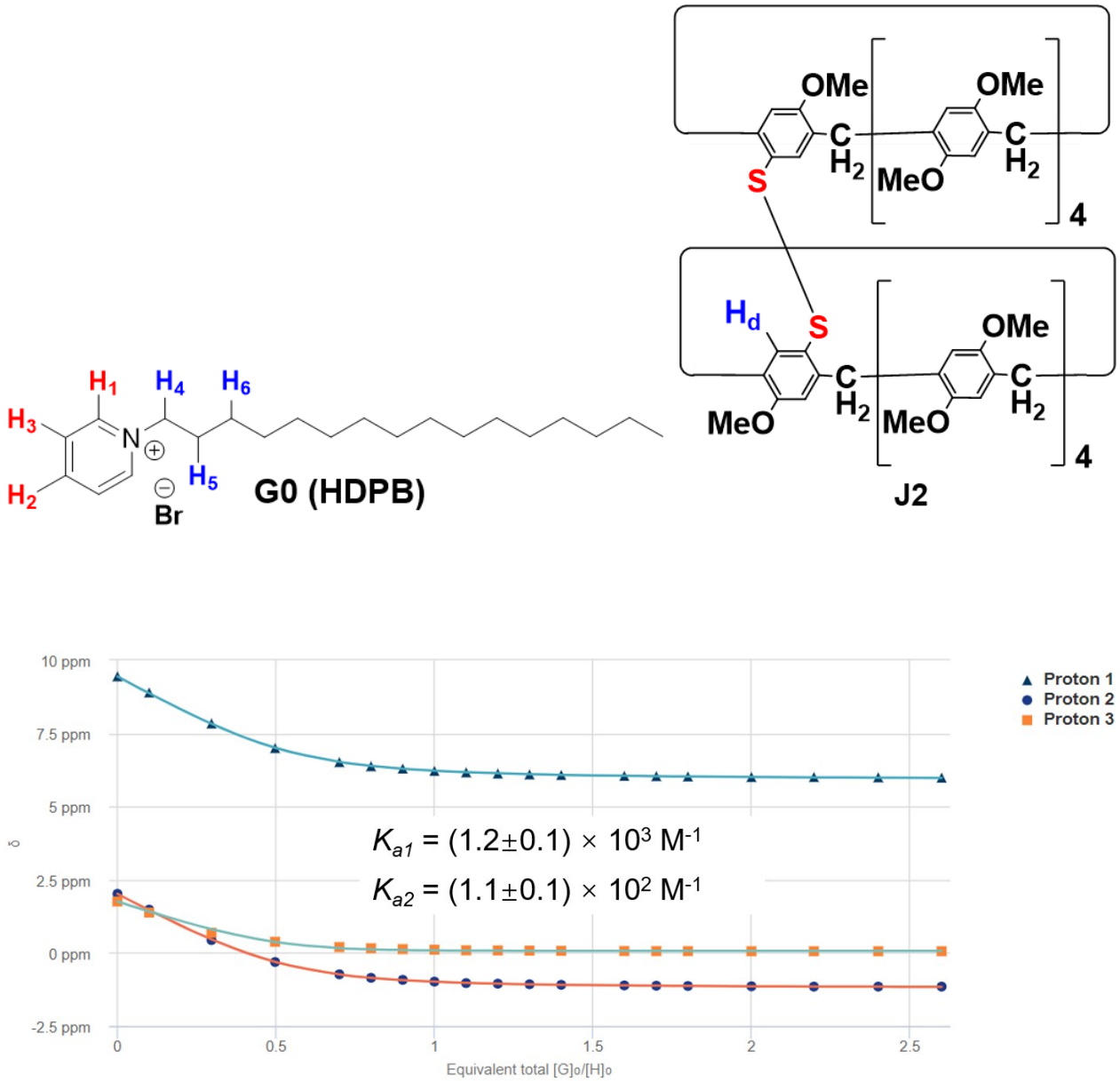

Fig. S68. The chemical shift changes and the nonlinear-fitting curves by BindFit v0.5 of $\mathbf{H_1}$ (Proton 1), $\mathbf{H_5}$ (Proton 2) and $\mathbf{H_6}$ (Proton 3) of **G0** (42 mM) upon the addition of **H1** (0–2.60 eq).

5. The Reversible Redox Conversion of the Host-guest Complexes between G0⊂J1 and $(G0)_2$⊂J2.

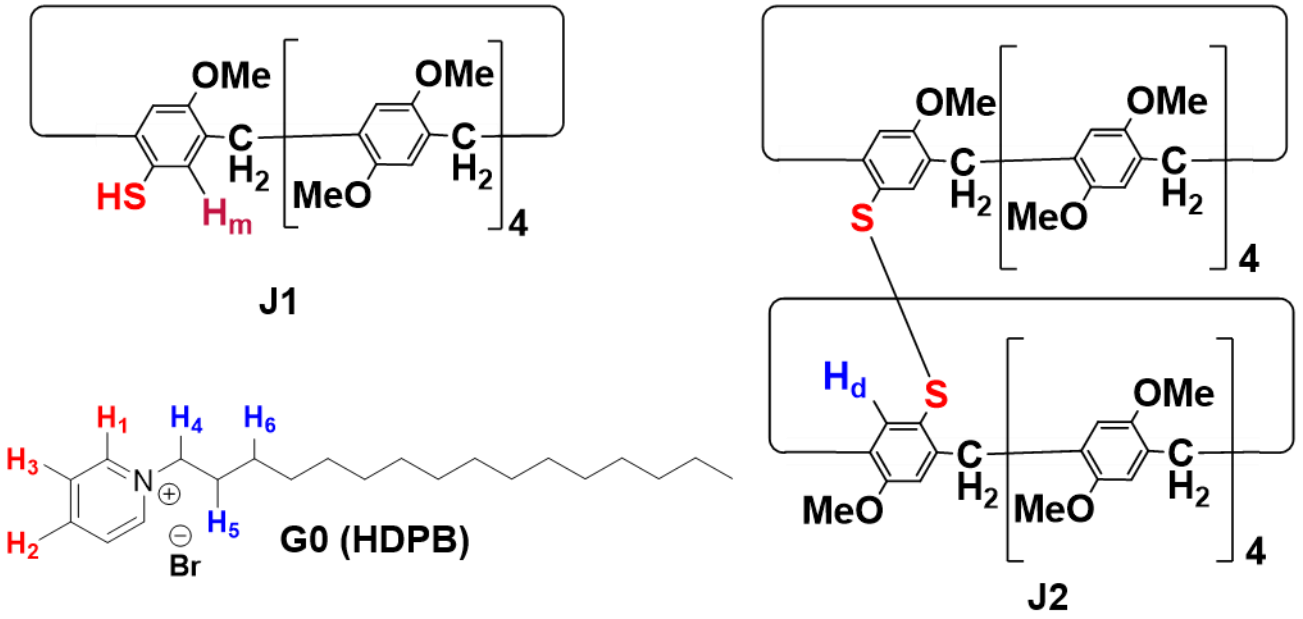

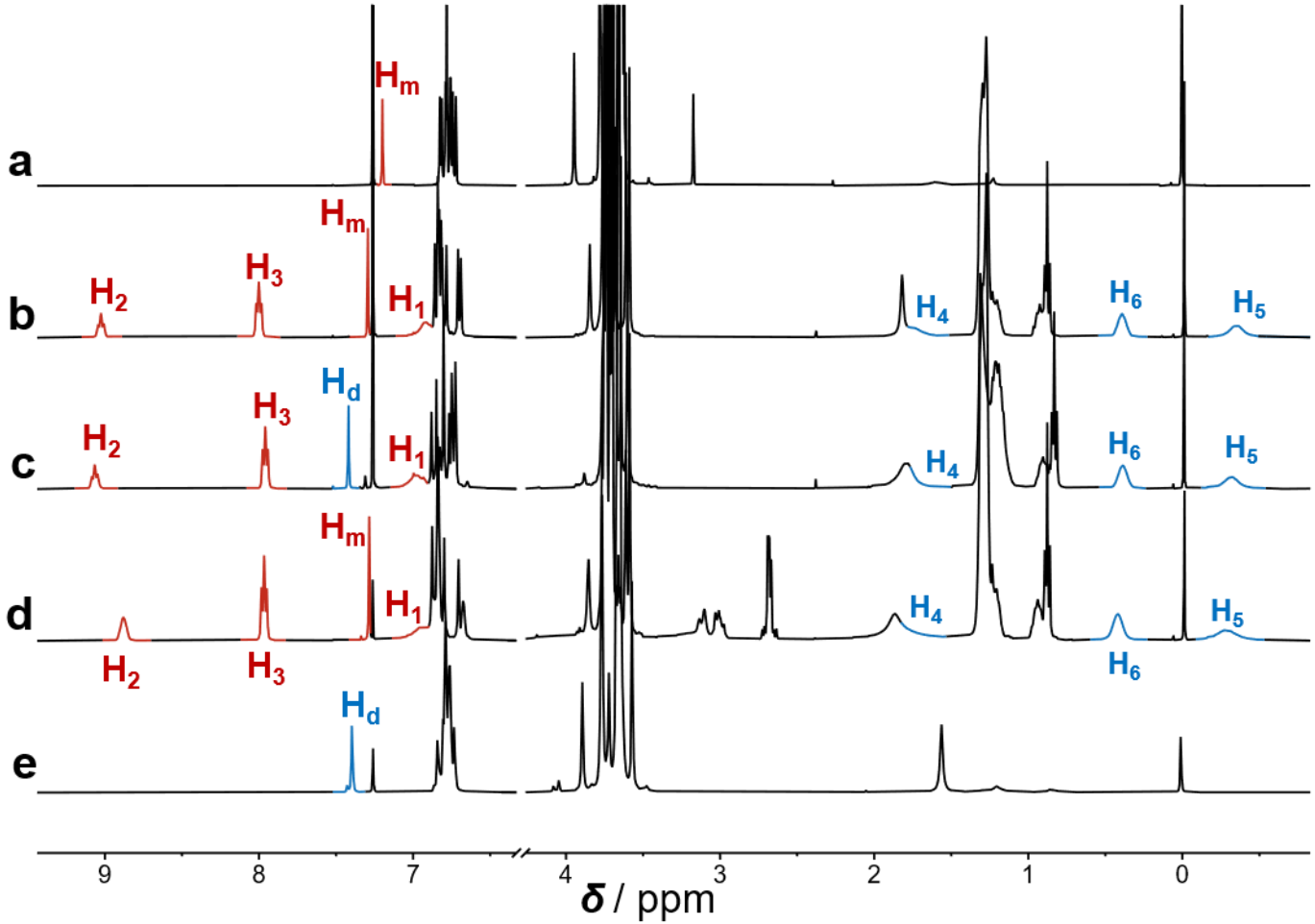

Fig. S69. ^{1}H NMR spectroscopic analysis of reversible redox conversion of the host-guest complexes between **G0⊂J1** and **(G0)$_2$⊂J2**. Partial ^{1}H NMR spectra (400 MHz, $CDCl_3$, 293 K) of (a) the **mono-SH-pillar[5]arene J1**, (b) the host-guest complex **G0⊂J1**, (c) a reaction mixture containing **(G0)$_2$⊂J2** after performing oxidation by O_2 in the air for 4 h, (d) a reaction mixture containing **G0⊂J1** after performing reduction by adding DTT (dithiothreitol) for 68 min, and (e) the **di(mono-SH-pillar[5]arene)mer J2**. Peaks are highlighted in red and blue for **J1** (H_m) and **J2** (H_d), respectively; peaks which chemical shifts changed are highlighted in red, blue, for H_1, H_2, H_3 and H_4, H_5, H_6 of **G0**, respectively.

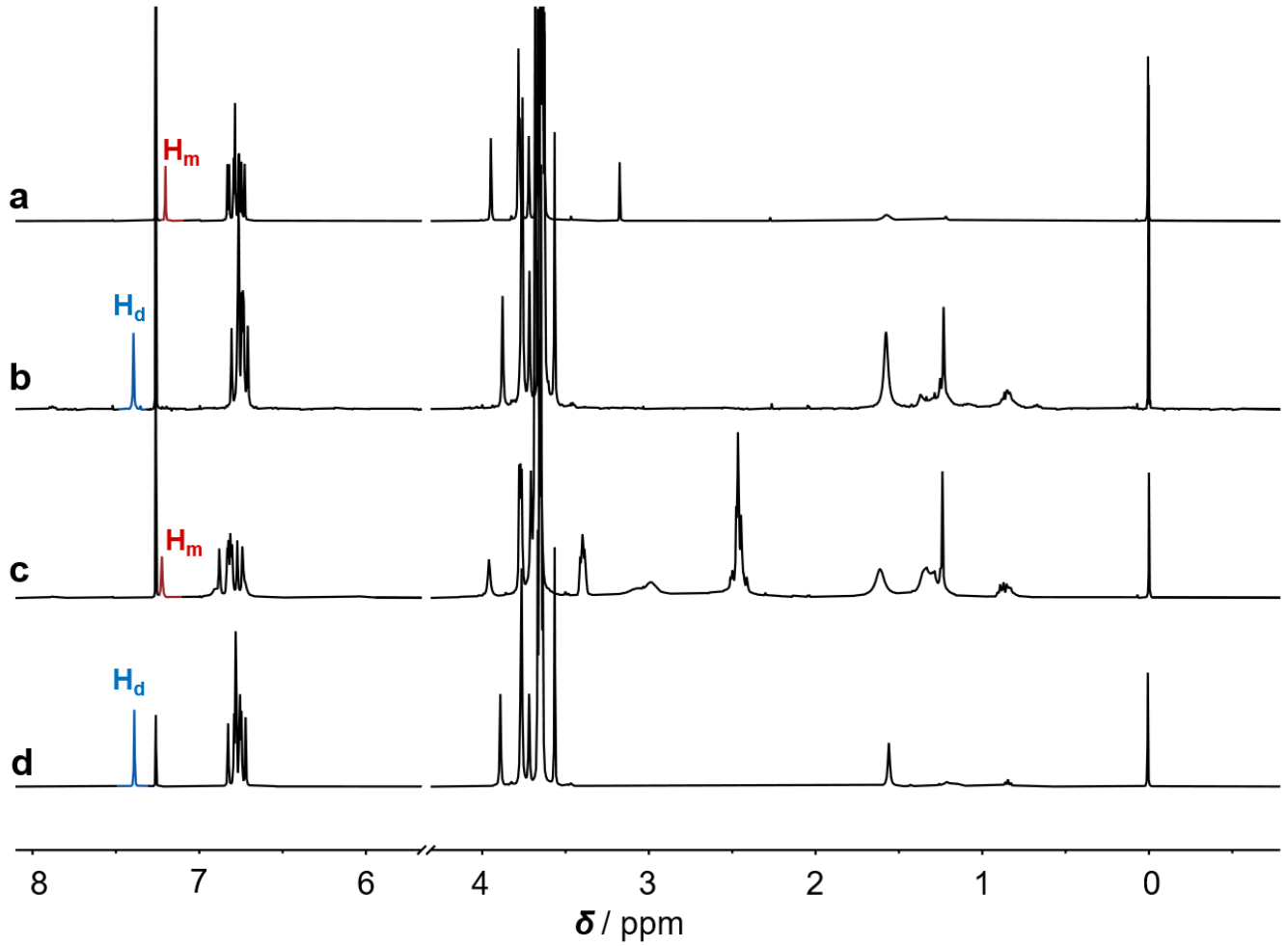

Fig. S70. ^{1}H NMR spectroscopic analysis of reversible redox conversion between **J1** and **J2** in the presence of catalytic amount of **G0** (9 mol%). Partial ^{1}H NMR spectra (400 MHz, $CDCl_3$, 293 K) of (a) **mono-SH-pillar[5]arene J1**, (b) a reaction mixture containing **J2** and catalytic amount of **G0** after performing oxidation by O_2 in the air for 5 d, (c) a reaction mixture containing **J1** and catalytic amount of **G0** after performing reduction by adding DTT (dithiothreitol) for 130 min, and (d) **di(mono-SH-pillar[5]arene)mer J2**. Peaks are highlighted in red and blue for **J1** (H_m) and **J2** (H_d), respectively.

Table S1 Association constants of host (**J1**, **J2**) with guest (**G0**), the time of redox conversion between **J1** and **J2** in the absence or presence of **G0**.

Host	K_a / M^{-1}	Reaction	t_c[a]	t_c'[b]
J1	270	Dimerization	53 d[c]	4 h
J2	1200 110	Reduction	56.5 h[d]	68 min

[a]The time of redox conversion between **J1** and **J2** in the absence of **G0**
[b]The time of redox conversion between **J1** and **J2** in the presence of **G0**
[c]Conversion ratio of **J1** (71%) by ^{1}H NMR
[d]Conversion ratio of **J2** (76%) by ^{1}H NMR

6. Control Experiments for Further Elucidating the Mechanism of Accelerated Redox Conversion Process.

In order to elucidate the mechanism of accelerated redox conversion process between **J1** and **J2** in the presence of **G0** (pyridinium salt), several control experiments have been performed. Since we realized the redox reactions are heterogeneous systems owing to the low solubility of base (K_2CO_3) in $CHCl_3$, we first replaced **G0** with **TBAB** (tetrabutylammonium bromide) and found out that **TBAB** can accelerate the reaction (Fig S75, S76, Table S2). The result of **TBAB** confirms that phase transfer catalyst can accelerate the reaction, but not as good as **G0** because **TBAB** is too bulky to get into the cavity of **J1** and **J2**. So, we think the host-guest interaction is also important. To further confirm this hypothesis, we mixed **G0** with 4-methoxybenzenethiol (**MBT**) and found that the dimerization of **MBT** was accelerated (Fig S72, S73, Table S2), which confirms that **G0** also functions as a phase transfer catalyst.[9] The acceleration effect is not as good as **J1** again because there is no host-guest interaction between **G0** and **MBT**.

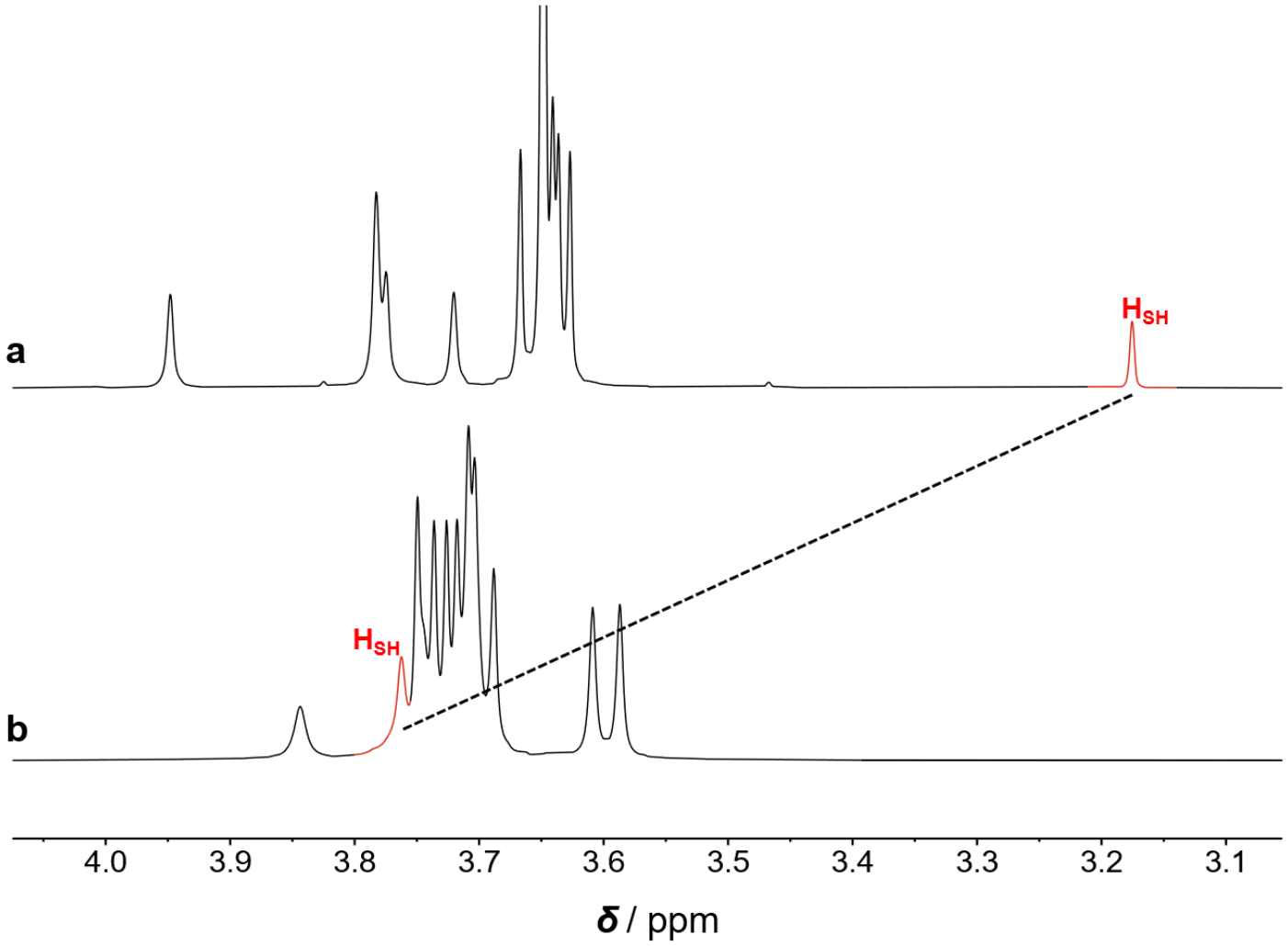

Fig. S71. Partial ^{1}H NMR spectra (400 MHz, $CDCl_3$, 293 K) of (a) **J1**, (b) **J1** in the presence of **G0** (**HDPB**). The H_{SH} assigned to **G0⊂J1** experienced significant downfield shift compared with **J1** owing to deshielding effect derived from complexation of electron-deficient **G0** and **J1**.

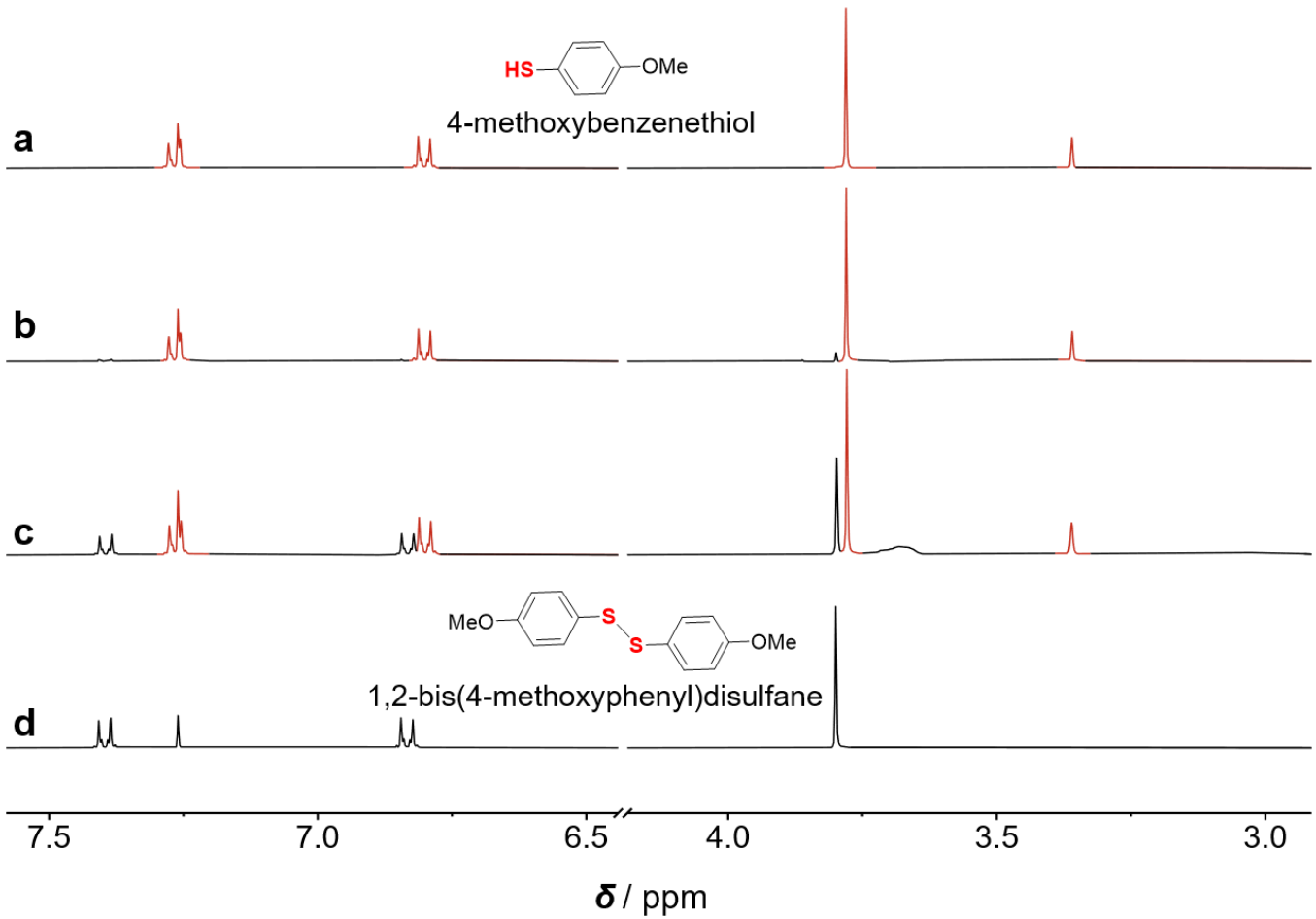

Fig. S72. ^{1}H NMR spectroscopic analysis of reversible redox conversion between **4-methoxybenzenethiol** and **1,2-bis(4-methoxyphenyl)disulfane** in the absence of **G0**. Partial ^{1}H NMR spectra (400 MHz, $CDCl_3$, 293 K) of (a) **4-methoxybenzenethiol**, (b) a reaction mixture containing **4-methoxybenzenethiol** and K_2CO_3 after performing oxidation by O_2 in the air for 72 h (conversion ratio: 7%), (c) a reaction mixture containing **4-methoxybenzenethiol** (conversion ratio: 50%) and K_2CO_3 after performing reduction by adding DTT (dithiothreitol) into **1,2-bis(4-methoxyphenyl)disulfane** for 59 h 52 min, and (d) **1,2-bis(4-methoxyphenyl)disulfane**. Peaks are highlighted in red for **4-methoxybenzenethiol**.

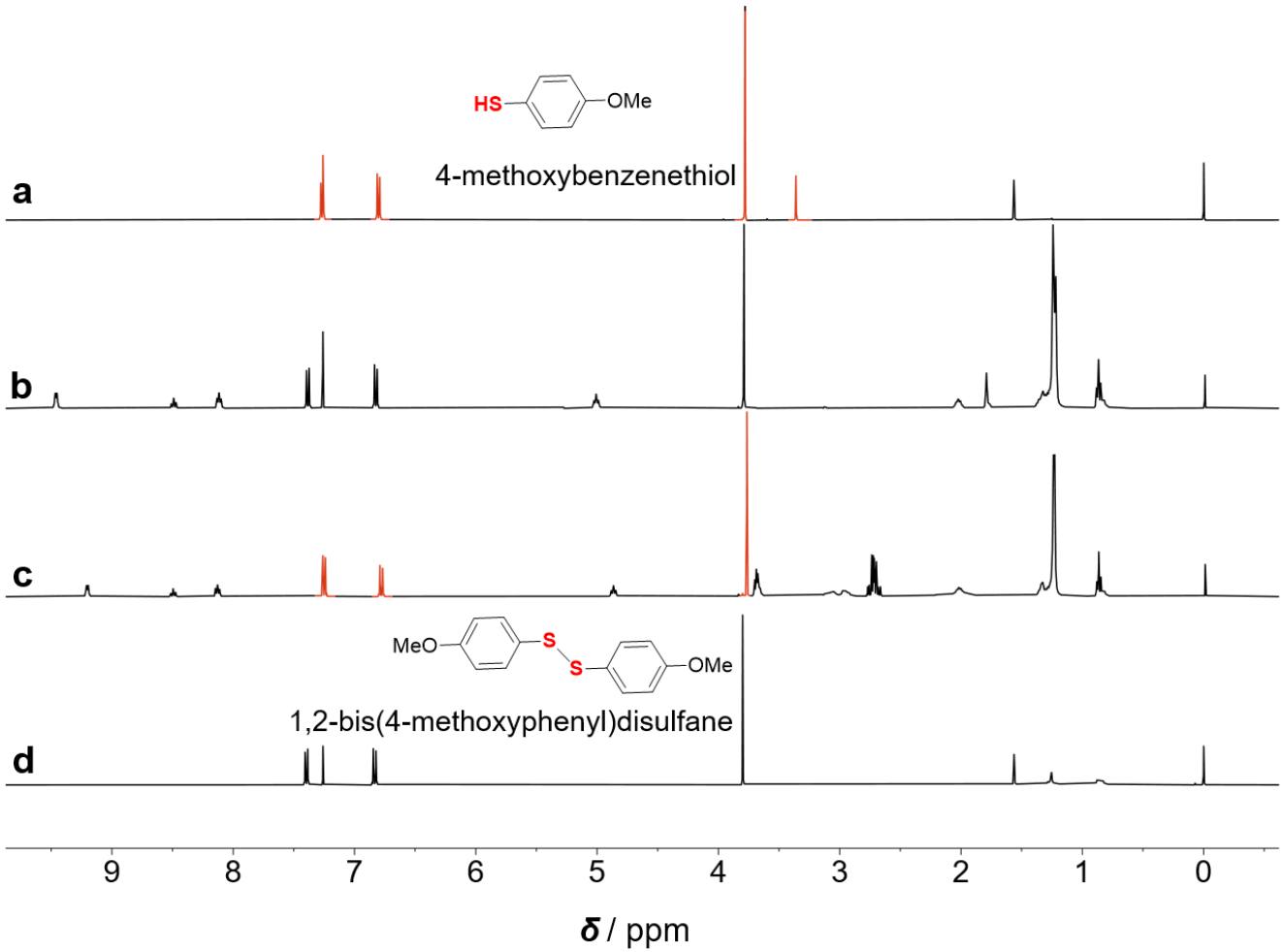

Fig. S73. ^{1}H NMR spectroscopic analysis of reversible redox conversion between **4-methoxybenzenethiol** and **1,2-bis(4-methoxyphenyl)disulfane** in the presence of **G0**. Partial ^{1}H NMR spectra (400 MHz, $CDCl_3$, 293 K) of (a) **4-methoxybenzenethiol**, (b) a reaction mixture containing **4-methoxybenzenethiol**, **G0** and K_2CO_3 after performing oxidation by O_2 in the air for 16 h 10 min, (c) a reaction mixture containing **1,2-bis(4-methoxyphenyl)disulfane**, **G0** and K_2CO_3 after performing reduction by adding DTT (dithiothreitol) for 165 min, and (d) **1,2-bis(4-methoxyphenyl)disulfane**. Peaks are highlighted in red for **4-methoxybenzenethiol**.

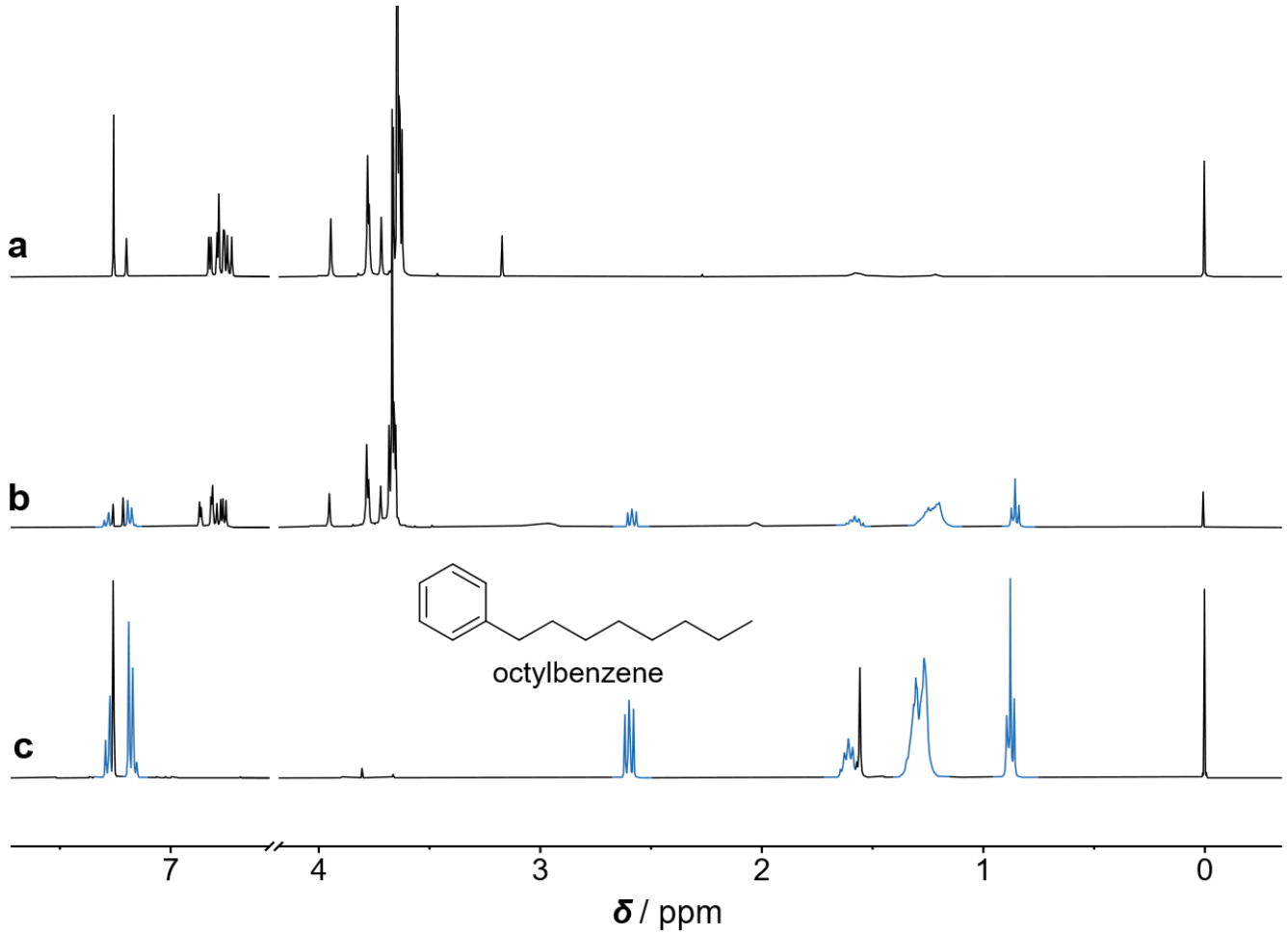

Fig. S74. ^{1}H NMR spectroscopic analysis of host-guest complexation between **J1** and **octylbenzene**. Partial ^{1}H NMR spectra (400 MHz, $CDCl_3$, 293 K) of (a) **mono-SH-pillar[5]arene J1**, (b) a reaction mixture containing **J1** and **octylbenzene**, and (c) **octylbenzene**. No host-guest complexation between **J1** and **octylbenzene**.

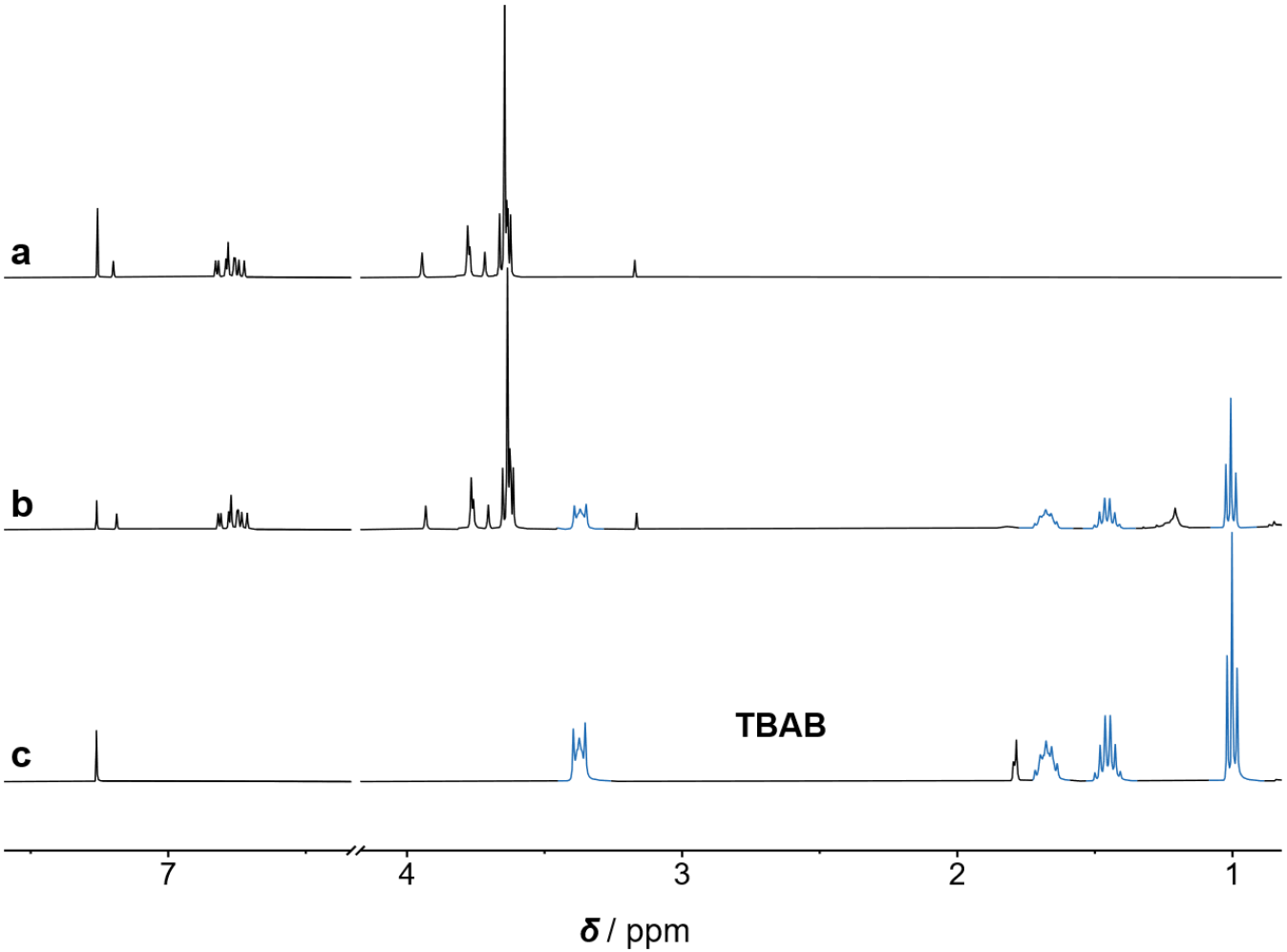

Fig. S75. ^{1}H NMR spectroscopic analysis of host-guest complexation between **J1** and **TBAB** (tetrabutylammonium bromide). Partial ^{1}H NMR spectra (400 MHz, $CDCl_3$, 293 K) of (a) **mono-SH-pillar[5]arene J1**, (b) a reaction mixture containing **J1** and **TBAB**, and (c) **TBAB**. No host-guest complexation between **J1** and **TBAB**.

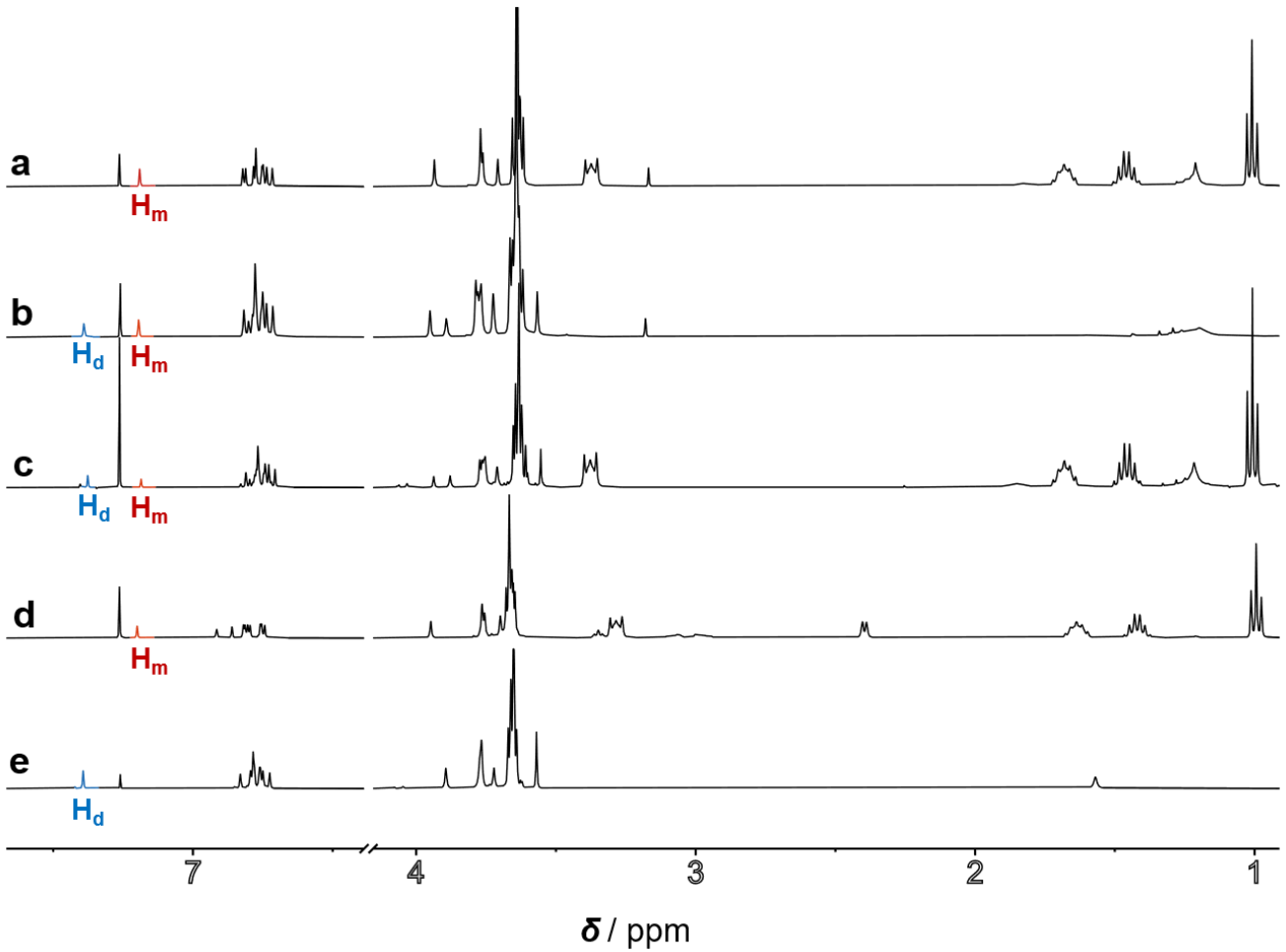

Fig. S76. ^{1}H NMR spectroscopic analysis of reversible redox conversion between **J1** and **J2** in the presence of **TBAB**. Partial ^{1}H NMR spectra (400 MHz, $CDCl_3$, 293 K) of (a) a reaction mixture containing **J1** and **TBAB**, (b) a reaction mixture containing **J2** (conversion ratio: 50%) and K_2CO_3 after performing oxidation by O_2 in the air for 25 d, (c) a reaction mixture containing **J2** (conversion ratio: 59%), **TBAB** and K_2CO_3 after performing oxidation by O_2 in the air for 49 h 50 min, (d) a reaction mixture containing **J1**, **TBAB** and K_2CO_3 after performing reduction by adding DTT (dithiothreitol) for 5 h 49 min, and (e) **di(mono-SH-pillar[5]arene)mer J2**. Peaks are highlighted in red and blue for **J1** (H_m) and **J2** (H_d), respectively.

Table S2 The time of redox conversions between monomers and dimers in the absence or presence of **G0**, **TBAB**.

System	Reaction	t_{ox}	t_{red}
J1	Dimerization	25 d[a], 53 d[b]	—
J2	Reduction	—	56.5 h[c]
J1+G0	Dimerization	4 h	—
J2+G0+DTT	Reduction	—	68 min
J1+TBAB	Dimerization	49 h 50 min[d]	—
J2+TBAB+DTT	Reduction	—	5 h 49 min
MBT	Dimerization	72 h[e]	—
BMPD	Reduction	—	59 h 52 min[f]
MBT+G0	Dimerization	16 h 10 min	—
BMPD +G0+DTT	Reduction	—	165 min

[a]Conversion ratio of **J1** (50%) by ^{1}H NMR
[b]Conversion ratio of **J1** (71%) by ^{1}H NMR
[c]Conversion ratio of **J2** (76%) by ^{1}H NMR
[d]Conversion ratio of **J1** (59%) by ^{1}H NMR
[e]Conversion ratio of **MBT** (7%) by ^{1}H NMR, **MBT: 4-methoxybenzenethiol**
[f]Conversion ratio of **BMPD** (50%) by ^{1}H NMR, **BMPD: 1,2-bis(4-methoxyphenyl)disulfane** (dimer of **4-methoxybenzenethiol**)

The Proposed Mechanism of a Faster Reversible Redox Conversion in the Presence of Guest

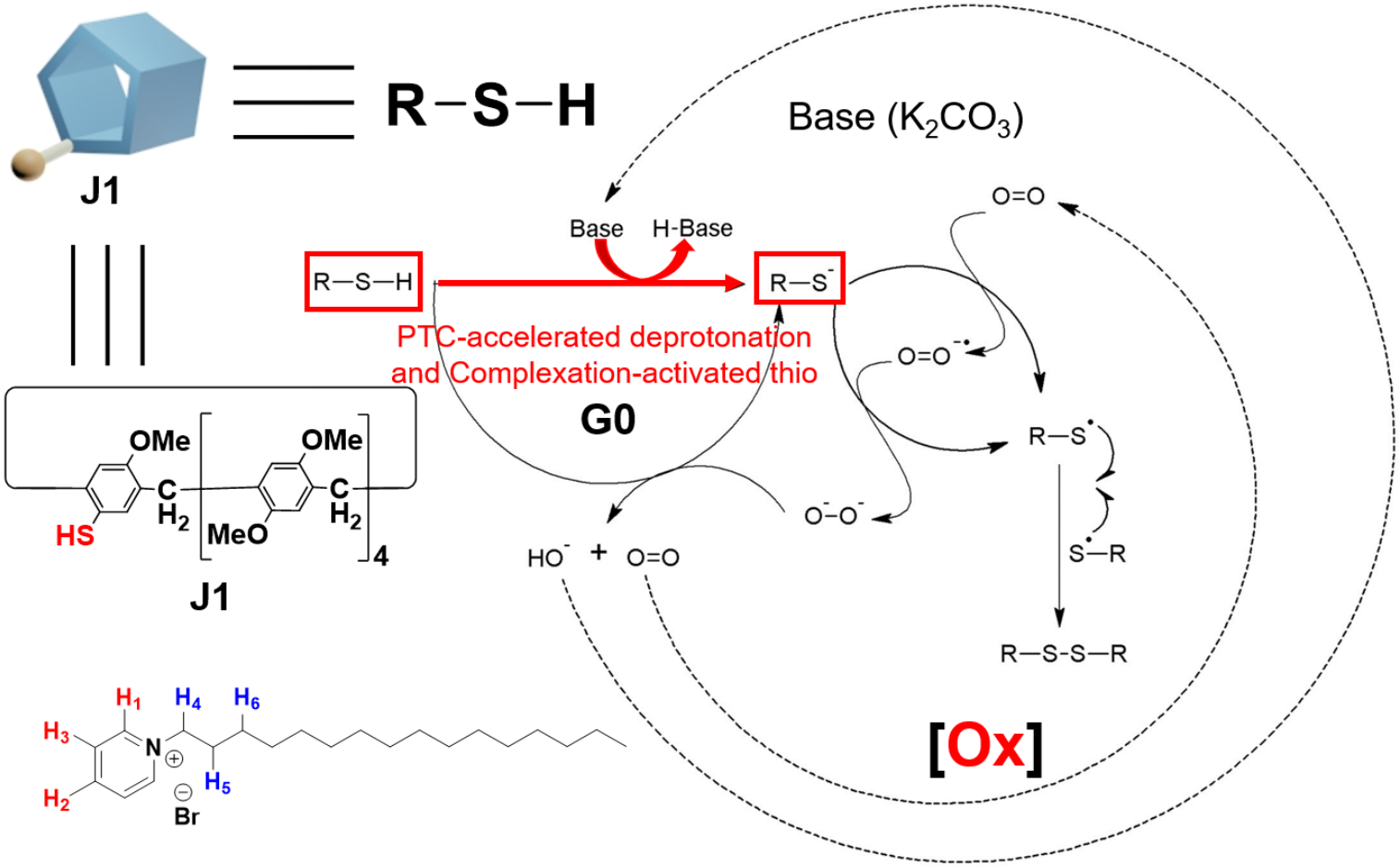

G0 (quaternary ammonium salt, phase transfer catalyst (PTC) & Guest)

Fig. S77. The proposed mechanism of the faster oxidative dimerization of **J1**.[10]

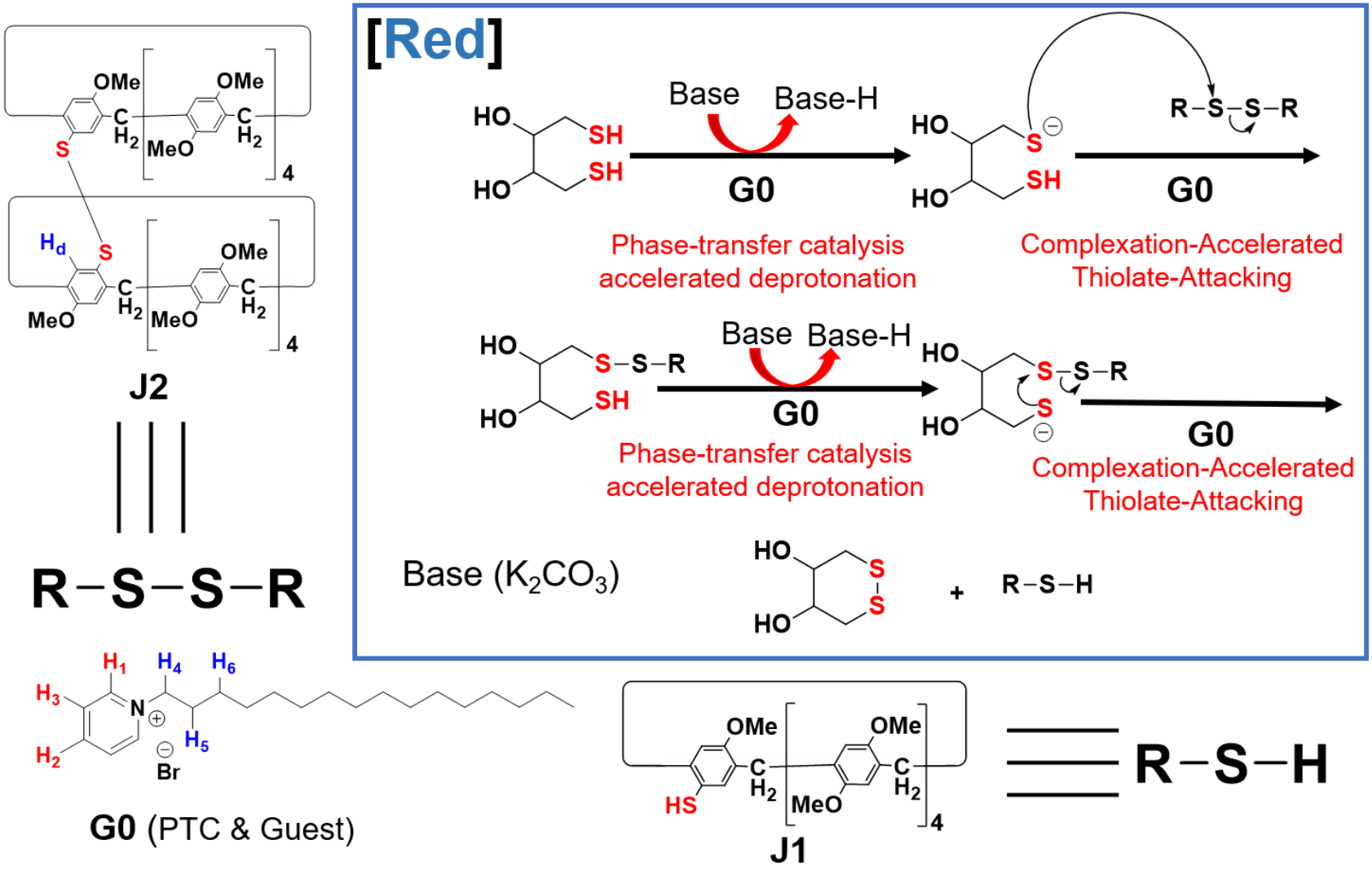

Fig. S78. The proposed mechanism of the faster reduction of **J2**.[11]

7. References

1. L. Z. Liu, D. R. Cao, Y. Jin, H. Q. Tao, Y. H. Kou and H. Meier, *Org. Biomol. Chem.*, 2011, **9**, 7007–7010.
2. Y. Chen, M. Q. He, B. Q. Li, L. Y. Wang, H. Meier and D. R. Cao, *RSC Adv.*, 2013, **3**, 21405–21408.
3. Y. Ding, A. R. Hlil and A. S. Hay, *Macromolecules*, 1999, **32**, 315-321.
4. M. S. Newman and H. A. Karnes, *Newman and Karnes*, 1966, **31**, 3980-3984.
5. D. Lee, S. W. Stone and J. P. Ferraris, *Chem. Commun.,* 2011, **47**, 10987–10989.
6. C.-L. Sun, J.-F. Xu, Y.-Z. Chen, L.-Y. Niu, L.-Z. Wu, C.-H. Tung and Q.-Z. Yang, *Polym. Chem.*, 2016, **7**, 2057–2061.
7. D. B. Hibbert and P. Thordarson, *Chem. Commun.,* 2016, **52**, 12792-12805.
8. P. Thordarson, *Chem. Soc. Rev.*, 2011, **40**, 1305-1323.
9. Y.-T. Li, Study on the Synthesis and Catalysis of New Phase Transfer Catalyzer, http://www. cnki. net.
10. E. Q. Rosenthal-Kim and J. E. Puskas, *Pure Appl. Chem.*, 2012, **84**, 2121–2133.
11. W. W. Cleland, *Biochemistry*, 1964, **3**, 480-482.